NASA TECHNICAL NOTE

NASA TN D-6457

NASA TN D-6457

EVALUATION OF EFFECTS OF HIGH-ALTITUDE TURBULENCE ENCOUNTERS ON THE XB-70 AIRPLANE

by Ronald J. Wilson, Betty J. Love, and Richard R. Larson

Flight Research Center
Edwards, Calif. 93523

NATIONAL AERONAUTICS AND SPACE ADMINISTRATION • WASHINGTON, D. C. • JULY 1971

1. Report No.	2. Government Accession No.	3. Recipient's Catalog No.
NASA TN D-6457		

4. Title and Subtitle	5. Report Date
EVALUATION OF EFFECTS OF HIGH-ALTITUDE TURBULENCE ENCOUNTERS ON THE XB-70 AIRPLANE	July 1971
	6. Performing Organization Code

7. Author(s)	8. Performing Organization Report No.
Ronald J. Wilson, Betty J. Love, and Richard R. Larson	H-631
	10. Work Unit No. 720-51-00-04-24
9. Performing Organization Name and Address	11. Contract or Grant No.
NASA Flight Research Center P.O. Box 273 Edwards, California 93523	
	13. Type of Report and Period Covered
12. Sponsoring Agency Name and Address	Technical Note
National Aeronautics and Space Administration Washington, D. C. 20546	14. Sponsoring Agency Code

15. Supplementary Notes

16. Abstract

A turbulence response investigation was conducted with the XB-70 airplane. No special turbulence penetration techniques, speeds, or other restrictions were specified for the investigation, nor were any flights made solely to obtain turbulence data. During 79 flights, turbulence was encountered, and recorded on a VGH recorder, 6.2 percent of the total flight distance at supersonic speeds above an altitude of 12,192 meters (40,000 feet). Geographical locations are given for selected turbulence encounters.

For 22 flights the airplane was instrumented to measure true gust velocities and the structural acceleration response to turbulence. The turbulence intensities measured were very low in comparison with those measured at high altitudes in other investigations. Acceleration response spectra, frequency response transfer functions, and coherence functions were computed from three turbulence encounters at Mach numbers of 0.88, 1.59, and 2.35. Results are compared with calculated studies. Frequencies from the vertical and lateral structural modes, dominant in the airplane acceleration responses, were compared with the natural frequencies of the human body in the vertical and lateral directions.

17. Key Words (Suggested by Author(s))	18. Distribution Statement
Structural dynamics Atmospheric turbulence XB-70 airplane Human factors	Unclassified - Unlimited

19. Security Classif. (of this report)	20. Security Classif. (of this page)	21. No. of Pages	22. Price*
Unclassified	Unclassified	84	$3.00

*For sale by the National Technical Information Service, Springfield, Virginia 22151

EVALUATION OF EFFECTS OF HIGH-ALTITUDE TURBULENCE ENCOUNTERS ON THE XB-70 AIRPLANE

Ronald J. Wilson, Betty J. Love, and Richard R. Larson
Flight Research Center

SUMMARY

A turbulence response investigation was conducted with the XB-70 airplane. No special turbulence penetration techniques, speeds, or other restrictions were specified for the investigation, nor were any flights made solely to obtain turbulence data. Out of a total of 129 flights on which a VGH recorder was used, 79 flights covered 150,680 kilometers (93,628 miles) at supersonic speeds above an altitude of 12,192 meters (40,000 feet). During these 79 flights, turbulence was encountered for 9333 kilometers (5799 miles) or for 6.2 percent of the total flight distance. Data concerning geographical locations, date, time of day, altitude, and maximum acceleration are also given for selected turbulence encounters.

For 22 flights the airplane was instrumented to measure true gust velocities and the structural acceleration response to turbulence. In general, the turbulence intensities measured were very low in comparison with those measured at high altitudes in other investigations. Results from acceleration response spectra data, which were used to identify the structural mode natural frequencies, showed good agreement with analytical predictions when updated XB-70 mode frequencies, mode shapes, mass, and structural characteristics were used. Results also showed that the frequencies of the vertical and lateral structural modes, dominant in the airplane acceleration responses, corresponded with the natural frequencies of the human body in the vertical and lateral direction. This resulted in marginal ride characteristics for the crew members during turbulence encounters.

Frequency response transfer functions and coherence functions were obtained from turbulence encounters at Mach numbers of 0.88, 1.59, and 2.35. The transfer functions are compared with results from a theoretical study in which early estimates of XB-70 mass, structural, and aerodynamic data were used.

INTRODUCTION

Analytical models of aircraft response to atmospheric turbulence now use true gust velocities, power spectral density techniques, and discrete gust velocities, whereas the earlier models used only the discrete gust velocities. Reference 1 is a comprehensive study of the methods used to define the atmospheric turbulence spectra and the power spectral density techniques with which aircraft response to turbulence excitation is analyzed.

Introduction of the present analytical models and the related spectra techniques required the collection of a large number of flight data samples to verify assumptions and extend statistical descriptions of turbulence in the atmosphere. To provide the required test data, extensive flight tests were conducted at high altitudes to obtain true gust velocities and statistical and spectral data on clear-air turbulence. References 2 to 4 are representative of these studies. Other investigators conducted tests of dynamic response to turbulence for rigid and flexible aircraft in the subsonic flight region; these results are reported in references 5 to 9. A study of the response of a delta-wing fighter in the supersonic region is presented in reference 1.

The design of large, flexible, supersonic cruise vehicles required that data be obtained in a supersonic cruise environment. To provide these flight-test data, a program was conducted on the XB-70 airplane using a VGH recorder to measure the turbulence encountered at altitudes greater than 12,192 meters (40,000 feet) at supersonic speeds. The results of this study, including preliminary airplane response to turbulence, were reported in reference 10. As a continuation of this study, instrumentation was installed for 22 flights to measure true gust velocities and the structural acceleration response to turbulence experienced at various locations on the airplane. No special techniques, speeds, or other restrictions were specified for the investigation, nor were any flights made solely to obtain turbulence data.

This report presents and discusses the flight-test results from the XB-70 turbulence response program. Atmospheric turbulence data are presented as turbulence spectra of the true gust velocities and the percentage of turbulence encountered in various altitude intervals. The airplane's response to turbulence is shown as acceleration response spectra, frequency response transfer functions, and coherence functions.

SYMBOLS

Units for the physical quantities defined in this report are given first in the International System of Units (SI) and then parenthetically in U.S. Customary Units. Measurements used in the investigation were taken in U.S. Customary Units. Factors relating the two systems are presented in reference 11.

Symbols used in appendix C are defined therein.

a_n, a_y	normal and lateral acceleration, g or meters/second^2 (feet/second^2)
Δa_n	peak-to-peak increments in normal acceleration at the airplane center of gravity, g
B_e	equivalent resolution bandwidth for power spectra calculations, cycles/second
f	frequency, cycles/second or radians/second
f_c	cutoff frequency (Nyquist frequency), cycles/second

g	acceleration due to gravity, meters/second^2 (feet/second^2)
$\left\|H_{(f)}\right\|$	frequency response transfer function
$\left\|H_{(f)}\right\|_c$	frequency response transfer function determined by use of cross-spectral relations
$\left\|H_{(f)}\right\|_s$	frequency response transfer function determined from power spectral relations
h_p	pressure altitude, meters (feet)
l_x, l_z	longitudinal and vertical distance from accelerometer to flow-direction vane, meters (feet)
$N(f)$	signal-to-noise ratio (appendix B)
T_r	track record, seconds
t	time, seconds
Δt	time interval between samples, seconds
V	airplane speed, meters/second (feet/second)
v_g	lateral component of true gust velocity, meters/second (feet/second)
w_g	vertical component of true gust velocity, meters/second (feet/second)
α	vane-corrected angle of attack, degrees or radians
β	vane-corrected angle of sideslip, degrees or radians
γ^2	coherence function
δ_{t_p}	wing-tip position, degrees
ϵ	normalized standard error
η	statistical degrees of freedom
θ	pitch angle, degrees or radians
λ	wavelength, V/f, meters/radian (feet/radian)
σ	root mean square

σ_1	truncated-root-mean-square values
$\bar{\Phi}$	power spectral density
$\bar{\Phi}_{n(f)}$	noise spectrum (appendix B)
φ	roll angle, degrees or radians
ψ	yaw angle, degrees or radians

Subscript:

max	maximum

A dot over a value represents differentiation with respect to time. A bar over a value represents the mean value for the indicated variable.

DESCRIPTION OF THE XB-70 AIRPLANE

The large, delta-wing, multijet-engine XB-70 airplane was designed for supersonic cruise at a Mach number of 3 and altitudes above 21,336 meters (70,000 feet). Two airplanes were built by North American Aviation, Inc., designated the XB-70-1 and XB-70-2. The three-view drawing of the XB-70 airplane in figure 1 shows the general configuration and overall dimensions. The basic design incorporated a thin, low-aspect-ratio wing with a 65.57° sweptback leading edge and folding tips, twin vertical stabilizers, and a movable canard with trailing-edge flaps. Geometric characteristics of the airplane are presented in table 1; a more detailed description is included in reference 12.

INSTRUMENTATION AND DATA ACQUISITION

The basic turbulence response instrumentation system used to measure atmospheric disturbances and aircraft response parameters consisted of: low inertia flow-direction vanes, attitude and rate sensing gyros, vertical and lateral accelerometers, and total-temperature and static- and dynamic-pressure probes.

Pertinent parameters for this investigation are listed in table 2. The parameters are grouped according to their primary area of use: vertical gust velocity, lateral gust velocity, basic airplane data, vertical airplane response, lateral airplane response, and NASA VGH recorder. The table also shows the type of transducer, its range of measurement, system resolution, accuracy, sampling rate, and location. Approximate locations of the more pertinent XB-70 sensors used for this investigation are illustrated in figure 2.

The turbulence response data were recorded with a digital data-acquisition system utilizing pulse code modulation (PCM) techniques. The system used a 40-sample-per-second sampling rate for the turbulence response parameters and had a total recording

time of 90 minutes per flight. A NASA VGH recorder provided up to 3 hours of continuous recording of airspeed, altitude, and normal acceleration at the airplane center of gravity and pilot position. Instrumentation, data acquisition, and data reduction are discussed further in appendix A.

FLIGHT-TEST PROCEDURES

A typical XB-70 flight plan included instructions that, when turbulence was encountered, the pilot could, if he desired, terminate all scheduled tests, recover attitude, and turn the data recorder to continuous record. Because most of the flight time was used for test purposes, the airplane condition was seldom that desired for turbulence penetration, that is, constant speed, constant altitude with the aircraft trimmed straight and level, and continuous data recording. With the limited total recording time of 90 minutes, the data were not recorded continuously on some of the turbulence encounters. These factors limited acquisition of turbulence data, because a turbulence penetration would often be complete before attitude could be recovered and the data recorder energized. Continuous recording was available on the NASA VGH recorder, thus these data were used to determine the total XB-70 turbulence environment and to assist in data editing.

On the day of a scheduled flight, areas of predicted severe or moderate turbulence were avoided by following an alternate route. No attempt was made during the tests to penetrate known severe or moderate turbulent areas.

DATA-ANALYSIS PROCEDURE

VGH Data

The VGH records were evaluated to determine the complete turbulence environment that the airplane was subjected to, that is, the percentage of turbulence at various altitude intervals, length of the turbulent areas encountered, and intensity of turbulence encountered in the form of acceleration magnitude. To evaluate the records, a value of the threshold of peak accelerations at the center of gravity of $\pm 0.06g$ was used, as established in reference 10. In addition, the airspeed trace showed irregular disturbances in the presence of turbulence, which aided in the determination of turbulence onset. By using the aircraft instrumentation, which could measure within the state of the art such quantities as pilot inputs, control positions, engine parameters, and duct variations, it was qualitatively determined whether the disturbance was caused by turbulence or the inputs just noted. Only those records in which turbulence disturbances could be identified were evaluated.

The length of turbulent areas and the percentage of miles in rough air were determined by considering the airplane to be in rough air whenever the airspeed trace showed irregular disturbances and the envelope of the incremental normal-acceleration trace remained greater than $\pm 0.06g$. The length of each turbulent area was obtained by multiplying the true airspeed by the time spent in rough air at each altitude interval. The summation of the lengths of the individual areas of rough air

was divided by the total flight distance for the given altitude interval to obtain the percentage of rough air for each altitude interval.

Gust Velocity

The true gust velocity was determined by using the method presented in reference 1, which relates the vertical gust velocity to the vane-corrected angle of attack and airplane motions, as in equation (1). For the vertical component of true gust velocity,

$$w_g = V\alpha - V\theta + \int a_n dt + l_x\dot{\theta} \tag{1}$$

For the lateral component of true gust velocity,

$$v_g = -V\beta - V\psi + l_x\dot{\psi} + \int (a_y + g\varphi)dt + l_z\dot{\varphi} \tag{2}$$

In applying these equations, the measurements were taken as increments from the mean value for the entire record. Essentially, the vertical component of true gust velocity would be given by the expression

$$w_g = V(\alpha - \bar{\alpha}) - V(\theta - \bar{\theta}) + \int (a_n - \bar{a}_n)dt + l_x(\dot{\theta} - \dot{\bar{\theta}}) \tag{3}$$

The expression for the lateral component would be similar. The equations are based on the assumptions that (1) all disturbances are small and (2) the effects of variations in upwash on the vane-indicated angle of attack are negligible.

Resolution of the gust velocity data is discussed in appendix B.

Power Spectral Analysis

A power spectral analysis computer program was used to perform a standard Blackman-Tukey type of spectral analysis on one or more data sequences. This procedure consisted of computing correlation functions from the data sequences and then taking a Fourier transform to generate spectral density estimates. Other relations used were: autocorrelation, cross correlation, cross-spectral density, amplitude and phase of frequency response transfer function, and coherence function. Specific details concerning the equations used are presented in appendix C.

Several considerations and compromises were examined in selecting frequency range, sample size, and other digital parameters to achieve digitally accurate results for the turbulence response data. For example, to avoid aliasing errors, reference 13 suggests that the cutoff frequency (Nyquist frequency) be at least 1 1/2 or two times greater than the maximum frequency of interest. The cutoff frequency is defined as

$f_c = \frac{1}{2\Delta t}$, where Δt is the time interval between samples. Results from initial computations and ground vibration tests on the XB-70 airplane indicated significant responses ranging from 0 cps to 10 cps, with some additional response modes to 15 cps. To examine the airplane response in the frequency range of 0 cps to 15 cps, a sampling rate of 40 samples per second was selected, resulting in a cutoff frequency of 20 cps. During reduction of the turbulence and structural response data, a low-pass digital filter with a cutoff frequency of 10 cps was used.

True gust velocity power spectra. – Computation of the true gust velocity spectra required compromises in determining minimum sample size. Using reference 1 as a guide, an initial attempt was made to maintain the statistical degrees of freedom ($\eta = 2B_eT_r$) near 80 or greater. However, the turbulence track record obtained during the XB-70 flight tests was usually very short (6 seconds to 53.5 seconds). With the given data samples, a minimum track record of 20 seconds with $B_e = 1.0$ cps and $\eta = 40$ was established. For presentation purposes, a common B_e of 1.0 cps was selected for the turbulence spectra to maintain comparison capability between each of the measured true gust velocity power spectra.

Structural response spectra. – For proper response resolution, reference 14 suggests that the filter bandwidth be one-fourth the bandwidth of the narrowest peak in the power spectrum. The approximate structural response bandwidth of 0.4 cps was obtained from in-flight data by using a shaker system (ref. 15).[1] Following these criteria, the suggested bandwidth would be 0.1 cps. Combining the suggested bandwidth with the track records from the flight data would result in very low statistical degrees of freedom. As a compromise, considering the resolution errors occurring from the choice of bandwidth and statistical uncertainty errors (as presented in ref. 16), a common spectral bandwidth of 0.4 cps was selected for use in reducing the structural-response data.

RESULTS AND DISCUSSION

Atmospheric Turbulence

Of a total of 129 XB-70 flights, 79 flights attained altitudes greater than 12,192 meters (40,000 feet) and supersonic speeds. A summary of the turbulence experienced by the airplane, for a center-of-gravity acceleration threshold of ±0.06g, during the 79 flights is presented in table 3. As shown, the airplane flew a total of 150,680 kilometers (93,628 miles) at these altitudes and encountered turbulence 6.2 percent of the distance, or 9333 kilometers (5799 miles).

Figure 3 illustrates the total number of kilometers (miles) flown in altitude bands

[1] The shaker system was installed on the XB-70 airplane to provide a known and controlled sinusoidal force input. The system consisted of two 0.185-square-meter (2-square-foot) trapezoidal planform surfaces symmetrically mounted at the airplane nose just forward of the pilot's station. The amplitude and frequency of these surfaces were controlled by a servohydraulic actuator. The system allowed for trim, amplitude, and frequency control by the copilot. The aerodynamic surfaces had amplitude capabilities of up to $\pm 12^{\circ}$ over the frequency range of 1.4 cps to 8.0 cps.

of 1524 meters (5000 feet). Figure 4 presents the variation of distance flown in turbulence by altitude bands, and figure 5 shows the probability of equaling or exceeding turbulence samples of various lengths. For comparison purposes, figures 3 to 5 present data obtained during flights over the western United States from references 2 and 3. The data from reference 2 and the XB-70 airplane were from flights on which turbulence was recorded when encountered during routine tests. The investigation of reference 3 collected flight data from deliberate turbulence penetrations.

Figure 3 shows that the XB-70 airplane flew more kilometers over the western United States than were flown in each altitude band in the studies of references 2 and 3, with two exceptions: in the interval from 15,240 meters (50,000 feet) to 16,764 meters (55,000 feet) and 21,336 meters (70,000 feet) to 22,860 meters (75,000 feet) in reference 2. Figure 4 indicates that the XB-70 airplane experienced a fairly consistent 6 percent to 7 percent of kilometers in turbulence between 12,192 meters (40,000 feet) and 19,812 meters (65,000 feet). The data from reference 2 generally exhibited 0 percent to 2 percent of kilometers in turbulence for these altitude intervals. The data from reference 3 exceeded the XB-70 airplane flight results between the altitude intervals of 13,716 meters (45,000 feet) to 18,288 meters (60,000 feet). Some of these differences may exist because of the method used to evaluate the presence of turbulence and the method used to obtain turbulence penetrations. In reference 2 a derived gust velocity threshold of 0.6096 meter/second (2.0 feet/second) was used. In reference 3 the criterion that the center-of-gravity acceleration trace should be continuously disturbed (±0.05g) and should exhibit frequency peaks in excess of ±0.10g was used. The value of ±0.06g threshold peak acceleration for this report was determined (ref. 10) to assure that the results would include values of the derived gust velocity greater than 0.46 meter/second (1.5 feet/second). In addition, the XB-70 data were obtained for supersonic conditions, whereas the referenced data were obtained for subsonic conditions.

The probability of equaling or exceeding a turbulence sample of a given length plotted in figure 5 shows that the XB-70 data generally fall between the two referenced studies. The XB-70 data also show that the probability of encountering turbulence equal to or greater than 254.3 kilometers (158 miles) in length was approximately 1 percent. The longest turbulent area, 724.2 kilometers (450 miles), was encountered at an altitude between 18,288 meters (60,000 feet) and 19,812 meters (65,000 feet). The turbulent areas of approximately 321.9 kilometers (200 miles) were encountered at altitudes between 16,764 meters (55,000 feet) and 18,288 meters (60,000 feet). This figure illustrates the problem of obtaining data samples of sufficient length in high-speed aircraft to provide high accuracy during data analysis.

Geographical locations of the turbulent areas encountered at altitudes above 12,192 meters (40,000 feet) for flights between May 12, 1967, and February 4, 1969, are discussed in appendix D, along with the time of day, $(\Delta a_n)_{max}$, length, and altitude for each turbulent encounter. Additional information concerning turbulence encounters for test flights made before May 12, 1967, is presented in reference 17.

Turbulence spectra. – The true gust velocity encountered by the XB-70 airplane was measured during the last 22 flights of the program, between May 12, 1967, and February 4, 1969. The overall envelopes of the gust velocity power spectral density obtained from the XB-70 flights, U-2 flights in which atmospheric turbulence was sought (ref. 3), and F-106 flights through severe storms (ref. 18) are compared in

figure 6. The comparison indicates the relatively low magnitude of the turbulence experienced by the XB-70 airplane in avoiding turbulent areas, and the level of turbulence intensity that could be encountered either during operational use or by deliberately seeking turbulence. The range of turbulence intensities measured with the XB-70 airplane was rated subjectively by the XB-70 pilots as being "very light" to short periods of "moderate."

To examine the turbulence spectra for comparison with theoretical turbulence models and probable isotropic turbulence, a representation of the vertical and lateral turbulence spectra computed from the XB-70 flight data is presented in figure 7. (Flight and data conditions for each of the encounters are listed in table 4.) The vertical turbulence spectra reveal response peaks for the higher values of reduced frequency. These response peaks correspond to the third and fifth structural modes, discussed in a later section, and have peaks of increasing magnitude with increasing turbulence intensities. The peaks indicate that the response or phasing, or both, of one or more of the parameters in equation (1) was insufficient to remove the aircraft response frequencies from the angle-of-attack parameter. Examination of the spectrum for the individual parameters from which the vertical gust velocity is derived and attempts to identify the contributing parameters through roller coaster maneuvers and ground calibration checks were inconclusive.

The comparisons of the vertical and lateral components of turbulence spectra in figure 7 generally show a lack of isotropic turbulence due to a difference in slopes and magnitudes. The slopes of the vertical turbulence spectra vary from approximately -1.5 to -1.0, compared to the slope of a theoretical turbulence model of -1.67. The slopes of the lateral turbulence spectra vary from -1.6 to -1.2. In general, the slope of the lateral turbulence spectrum is steeper than that of the vertical turbulence spectrum, a trend similar to that shown in reference 3. The relative difference between the lateral and vertical turbulence spectra can be seen by comparing the ratio of the lateral to vertical root-mean-square values which ranged from 1.08 to 1.63. Although the turbulence encountered by the XB-70 airplane was of low intensity and low statistical degree of freedom, the resulting degree of data variability is similar to that obtained in previous studies for similar data conditions. For example, selected turbulence spectra presented in reference 3 for low-intensity turbulence and low statistical degree of freedom show approximate slope variations from -1.9 to -0.8 for the vertical turbulence spectra and from -1.7 to -1.2 for the lateral turbulence spectra. However, with the limited amount of turbulence encounter data from the XB-70 flights, it is not possible to arrive at values of average spectrum slopes with any reasonable degree of statistical confidence.

Airplane Response

Time history data. – Time histories are presented in figure 8 to illustrate the nature of the response of the XB-70 airplane to a turbulence encounter at an altitude of 11,979 meters (39,300 feet) and a Mach number of 1.59 for approximately 45.4 seconds. The pilot rated this encounter as "moderate." The data are grouped into vertical gust velocity, lateral gust velocity, basic airplane, and airplane vertical and lateral response parameters. The vertical gust velocity (fig. 8(a)) ranged from 4.48 meters/second (14.7 feet/second) to -2.35 meters/second (-7.7 feet/second) as the lateral gust velocity (fig. 8(b)) varied from 5.18 meters/second (17 feet/second) to -4.27 meters/second (-14 feet/second). The maximum peak-to-peak increments in normal

acceleration at the pilot station and center of gravity were 0.65g and 0.25g, respectively. The corresponding peak-to-peak incremental lateral accelerations were 0.26g and 0.30g. The acceleration time histories also show a predominance of the oscillations of the structural elastic modes except for the lateral acceleration at the mixer bay (fig. 8(e)), which appears to be influenced somewhat by the elevon input (fig. 8(c)).

Acceleration response spectra. – Response spectra are presented to illustrate the effects of random turbulence excitation, identify major vertical and lateral response modes, and compare acceleration root-mean-square levels. Figure 9 compares the normal acceleration response spectra for a maximum intensity turbulence encounter (flight A) with data from a minimum intensity encounter during straight and level flight (flight E) with minimum control inputs. Figure 10 presents a similar comparison for the lateral acceleration response data. Flight conditions for these data are included in table 4.

As an aid in interpreting the responses of figure 9, figures 11(a) to 11(d) represent the calculated fuselage vertical deflections (normalized to unit wing-tip deflection) for the first four symmetrical modes of the airplane. Figure 11(e) is a planform view of the airplane showing the calculated node lines for these four symmetrical modes and various accelerometer locations. The data presented in figure 11 are from an unpublished study conducted as a follow-on to the investigation of reference 19. Reference 19 predicted the structural response modes by using early estimates of the XB-70 airplane mass, structural, and aerodynamic characteristics; however, the analytical predictions did not agree with flight data. The follow-on study updated the total weight and weight distribution for three typical flight conditions. In addition, the updated information was combined with data from ground vibration tests to obtain an accurate description of the structural modes. In general, the spectra presented in figure 9 show that the response of the structural modes contributed appreciably to the total turbulence response. The figure also shows that the responses of the structural modes for the low level and high level turbulence are similar, with the high level encounter resulting in more clearly defined response peaks. The defined response peaks, shown by the normal acceleration spectra, indicate a response in the rigid body longitudinal short-period mode (0.2 cps). The first structural mode appears at approximately 2.2 cps, whereas the second, third (the more predominant mode), and fourth modes appear at 4.0, 5.0, and 7.2 cps, respectively. These frequencies and the relative strengths of each mode show good agreement with the calculated predictions in figure 11. The results of figure 9 also show a fifth mode at 8.8 cps, which was predicted in the analytical study but is not illustrated in figure 11. Reference 10, which extended the response to 20.0 cps, also illustrates response indications at 12.0 cps and 15.0 cps.

Exceptions to these observations are probably due to accelerometer locations in relation to the response node lines. For example, the center-of-gravity accelerometer does not indicate a response at 4.0 cps. The mode shapes from figure 11(e) indicate that the node line for the 3.78 cps mode was close to the center-of-gravity accelerometer. The aft wing, fuselage, and wing-tip accelerometers do not show the 5.0 cps mode, indicating that the 5.29 cps node line from figure 11(e) may be closer to the accelerometer locations than is illustrated. Other exceptions may be found in figure 9; these exceptions may be clarified by comparing the node lines and accelerometer locations from figure 11(e). The normal acceleration root-mean-square values show fairly consistent readings from 0.027g to 0.0657g for the low turbulence condition throughout the airplane. The normal acceleration root-mean-square values for the stronger turbulence condition show increases from 0.0606g to 0.2952g. The

acceleration root-mean-square values at the pilot station and center-of-gravity locations for the strong turbulence encounter are 3.3 and 2.0 larger, respectively, than the values obtained for the low turbulence condition.

The lateral acceleration response spectra of figure 10 show the major response mode at 2.0 cps. Other modes are indicated at 4.0 cps and 6.0 cps. The center-of-gravity data also indicate a response at 9.6 cps. The lateral acceleration data at the mixer bay show a large response to the frequencies below 1 cps. This may be caused in part by the elevon input previously mentioned (figs. 8(e) and 8(c)). The acceleration root-mean-square values at the mixer bay are approximately the same for the two turbulence encounters. The acceleration root-mean-square values at the pilot station and center-of-gravity locations for the strong turbulence encounter are 4.5 and 6.4 larger, respectively, than the values obtained for the low turbulence condition.

Acceleration response and human factors. – The effect of the vertical and lateral low-frequency response on the crew members was particularly noticeable during turbulence encounters. Previous studies (ref. 20, for example) have shown that the natural frequency of the whole human body, seated, responds vertically from 4.0 cps to 6.0 cps. In addition, the transverse natural frequencies of the human body, shoulder and head, are 2 cps to 3 cps. The vertical body response frequencies correspond to the major normal structural response modes of 4.0 cps and 5.0 cps (fig. 9). The human lateral response also corresponds to the major structural lateral mode of 2.0 cps (fig. 10). Pilot comments from references 21 and 22 state that the lateral accelerations were noted only with respect to turbulence response. This type of turbulence response usually resulted in the crew members rating a patch of turbulence more severe than the rating given by the pilot of an accompanying support aircraft.

The crew members also reported that the response to even light turbulence at low speeds and altitudes would be unacceptable for a commercial transport and would be only marginally acceptable for a military airplane. However, at no time were the pilots unable to perform their functions or maintain control of the airplane because of cockpit response.

Frequency response transfer function. – Examples of the airplane frequency response transfer function, the turbulence input spectra, the acceleration response output spectra, and coherence data are presented in figures 12 to 17. (Flight-test and data-reduction conditions are listed in table 4.) The acceleration response output data are presented for seven airplane locations, four on the fuselage--nose, cockpit, center of gravity, and mixer bay--and three on the wing--forward left wing near the quarter span, aft left wing near the quarter span, and left wing tip. The figures illustrate results from three turbulence encounters at Mach numbers of 0.88, 1.59, and 2.35.

The turbulence input spectrum for each flight condition is presented in figures 12, 14, and 16. Using the data from the turbulence input and acceleration response, a cross-spectrum frequency response function, $\left|H_{(f)}\right|_c$, was computed from the relations given in appendix C. The acceleration response spectra, the computed cross-spectra frequency response transfer functions, and the coherence functions are presented for each of the flight conditions in figures 13, 15, and 17.

A theoretical turbulence spectrum, shown in figures 12, 14, and 16, was fitted to the turbulence spectrum measured in flight. The theoretical spectrum represents a von Kármán turbulence model with a -5/3 slope having a σ_1 value equal to the σ_1

value obtained from flight measurements. The fitted theoretical spectrum was used to compute a set of spectrum frequency response transfer functions, $|H_f|_s$, to compare with the cross-spectrum frequency response transfer functions. The transfer functions are compared for the normal acceleration at the center of gravity in figures 13(c), 15(c), and 17(c).

A third set of frequency-response transfer functions was obtained from the theoretical study of reference 23. Flight conditions considered for this study are listed in table 4. It should be emphasized that the theoretical data represent the expected flight conditions, and the structural response modes were predicted by using early estimates of the XB-70 mass, structural, and aerodynamic characteristics. No attempt was made during the flight tests to obtain identical conditions.

In comparing the frequency response transfer functions obtained from flight tests with those of the theoretical study, the following factors should be considered. Ideally, if long-time data samples can be collected and the random input process is assumed to be stationary, small statistical uncertainty and high spectral resolution can be obtained by using a narrow bandwidth filter. This small statistical uncertainty and high spectral resolution can be seen by examining the standard error, ϵ, associated with a measured spectrum estimate, that is,

$$\epsilon \approx \frac{1}{\sqrt{B_e T_r}}$$

However, in the XB-70 flight vibration measurements, the short-time data samples and lack of stationarity precluded high spectral resolution because of the contradiction between bandwidth requirements and data sample time for the standard error. In view of these considerations and those discussed previously in regard to power spectra calculations, XB-70 flight data and theory should be compared only in relation to the frequency at which peaks occur and the relative magnitude of the peaks. In general, the frequencies at which peaks occur in the flight data and the theoretical calculations are approximately the same at the center-of-gravity, wing-tip, and mixer-bay locations for the supersonic conditions considered. Discrepancies may be caused by differences between the airplane configuration used in flight and that used in the theoretical analysis. For example, the wing tips for the subsonic turbulence encounter were folded to 25° during flight and were considered to be at 0° for analysis. Another consideration would be a difference between the structural model used in the analysis and the actual structure.

Comparison of the transfer functions in figures 13(c), 15(c), and 17(c), which were obtained by using the cross-spectrum and power-spectrum techniques (in which the measured turbulence spectrum and fitted theoretical spectrum were used, respectively), shows good agreement up to 4.5 cps between the relative amplitudes of the peaks and the frequencies at which the peaks occur. From 4.5 cps to 10.0 cps the relative amplitude of the frequency response transfer functions between the two methods differs with the intensity of the turbulence encounter. This difference is attributed to components of fuselage response that could not be removed from the turbulence data which, in turn, affected the results of the cross-spectrum data.

Coherence function. – A criterion commonly used to evaluate response data is the coherence function. If the measured gust velocity and the measured acceleration response at various locations on the airplane are linearly related, the coherence function would be equal to unity. If the input signal (gust velocity) and output signal (acceleration response) are completely unrelated, the coherence function would be zero. For coherence functions greater than zero but less than unity, one or more of three possible situations exists: extraneous noise is present in the measurements; the system relating to the input and output signal is not linear; the output is due to other input sources in addition to turbulence. The coherence functions obtained in this study (figs. 13, 15, and 17) generally show values between zero and unity, indicating the presence of one or more of these factors in the data.

The influence of extraneous noise is illustrated in figure 18, in which the coherence functions are compared for flights A and D for the normal acceleration at the center of gravity. These two flights represent a high and a low turbulence intensity for the three flight conditions presented. The comparison indicates that the high intensity turbulence encounter resulted in data with a coherence function closer to unity than those from the low intensity encounter, because a stronger turbulence intensity placed the signal input farther from the noise level. The sources of noise at the input are not known explicitly.

Nonlinear effects may be present. For example, real elastic structures such as aircraft panels can demonstrate characteristics of a nonlinear spring. Structures may also exhibit hysteresis damping, with the damping resulting from internal friction. These phenomena could be expected to affect the results.

It is also possible that other inputs to the airplane, such as control inputs and engine and inlet fluctuations, affect the results. The control inputs were recorded and examined, and only those turbulence encounters during which minimum control inputs were used were considered. Because the data sampling rates for the control parameters and turbulence parameters differed, cross-spectra techniques could not be used for analysis. In turbulence, thrust fluctuations and rpm variations were not detected in these data. Data analysis showed that engine thrust fluctuations within 3 percent to 4 percent of total thrust were detectable.

CONCLUDING REMARKS

An investigation was made with the XB-70 airplane to obtain information on the turbulence environment above an altitude of 12,192 meters (40,000 feet), to measure the true gust velocities encountered, and to determine the resulting responses of a large, flexible, supersonic cruise vehicle. Of 129 flights, 79 flights covered 150,680 kilometers (93,628 miles) at supersonic speeds above an altitude of 12,192 meters (40,000 feet). In these flights, turbulence was encountered for 6.2 percent of the total flight distance, or 9333 kilometers (5799 miles). The resultant data showed that the probability of encountering turbulence equal to or greater than 254.3 kilometers (158 miles) in length was approximately 1 percent.

The turbulence intensities measured on 22 flights for which the airplane was instrumented to measure true gust velocities were very low in comparison with those

from other investigations made at high altitudes. The primary reason for this difference was that turbulence was avoided in the XB-70 flight tests, whereas it was deliberately sought in the other investigations. In general, the slopes of the vertical turbulence spectra varied from -1.5 to -1.0, and those of the lateral turbulence spectra varied from -1.6 to -1.2.

Power spectral density estimates of the normal and lateral acceleration response to turbulence at various locations on the airplane showed that the response of the structural modes contributed appreciably to the total response, particularly at the pilot station.

Results from acceleration response spectra data which were used to identify the structural modes showed good agreement with analytical predictions when updated XB-70 weight and weight distribution data combined with ground vibration tests were used.

The normal and lateral acceleration response at the pilot station showed major responses at 4.0 cps to 5.0 cps and 2.0 cps, respectively. These frequencies corresponded with the natural vertical frequency of the whole human body, seated, and the transverse natural frequencies of the human body, shoulder and head. The resulting ride characteristics in the cockpit during turbulence encounters were marginal.

Frequency response transfer functions obtained from turbulence encounters at Mach numbers of 0.88, 1.59, and 2.35 were compared with theoretical calculations. The calculations were representative of the expected flight conditions, and the structural response modes were predicted by using early estimates of the XB-70 mass, structural, and aerodynamic characteristics. The comparisons show general agreement of the frequencies at which peaks occurred, for supersonic conditions, at the center-of-gravity, wing-tip, and mixer-bay accelerometer positions. Comparison of frequency response transfer functions computed from the measured turbulence spectra and a fitted theoretical spectra showed good agreement in relative amplitudes and frequencies at which peaks occurred from 0 cps to 4.5 cps.

The coherence function showed low correlation between the turbulence input and the resultant response. Results indicated that the intensity of the turbulence may have been too low to obtain high coherence values and that noise or other inputs not known explicitly were probably present in the turbulence measurements.

Flight Research Center,
National Aeronautics and Space Administration,
Edwards, Calif., February 12, 1971.

APPENDIX A

INSTRUMENTATION, DATA ACQUISITION, AND DATA REDUCTION

Instrumentation

The basic measurement problem was that of sensing the disturbance due to turbulence and the resulting aircraft motion. The low inertia flow-direction vanes were used to sense turbulence; however, they also responded to aircraft motion. Position and rate sensing gyros and vertical and lateral accelerometers provided measurements of aircraft motion. By removing the aircraft motion from the low inertia flow-direction-vane measurements, the required turbulence information was obtained.

The low inertia vanes, attached to the nose boom, were mass balanced. The span of each vane was 0.0603 meter (2.375 inches), with a chord of approximately 0.1130 meter (4.75 inches) and a thickness of 0.0032 meter (0.125 inch). The vanes were fabricated by laminating 0.0064-meter- (0.25-inch-) wide strips of lightweight balsa having a density of 96 kilograms/meter^3 (6 pounds/feet^3) to 128 kilograms/meter^3 (8 pounds/feet^3) and bonding with polyester resin. Protective covering to prevent damage to the vanes from aerodynamic heating was not used during the XB-70 flight tests. At the completion of the flight tests, the vanes had withstood sustained supersonic cruise at Mach numbers between 2.50 and 2.55 for periods up to 37 minutes without detectable deterioration.

The nose boom, used to support the flow vanes, was fabricated from PH15-7 MO CRES tubing. The outside diameter was 0.064 meter (2.5 inches), with wall thickness varying from 0.0034 meter (0.134 inch) at the base to 0.00165 meter (0.065 inch) at the tip of the boom. The overall length of the boom from the nose of the airplane was 1.975 meters (77.75 inches). The vertical and lateral vanes were 0.902 meter (35.5 inches) and 1.636 meters (64.41 inches), respectively, aft of the nose-boom tip. The boom-bending frequency for the vertical mode was 12.2 cps and for the lateral mode, 15.0 cps. Corrections to flow-direction vane angles because of boom deflections were applied by computing the slope of the boom at the flow vane. The slopes were computed from strain-gage values at the root of the boom, which had been calibrated for a range of boom deflections.

A prime instrumentation package, positioned 2.614 meters (102.9 inches) aft of the vertical flow vane, contained a vertical gyro, a yaw rate gyro, a vertical accelerometer, and a lateral accelerometer. A secondary package was installed 5.154 meters (202.9 inches) aft of the vertical flow vane to serve as a backup in the event of failure of one of the instruments in the major package. The secondary package contained three rate gyros to measure pitch, roll, and yaw rates.

Data-Acquisition System

Figure 19 is a block diagram of the XB-70 digital data-acquisition system (ref. 24) in which pulse code modulation techniques were used. Basically, a data sensor signal was passed through a signal conditioning network and a passive, low-pass filter

system. This resulted in a conditioned signal of ±20 millivolts, full scale, with a cutoff frequency of 20 cps. (The 20-cps filter characteristics are shown in figure 20.) The data signal was sampled, after filtering, by a subcommutator and master commutator switching system. Then the signal was amplified, converted from analog to digital format, and recorded on magnetic tape.

To assure reliable spectral information, the sample rate for all the turbulence response parameters was selected at twice the frequency cutoff, or 40 samples per second. Other parameters, used for monitoring, were sampled at either 20 samples per second or 4 samples per second.

Additional characteristics of the data-acquisition system were as follows:

Recording resolution	1/1024, 10 bits, analog input
Sample rate -	
Turbulence response data	40 samples per second
Basic airplane data	20 and 4 samples per second
Recording accuracy	±0.4 percent, full scale (analog input)
Frequency response -	
Turbulence response data	0 to 20 cps
Basic airplane data	0 to 4 cps
Time code, period/resolution	24 hours per 0.01 second
Recording time	90 minutes per flight
Recording sequence	Continuous record, interval long, interval short
Input signal level	±20 millivolts = ±460 counts

Data Processing

Figure 21 is a block diagram of the data-processing procedure used to convert the airborne digital recorded data, through a series of computer programs, to provide turbulence and aircraft response data. The first operation performed on the flight data through the PCM data system ground station (ref. 25) resulted in a quick-look data printout. The quick-look data had calibrations applied to selected parameters of the flight data, enabling the initial time editing of the data tape. After initial times were selected, the flight data were retrieved from the airborne magnetic tape by selecting channels, converting data to computer-compatible format, applying calibrations, converting to engineering units, and recording converted data on computer magnetic tape. The computer magnetic tape was then processed through a basic data program, resulting in data plots and the tabulation of turbulence response parameters. Final editing of the flight data was done by examining the basic data parameters, as well as the NASA VGH recorder. After the final start-stop times were selected, the flight data were processed to determine values of true gust velocities followed by the spectral and statistical analysis of the true gust velocities and aircraft response parameters.

APPENDIX B

RESOLUTION OF GUST VELOCITY DATA

To assure minimum separation of parameters in time during digital data sampling, the parameters were arranged in sequence according to their use in equations (1) and (2). For the vertical component of true gust velocity,

$$w_g = V\alpha - V\theta + \int a_n dt + l_x\dot{\theta} \tag{1}$$

For the lateral component of true gust velocity,

$$v_g = -V\beta - V\psi + l_x\dot{\psi} + \int (a_y + g\varphi)dt + l_z\dot{\varphi} \tag{2}$$

The sequentially arranged parameters in each equation were then assigned a position on the subcommutator and master commutator switching network of the data-acquisition system. The assigned positions assured that, within the equation, each parameter was sampled at 40 times per second. Each time each equation group was sampled, the spacing between each of the parameters was 0.05 millisecond.

Noise and long-term drift characteristics of the instrumentation were checked by recording the spurious signals from the gust velocity parameters with the aircraft on the ground. In effect, this resulted in a zero input. The spurious gust velocity was then computed by using the recorded noise of the turbulence parameters and substituting a true airspeed component to match the desired flight condition. From the computed gust velocity data, a noise spectrum was computed and compared with a theoretical spectrum of 0.30 meter/second (1 foot/second) representing a minimum signal. By dividing the power spectral density of the theoretical spectrum by similar values from the noise spectrum, an estimate of the instrumentation signal-to-noise ratio was obtained. The signal-to-noise ratio was defined as

$$N(f) = \frac{\Phi w_g(f)}{\Phi_{n(f)}}$$

where $N(f)$ is the signal-to-noise ratio, $\Phi w_g(f)$ is the theoretical spectrum, and $\Phi n(f)$ is the noise spectrum. Figure 22 presents the estimated signal-to-noise-ratio spectra for turbulence encounters at velocities equal to 274.32 meters/second (900 feet/second) and 695.86 meters/second (2283 feet/second). The two velocities bracket the turbulence penetration velocities encountered during the flight tests. The figure shows that the vertical gust velocity has a minimum level of signal-to-noise ratio of approximately 10 or greater on a power basis for the subsonic data. The minimum level for the high Mach number data decreases to 1 or greater, indicating the decrease in signal quality at high speeds.

APPENDIX C

POWER SPECTRAL ANALYSIS

The computation of the power spectra was programed for digital computer application in a manner similar to that used in reference 13. Details of the procedure are discussed in this appendix. The following notation is used:

$A(r), B(r)$	even and odd parts of cross-correlation function at lag, r, $A(r) = A_{xy}(rh)$, $B(r) = B_{xy}(rh)$
B_e	equivalent resolution bandwidth for power spectra
$C_{xy}(f)$	cospectrum, real part of $\bar{\phi}_{xy}(f)$ at frequency, f, $C_{xy}(k)$
f	frequency, cycles per second
f_c	Nyquist frequency, $\frac{1}{2h}$, cycles per second
$\left\|H(f)\right\|_c$	frequency response transfer function determined from cross-spectra relations
$\left\|H(f)\right\|_s$	frequency response transfer function determined from power spectral relations
h	time between data samples, seconds
j	complex number
k	harmonic number, $\frac{fm}{f_c}$
m	maximum lag number
N	number of discrete data samples
$Q_{xy}(f)$	quadrative spectrum, imaginary part of $\bar{\phi}_{xy}(f)$ at frequency, f, $Q_{xy}(k)$
$R_x(r)$	autocorrelation function of time series x at lag, r
$R_{xy}(r)$	cross-correlation function of time series x and y at lag, r, $R_{xy}(rh)$
r	lag number

APPENDIX C

x_n	n^{th} value of time series x for data sample transferred to deviation from zero mean
y_n	n^{th} value of time series y for data sample transferred to deviation from zero mean
$\gamma^2_{xy}(f)$	coherence function of time series x and y at frequency, f
$\measuredangle_{xy}(f)$	phase angle, radians
μ_n	n^{th} value of discrete, equispaced time series $\mu(t)$
$\bar{\Phi}_x(f)$, $\bar{\Phi}_y(f)$	power spectral density function of time series x or y at frequency, f
$\bar{\Phi}_{xy}(f)$	cross-spectral density function of time series x and y at frequency, f
$\overline{\quad}$	over a value represents the mean value for the time record
$\hat{}$	over a value denotes an estimate of the true value

Determination of Power Spectra and Cross Spectra by Digital Method

The mean of the data was first calculated and subtracted from each sample value to transform the data to a zero mean,

$$\bar{\mu} = \frac{1}{N}\sum_{n=1}^{N}\mu_n \tag{C1}$$

which defined a new data value,

$$x_n = \mu_n - \bar{\mu} \qquad n = 1, 2, \ldots N \tag{C2}$$

This would not have been done if the series were to be detrended. When a linear trend was present, the trend was removed by subtracting from each sample the corresponding time points along the least squares linear fit of the data. The data could then be prewhitened by performing the following transformation (only turbulence spectra with $B_e = 1.0$ were prewhitened):

$$x_n = x_n - x_{n-1} \qquad n = 1, 2, \ldots N - 1 \tag{C3}$$

However, because of the effects of prewhitening, the resulting spectrum had to be compensated for by postdarkening.

The autocorrelation is then computed as

$$\hat{R}_x(r) = \frac{1}{N - r} \sum_{n=1}^{N-r} x_n x_{n+r} \qquad r = 0, 1, 2, \ldots m \tag{C4}$$

The raw estimate of the power spectrum was obtained by using the expression

$$\hat{\bar{\phi}}_x(f) = 2h \left[\hat{R}_x(0) + 2 \sum_{r=1}^{m-1} \hat{R}_x(r) \cos\left(\frac{\pi r k}{m}\right) + (-1)^k \hat{R}_x(m) \right] \qquad k = 1, 2, \ldots m - 1 \tag{C5}$$

The raw estimates of the power spectrum are then smoothed by using the Hanning method,

$$\hat{\bar{\phi}}_x(0) = 0.5\hat{\bar{\phi}}_x(0) + 0.5\hat{\bar{\phi}}_x(1) \tag{C6}$$

$$\hat{\bar{\phi}}_x(k) = 0.25\hat{\bar{\phi}}_x(k - 1) + 0.5\hat{\bar{\phi}}_x(k) + 0.25\hat{\bar{\phi}}_x(k + 1) \qquad k = 1, 2, \ldots m - 1 \tag{C7}$$

$$\hat{\bar{\phi}}_x(m) = 0.5\hat{\bar{\phi}}_x(m - 1) + 0.5\hat{\bar{\phi}}_x(m) \tag{C8}$$

To compensate for the prewhitening (optional), the smoothed spectra were recolored by using the expression

$$\bar{\phi}_x(k) = \frac{\hat{\bar{\phi}}_x(k)}{2\left(1 - \cos\frac{\pi k}{m}\right)} \qquad k = 0, 1, 2, \ldots m \tag{C9}$$

The cross-correlation function was computed by using the following relationships:

$$\hat{R}_{xy}(rh) = \frac{1}{N - r} \sum_{n=1}^{N-r} x_n y_{n+r} \tag{C10}$$

and

$$\hat{R}_{yx}(rh) = \frac{1}{N - r} \sum_{n=1}^{N-r} y_n x_{n+r} \qquad r = 0, 1, 2, \ldots m \tag{C11}$$

APPENDIX C

The even and odd parts of the cross-correlation function can be written as

$$\hat{A}(r) \equiv \hat{A}_{xy}(rh) = \frac{1}{2}\left[\hat{R}_{xy}(rh) + \hat{R}_{yx}(rh)\right] \tag{C12}$$

$$\hat{B}(r) \equiv \hat{B}_{xy}(rh) = \frac{1}{2}\left[\hat{R}_{xy}(rh) - \hat{R}_{yx}(rh)\right] \qquad r = 0, 1, 2, \ldots m \tag{C13}$$

The cross-spectral density function was a complex-valued quantity defined by the equation

$$\hat{\bar{\phi}}_{xy}(f) = C_{xy}(f) - jQ_{xy}(f) \tag{C14}$$

where the cospectrum was

$$\hat{C}_{xy}(k) = 2h\left[\hat{A}(0) + 2\sum_{r=1}^{m-1}\hat{A}(r)\cos\left(\frac{\pi rk}{m}\right) + (-1)^k\hat{A}(r)\right] \qquad k = 0, 1, 2, \ldots m \tag{C15}$$

The quadrative spectrum was obtained from the expression

$$\hat{Q}_{xy}(k) = 4h\sum_{r=1}^{m-1}\hat{B}(r)\sin\left(\frac{\pi rk}{m}\right) \qquad k = 0, 1, 2, \ldots m \tag{C16}$$

Both the cospectrum and quadspectrum were smoothed by using the Hanning method before the final estimate was obtained. The amplitude and phase of the cross-spectrum were computed as

$$\left|\hat{\bar{\phi}}_{xy}(f)\right| = \left[C^2_{xy}(f) + Q^2_{xy}(f)\right]^{1/2} \tag{C17}$$

$$\measuredangle_{xy}(f) = \tan^{-1}\left[\frac{Q_{xy}(f)}{C_{xy}(f)}\right] \tag{C18}$$

Frequency Response Functions

The frequency response function, H(f), of a linear system was estimated by using the spectral input-output data,

$$\left|\hat{H}(f)\right|_s = \left(\frac{\hat{\bar{\phi}}_y(f)}{\hat{\bar{\phi}}_x(f)}\right)^{1/2} \tag{C19}$$

The expression was also computed by using the cross-spectra $\bar{\Phi}_{xy}(f)$ as shown in the expression

$$\left| H(f) \right|_C = \left| \frac{\hat{\bar{\Phi}}_{xy}(f)}{\hat{\bar{\Phi}}_x(f)} \right| \tag{C20}$$

Finally, the coherence function was given as

$$\gamma^2_{xy}(f) = \frac{\left| \bar{\Phi}_{xy}(f) \right|^2}{\bar{\Phi}_x(f)\bar{\Phi}_y(f)} \tag{C21}$$

APPENDIX D

XB-70 TURBULENCE ENCOUNTER DATA

Turbulence encounter data are presented in this appendix for flights of the XB-70 airplane over the western United States. A total of 22 flights was flown between May 12, 1967, and February 4, 1969; in nine of these flights turbulence data were obtained at an altitude greater than 12,192 meters (40,000 feet). Figure 23 is a relief map of the XB-70 test area showing the type of terrain covered by the flights. Figures 24(a) to 24(i) are maps of each of the data flights showing the locations at which turbulence was encountered. A solid line represents the flight track for the portion of the flight above 12,192 meters (40,000 feet) altitude. A short line across the flight track denotes turbulence encounters that were less than 8045 meters (5 miles) long; a solid square denotes encounters 8045 meters to 16,090 meters (5 miles to 10 miles) long. For encounters longer than 16,090 meters (10 miles), a thick line along the flight track represents the distance in turbulence. The adjacent numbers provide a cross reference between the encounter locations on the map and the accompanying table. The encounter number, time of day, $(\Delta a_n)_{max}$, length of each turbulence encounter, and altitude are listed in each table.

REFERENCES

1. Houbolt, John C.; Steiner, Roy; and Pratt, Kermit G.: Dynamic Response of Airplanes to Atmospheric Turbulence Including Flight Data on Input and Response. NASA TR R-199, 1964.

2. Coleman, Thomas L.; and Steiner, Roy: Atmospheric Turbulence Measurements Obtained From Airplane Operations at Altitudes Between 20,000 and 75,000 Feet for Several Areas in the Northern Hemisphere. NASA TN D-548, 1960.

3. Crooks, Walter M.; Hoblit, Frederic M.; Prophet, David T.; et al.: Project HICAT - An Investigation of High Altitude Clear Air Turbulence. Tech. Rep. AFFDL-TR-67-123, vols. I, II, and III, Air Force Flight Dynamics Lab., Wright-Patterson Air Force Base, Nov. 1967.

4. Crooks, Walter M.; Hoblit, Frederic M.; Mitchell, Finis A.; et al.: Project HICAT - High Altitude Clear Air Turbulence Measurements and Meteorological Correlations. Tech. Rep. AFFDL-TR-68-127, vols. I and II, Air Force Flight Dynamics Lab., Wright-Patterson Air Force Base, Nov. 1968.

5. Bennett, Floyd V.; and Pratt, Kermit, G.: Calculated Responses of a Large Sweptwing Airplane to Continuous Turbulence With Flight-Test Comparisons. NASA TR R-69, 1960.

6. Coleman, Thomas L.; Press, Harry; and Meadows, May T.: An Evaluation of Effects of Flexibility on Wing Strains in Rough Air for a Large Swept-Wing Airplane by Means of Experimentally Determined Frequency-Response Functions With an Assessment of Random-Process Techniques Employed. NASA TR R-70, 1960.

7. Peloubet, R. P.; and Haller, R. L.: Application of a Power Spectral Gust Design Procedure to Bomber Aircraft. Tech. Rep. AFFDL-TR-66-35, Air Force Flight Dynamics Lab., Wright-Patterson Air Force Base, June 1966.

8. Peloubet, R. P., Jr.; and Haller, R. L.: Parametric Study of B-58 Acceleration Response to Turbulence and Comparisons With Flight Data, August 1967 - August 1968. General Dynamics (NASA CR-66699), 1968.

9. Dempster, John B.; and Bell, Clarence A.: Summary of Flight Load Environmental Data Taken on B-52 Fleet Aircraft. J. Aircraft, vol. 2, no. 5, Sept.-Oct. 1965, pp. 398-406.

10. Kordes, Eldon E.; and Love, Betty J.: Preliminary Evaluation of XB-70 Airplane Encounters With High-Altitude Turbulence. NASA TN D-4209, 1967.

11. Mechtly, E. A.: The International System of Units - Physical Constants and Conversion Factors. NASA SP-7012, 1969.

12. Andrews, William H.: Summary of Preliminary Data Derived From the XB-70 Airplanes. NASA TM X-1240, 1966.

13. Bendat, Julius S.; and Piersol, Allan G.: Measurement and Analysis of Random Data. John Wiley & Sons, Inc., c. 1966.

14. Bendat, Julius S.; Enochson, Loren D.; Klein, G. Harold; and Piersol, Allan G.: The Application of Statistics to the Flight Vehicle Vibration Problem. ASD Tech. Rep. 61-123 (DDC No. AD 271 913), Aeronautical Systems Div., Wright-Patterson Air Force Base, Dec. 1961.

15. Wykes, John H.; and Kordes, Eldon E.: Analytical Design and Flight Tests of a Modal Suppression System on the XB-70 Airplane. Part 1: Design Analysis. Part 2: Flight Tests. Aeroelastic Effects From a Flight Mechanics Standpoint, AGARD Conf. Proc. No. 46, March 1970, pp. 23-1 - 23-18.

16. Forlifer, W. R.: The Effects of Filter Bandwidth in Spectrum Analysis of Random Vibration. Shock, Vibration and Associated Environments, Bulletin No. 33, Part II, Depart. of Defense, Feb. 1964, pp. 273-278.

17. Ehernberger, L. J.: Atmospheric Conditions Associated With Turbulence Encountered by the XB-70 Airplane Above 40,000 Feet Altitude. NASA TN D-4768, 1968.

18. Rhyne, Richard H.; and Steiner, Roy: Power Spectral Measurement of Atmospheric Turbulence in Severe Storms and Cumulus Clouds. NASA TN D-2469, 1964.

19. Wykes, John H.; Nardi, Louis U.; and Mori, Alva S.: XB-70 Structural Mode Control System Design and Performance Analyses. North American Rockwell Corp. (NASA CR-1557), 1970.

20. Runyan, Harry L.: Structural Dynamic Research Related to Manned Space Flight. AIAA/ASME Structures and Materials Conference, 7th, Cocoa Beach, Fla., April 18-20, 1966, pp. 328-336.

21. Irwin, Kirk, S.; and Andrews, William H.: Summary of XB-70 Airplane Cockpit Environmental Data. NASA TN D-5449, 1969.

22. Berry, Donald T.; and Powers, Bruce G.: Handling Qualities of the XB-70 Airplane in the Landing Approach. NASA TN D-5676, 1970.

23. Stenton, Thomas E.: Theoretical Frequency Response Functions and Power Spectra of the XB-70 Response to Atmospheric Turbulence. North American Rockwell Corp. (NASA CR-1621), 1970.

24. Ince, D. B.: Application Experience With the B-70 Flight Test Data System. Aerospace Instrumentation. Vol. 4 - Proceedings of the Fourth International Aerospace Symposium, College of Aeronautics, Cranfield, Eng., March 21-24, 1966, M. A. Perry, ed., Pergamon Press, Ltd., 1967, pp. 195-208.

25. Edwards, E. L.: A Data Processing Facility for the XB-70 Flight Test Program. Flight Test Instrumentation, AGARD Conf. Proc. No. 32, 1967, pp. 243-258.

TABLE 1. GEOMETRIC CHARACTERISTICS OF THE XB-70 AIRPLANE

Total wing -	
Total area (includes 230.62 m^2 (2482.34 ft^2) covered by fuselage but not 3.12 m^2 (33.53 ft^2) of the wing ramp area), m^2 (ft^2)	585.07 (6297.8)
Span, m (ft)	32 (105)
Aspect ratio	1.751
Taper ratio	0.019
Dihedral angle, deg:	
XB-70-1	0
XB-70-2	5
Root chord (wing station 0), m (ft)	35.89 (117.76)
Tip chord (wing station 16 m (630 in.)), m (ft)	0.67 (2.19)
Mean aerodynamic chord (wing station 5.43 m (213.85 in.)), m (in.)	23.94 (942.38)
Fuselage station of 25-percent wing mean aerodynamic chord, m (in.)	41.18 (1621.22)
Sweepback angle, deg:	
Leading edge	65.57
25-percent element	58.79
Trailing edge	0
Incidence angle, deg:	
Root (fuselage juncture)	0
Tip (fold line and outboard)	-2.60
Airfoil section:	
Root to wing station 4.72 m (186 in.) (thickness-chord ratio, 2 percent)	0.30 to 0.70 HEX (MOD)
Wing station 11.68 m (460 in.) to 16 m (630 in.)(thickness-chord ratio, 2.5 percent)	0.30 to 0.70 HEX (MOD)
Inboard wing —	
Area (includes 230.62 m^2 (2482.34 ft^2) covered by fuselage but not 3.12 m^2 (33.53 ft^2) wing ramp area), m^2 (ft^2)	488.28 (5256.0)
Span, m (ft)	19.34 (63.44)
Aspect ratio	0.766
Taper ratio	0.407
Dihedral angle, deg:	
XB-70-1	0
XB-70-2	5
Root chord (wing station 0), m (ft)	35.89 (117.76)
Tip chord (wing station 9.67 m (380.62 in.)), m (ft)	14.61 (47.94)
Mean aerodynamic chord (wing station 4.15 m (163.58 in.)), m (in.)	26.75 (1053)
Fuselage station of 25-percent wing mean aerodynamic chord, m (in.)	39.07 (1538.29)
Sweepback angle, deg:	
Leading edge	65.57
25-percent element	58.79
Trailing edge	0
Airfoil section:	
Root (thickness-chord ratio, 2 percent)	0.30 to 0.70 HEX (MOD)
Tip (thickness-chord ratio, 2.4 percent)	0.30 to 0.70 HEX (MOD)
Mean camber (leading edge), deg:	
Butt plane 0	0.15
Butt plane 2.72 m (107 in.)	4.40
Butt plane 3.89 m (153 in.):	
XB-70-1	3.15
XB-70-2	2.75
Butt plane 6.53 m (257 in.):	
XB-70-1	2.33
XB-70-2	2.60
Butt plane 9.32 m (367 in.) to tip	0
Canard —	
Area (includes 13.96 m^2 (150.31 ft^2) covered by fuselage), m^2 (ft^2)	38.61 (415.59)
Span, m (ft)	8.78 (28.81)
Aspect ratio	1.997
Taper ratio	0.388
Dihedral angle, deg	0
Root chord (canard station 0), m (ft)	6.34 (20.79)

TABLE 1. GEOMETRIC CHARACTERISTICS OF THE XB-70 AIRPLANE - Continued

Tip chord (canard station 4.39 (172.86 in.)), m (ft)	2.46 (8.06)
Mean aerodynamic chord (canard station 1.87 m (73.71 in.)), m (in.)	4.68 (184.3)
Fuselage station of 25-percent canard mean aerodynamic chord, m (in.)	14.06 (553.73)
Sweepback angle, deg:	
Leading edge	31.70
25-percent element	21.64
Trailing edge	-14.91
Incidence angle (nose up), deg	0 to 6
Airfoil section:	
Root (thickness-chord ratio, 2.5 percent)	0.34 to 0.66 HEX (MOD)
Tip (thickness-chord ratio, 2.52 percent)	0.34 to 0.66 HEX (MOD)
Ratio of canard area to wing area	0.066
Canard flap (one of two):	
Area (aft of hinge line), m^2 (ft^2)	5.08 (54.69)
Ratio of flap area to canard semi-area	0.263
Vertical tail (one of two) —	
Area (includes 0.83 m^2 (8.96 ft^2) blanketed area), m^2 (ft^2)	21.74 (233.96)
Span, m (ft)	4.57 (15)
Aspect ratio	1
Taper ratio	0.30
Root chord (vertical-tail station 0), m (ft)	7.03 (23.08)
Tip chord (vertical-tail station 4.57 m (180 in.)), m (ft)	2.11 (6.92)
Mean aerodynamic chord (vertical-tail station 1.88 m (73.85 in.)), m (in.)	5.01 (197.40)
Fuselage station of 25-percent vertical-tail mean aerodynamic chord, m (in.)	55.59 (2188.50)
Sweepback angle, deg:	
Leading edge	51.77
25-percent element	45
Trailing edge	10.89
Airfoil section:	
Root (thickness-chord ratio, 3.75 percent)	0.30 to 0.70 HEX (MOD)
Tip (thickness-chord ratio, 2.5 percent)	0.30 to 0.70 HEX (MOD)
Cant angle, deg	0
Ratio vertical tail to wing area	0.037
Rudder travel, deg:	
With gear extended	±12
With gear retracted	±3
Outboard wing —	
Area (one side only), m^2 (ft^2)	48.39 (520.90)
Span (one side only), m (ft)	6.33 (20.78)
Aspect ratio	0.829
Taper ratio	0.046
Dihedral angle, deg:	
XB-70-1	0
XB-70-2	5
Root chord (wing station 9.67 m (380.62 in.)), m (ft)	14.61 (47.94)
Tip chord (wing station 16.00 m (630 in.)), m (ft)	0.67 (2.19)
Mean aerodynamic chord (wing station 11.87 m (467.37 in.)), m (in.)	9.76 (384.25)
Sweepback angle, deg:	
Leading edge	65.57
25-percent element	58.79
Trailing edge	0
Airfoil section:	
Root (thickness-chord ratio, 2.4 percent)	0.30 to 0.70 HEX (MOD)
Tip (thickness-chord ratio, 2.5 percent)	0.30 to 0.70 HEX (MOD)
Down deflection from wing reference plane, deg:	
XB-70-1	0, 25, 65
XB-70-2	0, 30, 70
Skewline of tip fold, deg:	
Leading edge in	1.5
Leading edge down	3

TABLE 1. GEOMETRIC CHARACTERISTICS OF THE XB-70 AIRPLANE - Concluded

Wing-tip area in wing reference plane (one side only), m^2 (ft^2):			
	XB-70-1	XB-70-2	
Rotated down	25°	30°	43.85 (472.04)
Rotated down	65°	70°	20.44 (220.01)

	Wing tips	
	Up	Down
Elevons (data for one side):		
Total area aft of hinge line, m^2 (ft^2)	18.37 (197.7)	12.57 (135.26)
Span, m (ft)	6.23 (20.44)	4.26 (13.98)
Inboard chord (equivalent), m (in.)	2.95 (116)	2.95 (116)
Outboard chord (equivalent), m (in.)	2.95 (116)	2.95 (116)
Sweepback angle of hinge line, deg	0	0
Deflection, deg:		
As elevator		-25 to 15
As aileron with elevators at ±15° or less		-15 to 15
As aileron with elevators at -25°		-5 to 5
Total		-30 to 30
Fuselage (includes canopy) —		
Length, m (ft)		56.62 (185.75)
Maximum depth (fuselage station 22.30 m (878 in.)), m (in.)		2.72 (106.92)
Maximum breadth (fuselage station 21.72 m (855 in.)), m (in.)		2.54 (100)
Side area, m^2 (ft^2)		87.30 (939.72)
Planform area, m^2 (ft^2)		110.07 (1184.78)
Center of gravity:		
Forward limit, percent mean aerodynamic chord		19.0
Aft limit, percent mean aerodynamic chord		25.0
Duct —		
Length, m (ft)		31.96 (104.84)
Maximum depth (fuselage station 34.93 m (1375 in.)), m (in.)		2.31 (90.75)
Maximum breadth (fuselage station 53.34 m (2100 in.)), m (in.)		9.16 (360.70)
Side area, m^2 (ft^2)		66.58 (716.66)
Planform area, m^2 (ft^2)		217.61 (2342.33)
Inlet captive area (each), m^2 ($in.^2$)		3.61 (5600)
Surface areas (net wetted), m^2 (ft^2) —		
Fuselage and canopy		266.75 (2871.24)
Duct		460.49 (4956.66)
Wing, wing tips, and wing ramp		711.49 (7658.44)
Vertical tails (two)		87.02 (936.64)
Canard		49.32 (530.83)
Tail pipes		31.62 (340.45)
Total		1606.69 (17,294.26)
Engines		Six YJ93-GE-3

TABLE 2. – XB-70 INSTRUMENTATION CHARACTERISTICS

Parameter	Transducer		System resolution	Accuracy, percent full range	Sample rate, sample/second	Location					
	Type	Range				Fuselage station,		Butt plane,		Water plane,	
						meters	inches	meters	inches	meters	inches
Vertical component of true gust velocity –											
Normal acceleration at nose	Accelerometer	±2.84g	±0.0062g	2.0	40	4.947	194.75	-----	----	------	-----
Nose-boom angle of attack (high response)	Angle of attack and sideslip sensor	0° to 8.0°	±.0087°	.8	40	2.308	91.875	0.152	6.0	0.508	20.0
Angle of pitch at airplane nose	Attitude gyro	±4.24°	±.0092°	[a]5.0	40	4.947	194.75	-----	----	------	-----
Rate of pitch at airplane nose	Airplane electrical system	±5.0 deg/sec	±.0109 deg/sec	2.0	40	7.487	294.75	-----	----	------	-----
Nose-boom vertical bending	Bonded strain gage	±153,752,925 N/m^2 (±22,300 psi)	±334,245.5 N/m^2 (±48.48 psi)	2.5	40	3.251	128.00	-----	----	------	-----
Lateral component of true gust velocity –											
Lateral acceleration at airplane nose	Accelerometer	±1.086g	±0.00235g	2.0	40	4.921	193.75	-----	----	------	-----
Nose-boom angle of sideslip (high response)	Angle of attack and sideslip sensor	±4.0°	±.0087°	.8	40	3.069	120.81	0	0	0.330	13.0
Angle of yaw at airplane nose	Attitude gyro	±10.3°	±.0224°	2.0	40	4.947	194.75	-----	----	------	-----
Angle of roll at airplane nose	Attitude gyro	±34.5°	±.0750°	[a]7.0	40	4.947	194.75	-----	----	------	-----
Rate of yaw at airplane nose	Airplane electrical system	±5.0 deg/sec	±.0109 deg/sec	2.0	40	7.487	294.75	-----	----	------	-----
Rate of roll at airplane nose	Airplane electrical system	±5.0 deg/sec	±.0109 deg/sec	2.0	40	7.487	294.75	-----	----	------	-----
Nose-boom lateral bending	Bonded strain gage	153,752,925 N/m^2 22,300 (tension) to 22,300 (compression)	±334,245.5 N/m^2 (±48.48 psi)	2.0	40	3.251	128.00	-----	----	------	-----
Airplane basic data –											
True velocity	Airplane electrical system	66 to 1632 knots	±1.702 knots	[b]±0.1	40	-----	------	-----	----	------	-----
Angle of pitch at center of gravity	Attitude gyro	-10.45° to 35.3°	±.0497°	2.0	40	41.58	1637.0	-----	----	------	-----
Rate of pitch at center of gravity	Rate gyro	±5.33 deg/sec	±.0116 deg/sec	2.0	40	35.54	1399.0	-----	----	------	-----
Rate of yaw at center of gravity	Rate gyro	±5.7 deg/sec	±.0124 deg/sec	2.0	20	35.66	1404.0	0.406	16.0	-1.626	-64.0
Rate of roll at center of gravity	Rate gyro	±21.66 deg/sec	±.047 deg/sec	2.0	20	35.66	1404.0	.406	16.0	-1.626	-64.0
Left-hand elevon position at inboard actuator	Position transmitter	±30.0°	±.0652°	1.2	20	-----	------	-----	----	------	-----
Right-hand elevon position at inboard actuator	Position transmitter	±30.0°	±.0652°	1.2	20	-----	------	-----	----	------	-----
Outside air temperature, total (low range)	Temperature sensing probe	218° K to 433° K (-67° F to 320° F)	±.234° K (±.042° F)	1.2	4	-----	------	-----	----	------	-----
Outside air temperature, total (high range)	Temperature sensing probe	422° K to 650° K (300° F to 711° F)	±.248° K (±.45° F)	1.2	4	-----	------	-----	----	------	-----
Nose-boom total pressure	Absolute pressure transducer	0 to 206,843 N/m^2 (0 to 30 psia)	224.8 N/m^2 (.0326 psia)	.05	20	-----	------	-----	----	------	-----
Nose-boom static pressure	Absolute pressure transducer	0 to 110,316 N/m^2 (0 to 16 psia)	119.9 N/m^2 (.0174 psia)	.05	20	-----	------	-----	----	------	-----
Altitude (coarse)	Airplane subsystem	-304.8 to 30,480 m (-1000 to 100,000 ft)	33.5 m (109.8 ft)	2.0	40	-----	------	-----	----	------	-----
Airspeed (coarse)	Airplane subsystem	50 to 800 knots	.815 knots	2.0	40	-----	------	-----	----	------	-----
Mach number (coarse)	Airplane subsystem	.5 to 3.2 Mach number	.0029 Mach number	2.0	40	-----	------	-----	----	------	-----
Altitude (fine)	Airplane subsystem	1524 m/revolution (5000 ft/revolution)	1.66 m/revolution (5.43 ft/revolution)	2.0	40	-----	------	-----	----	------	-----
Airspeed (fine)	Airplane subsystem	70 knots/revolution	.076 knots/revolution	2.0	40	-----	------	-----	----	------	-----
Mach number (fine)	Airplane subsystem	.3 Mach number/revolution	.00033 Mach number/revolution	2.0	40	-----	------	-----	----	------	-----

TABLE 2. – XB-70 INSTRUMENTATION CHARACTERISTICS - Concluded

Parameter	Transducer		System resolution	Accuracy, percent full range	Sample rate, sample/second	Location					
						Fuselage station,		Butt plane,		Water plane,	
	Type	Range				meters	inches	meters	inches	meters	inches
Vertical airplane response -											
Normal acceleration at pilot station	Accelerometer	±3.0g	±0.0065g	2.0	40	11.125	438.00	0.305	12.0	0.914	36.0
Normal acceleration at center of gravity	Accelerometer	±1.37g	±.00298g	2.0	40	37.72	1485.0	.279	11.0	-1.803	-71.0
Normal acceleration at left-hand wing	Accelerometer	±5.88g	±.01275g	2.0	40	46.23	1820.0	9.53	375.0	------	-----
Normal acceleration at right-hand wing	Accelerometer	±6.40g	±.014g	2.0	40	46.23	1820.0	9.53	375.0	------	-----
Normal acceleration at left-hand wing	Accelerometer	±6.44g	±.014g	2.0	40	55.17	2172.0	9.53	375.0	------	-----
Normal acceleration at right-hand wing	Accelerometer	±6.81g	±.0148g	2.0	40	55.17	2172.0	9.53	375.0	------	-----
Normal acceleration at left-hand wing	Accelerometer	±9.24g	±.021g	2.0	40	55.88	2200.0	13.21	520.0	------	-----
Normal acceleration at mixer bay	Accelerometer	-1.2g to 3.2g	±.0048g	2.0	40	51.70	2035.5	-----	-----	------	-----
Lateral airplane response -											
Lateral acceleration at pilot's station	Accelerometer	±2.04g	±0.0044g	2.0	40	11.176	440.00	-----	-----	------	-----
Lateral acceleration at center of gravity	Accelerometer	±.299g	±.00065g	2.0	40	37.77	1487.0	-----	-----	------	-----
Lateral acceleration at mixer bay	Accelerometer	±.85g	±.00185g	2.0	40	51.70	2035.5	-----	-----	------	-----
VGH recorder -											
Normal acceleration at pilot's station	Accelerometer	-2 to 4g	0.20 percent	1.0	Continuous	11.94	470.00	0	0	-1.89	-74.5
Normal acceleration at center of gravity	Accelerometer	-2 to 4g	.20 percent	1.0	Continuous	37.59	1480.0	.53 right	21 right	0.64	25.0
Altitude	Airplane subsystem	105,337 to 0 N/m^2 (2200 to 0 psf)	.10 percent	1.0	Continuous	-----	------	-----	-----	------	-----
Airspeed	Airplane subsystem	0 to 105,337 N/m^2 (0 to 2200 psf)	.10 percent	1.0	Continuous	-----	------	-----	-----	------	-----

[a] Error minutes of arc.
[b] 0.1 Mach number.

TABLE 3.– DISTRIBUTION OF TOTAL FLIGHT KILOMETERS AND KILOMETERS IN TURBULENCE BY ALTITUDE BANDS OF 1524 METERS (5000 FEET)

Altitude range,		Distance flown –				Percent of distance in turbulence
		At altitude,		In turbulence,		
meters	feet	kilometers	miles	kilometers	miles	
12,192 to 13,716	40,000 to 45,000	21,050	13,080	1323	822	6.3
13,716 to 15,240	45,000 to 50,000	17,257	10,723	1072	666	6.2
15,240 to 16,764	50,000 to 55,000	20,318	12,625	1426	886	7.0
16,764 to 18,288	55,000 to 60,000	39,424	24,497	2559	1590	6.5
18,288 to 19,812	60,000 to 65,000	28,144	17,488	2074	1289	7.4
19,812 to 21,336	65,000 to 70,000	22,597	14,041	824	512	3.6
21,336 to 22,860	70,000 to 75,000	1,889	1,174	55	34	2.9
12,192 to 22,860	40,000 to 75,000	150,680	93,628	9333	5799	6.2

TABLE 4.–XB-70 TURBULENCE ENCOUNTER CONDITIONS FOR FLIGHT TESTS AND THEORETICAL CONDITIONS, INCLUDING DATA REDUCTION CHARACTERISTICS

Flight	True velocity,		Mach number	h_p,		Weight,		Center of gravity, percent mean aerodynamic chord	δ_{t_p}, deg	T_r, sec	Turbulence data						Vertical structural-response data	
											Vertical σ_1,		Lateral σ_1,		B_e	η	B_e	η
	m/sec	ft/sec		m	ft	kg	lb				m/sec	ft/sec	m/sec	ft/sec				
A	460	1508	1.59	11,979	39,300	173,362	382,200	21.05	65	45.4	0.6035	1.9799	0.6827	2.2398	1.0	90.8	0.4	36.3
A*	---	----	1.40	9,144	30,000	204,116	450,000	21.37	65	----	------	------	------	------	---	-----	---	----
B	358	1174	1.19	9,906	32,500	203,435	448,500	21.80	25	32.0	.3086	1.0124	.3340	1.0957	1.0	64.0	.4	25.6
C	696	2283	2.35	17,008	55,800	187,786	414,000	21.75	65	53.5	.3980	1.3058	.4839	1.5877	1.0	107.0	.4	42.8
C*	---	----	2.1	15,240	50,000	190,508	420,000	22.48	65	----	------	------	------	------	---	-----	---	----
D	274	900	.88	6,858	22,500	199,806	440,500	22.05	25	30.5	.2157	.7077	.3511	1.1520	1.0	60.0	.4	24.4
D*	---	----	.80	6,096	20,000	217,723	480,000	21.91	0	----	------	------	------	------	---	-----	---	----
E	608	1994	2.08	14,783	48,500	174,859	385,500	22.15	65	30.0	.1206	.3956	.1620	.5316	1.0	60.0	.4	24.0

*Condition used in theoretical study (ref. 23).

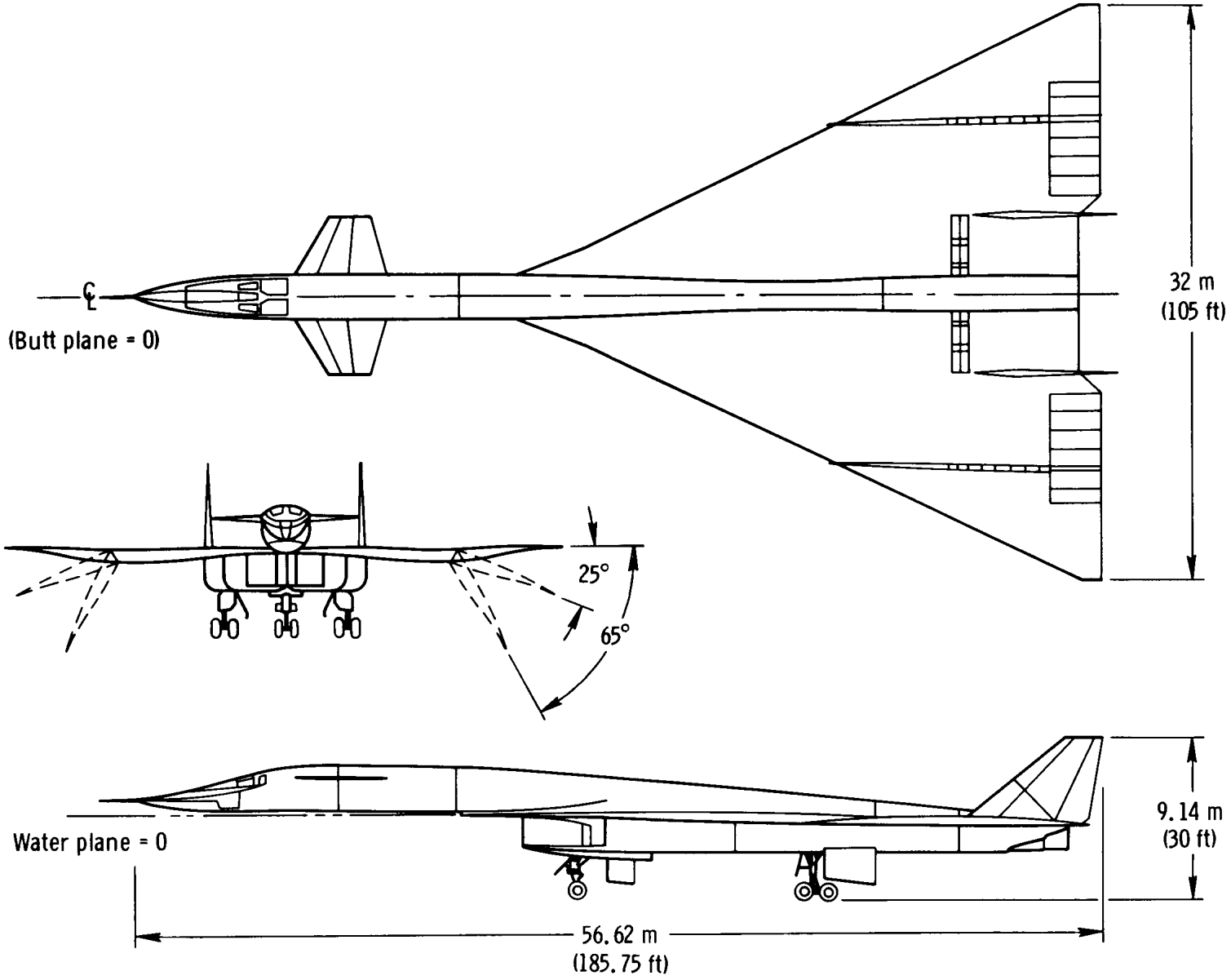

Figure 1. Three-view drawing of XB-70 airplane. Fuselage station 0 located 1.433 meters (56.4 inches) ahead of pitot tube. Dimensions in meters (feet).

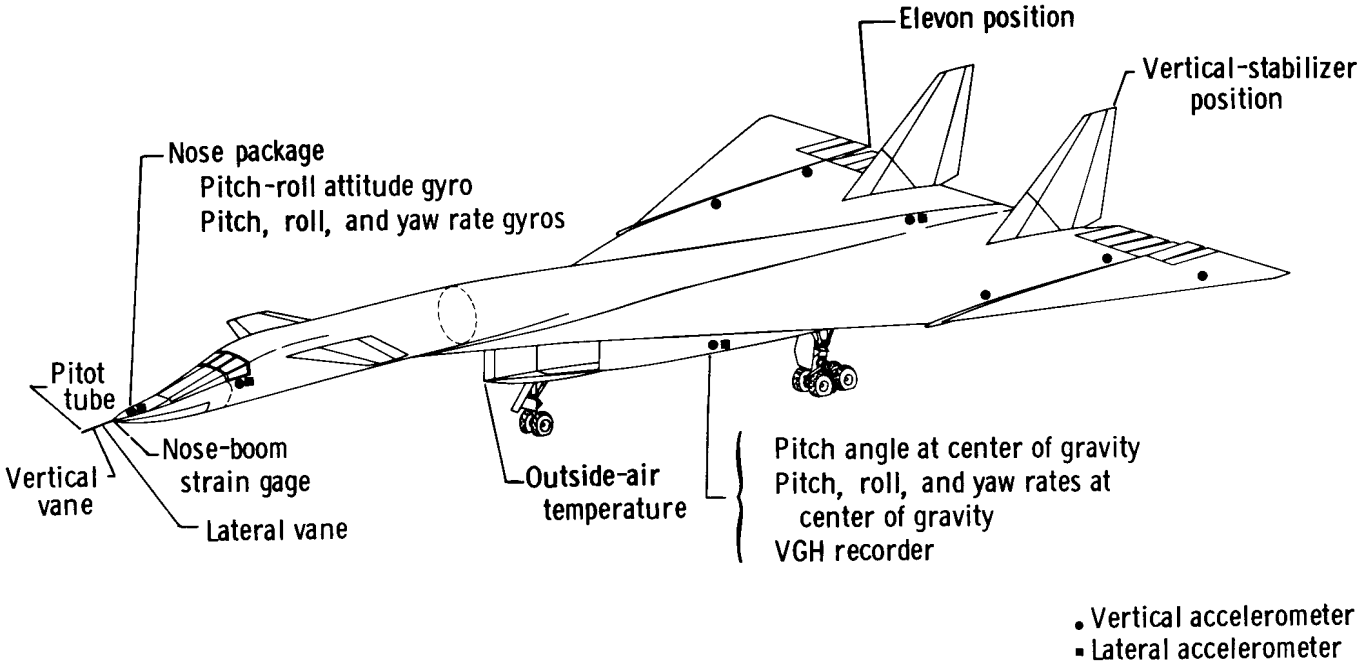

Figure 2. XB-70 instrumentation location.

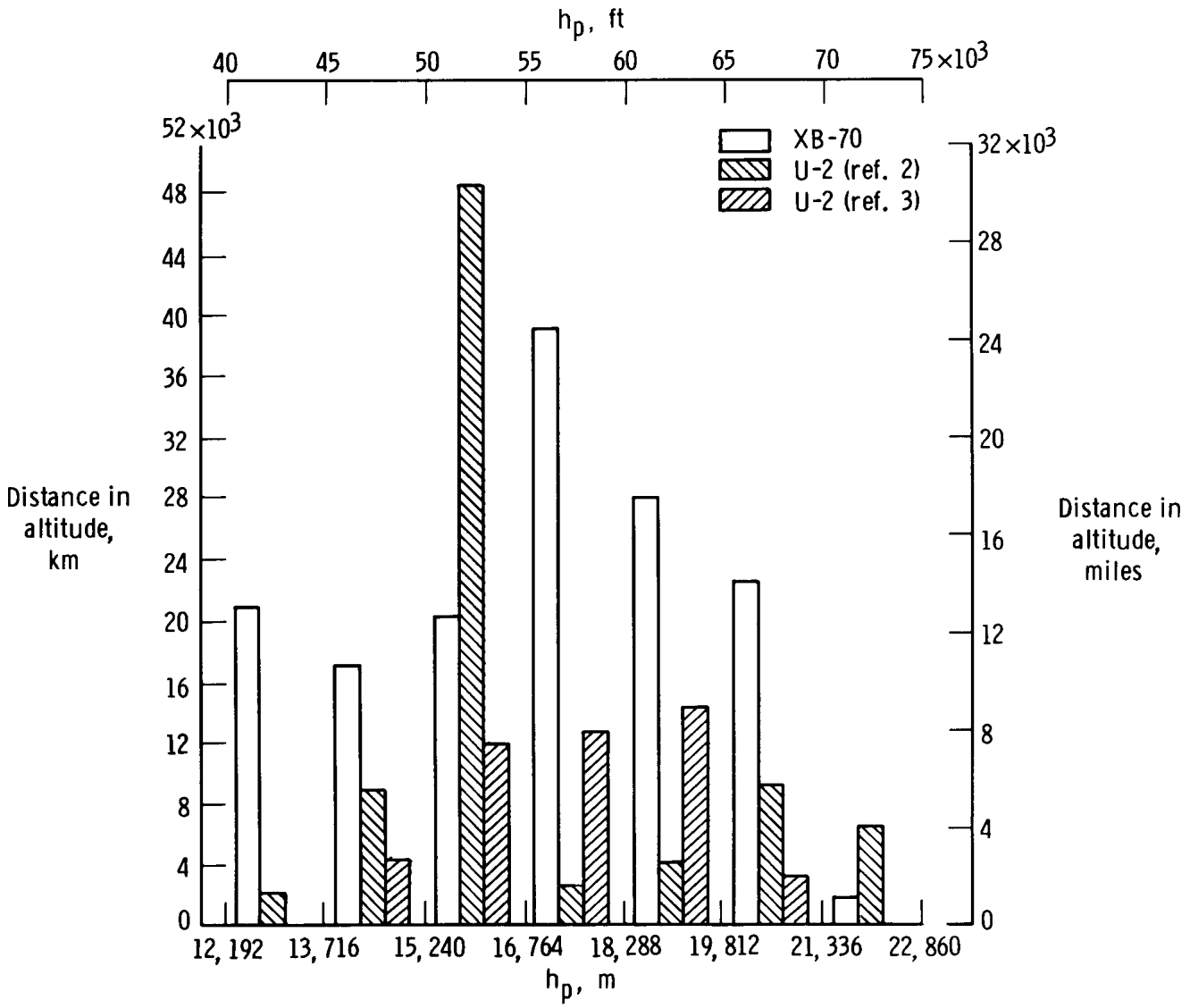

Figure 3. Comparison of distribution of XB-70 flight kilometers (miles) by 1524-meter (5000-foot) altitude bands with results from other turbulence investigations.

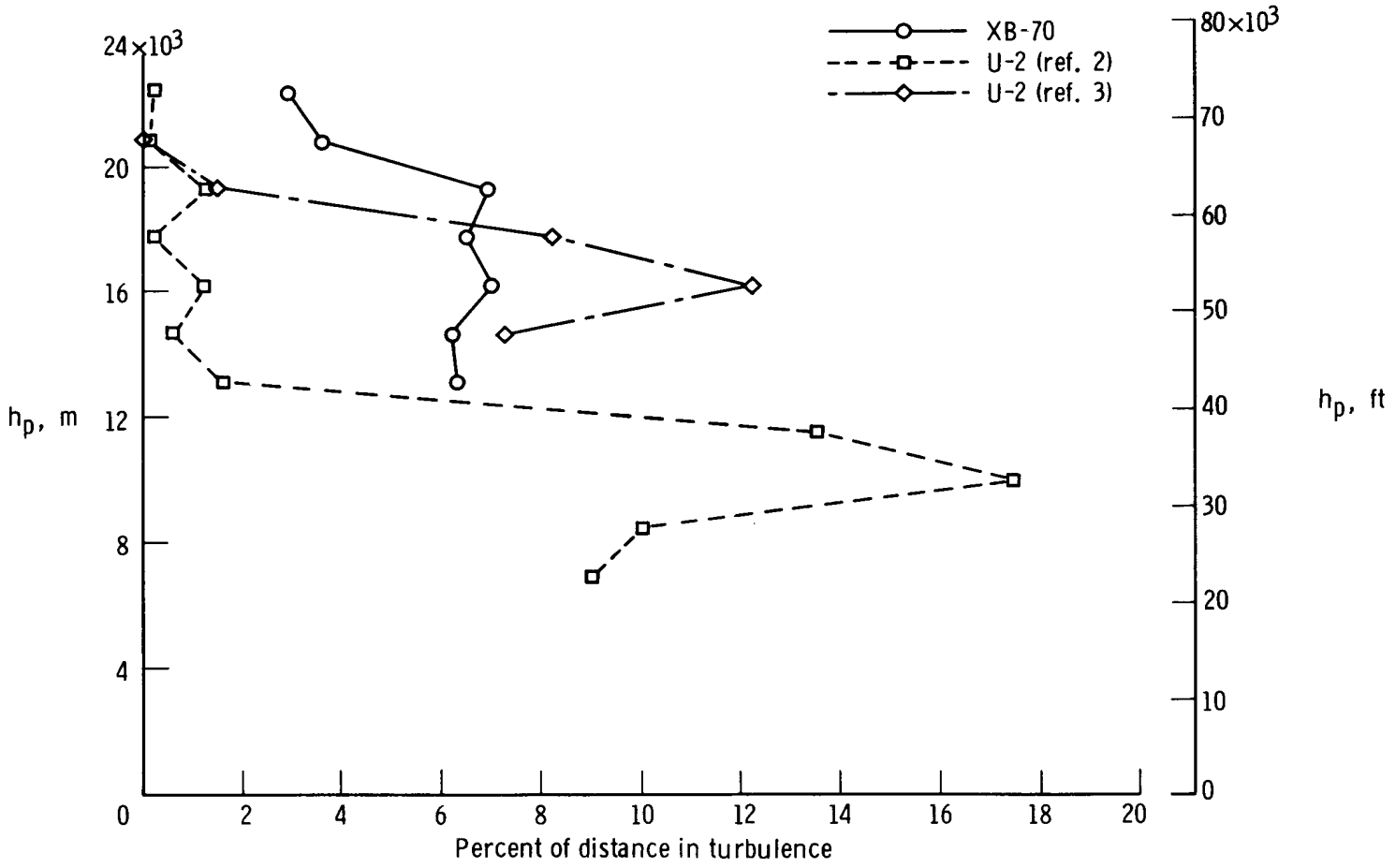

Figure 4. Comparison of variation in percentage of distance flown in turbulence with altitude for the XB-70 study with results from other turbulence investigations.

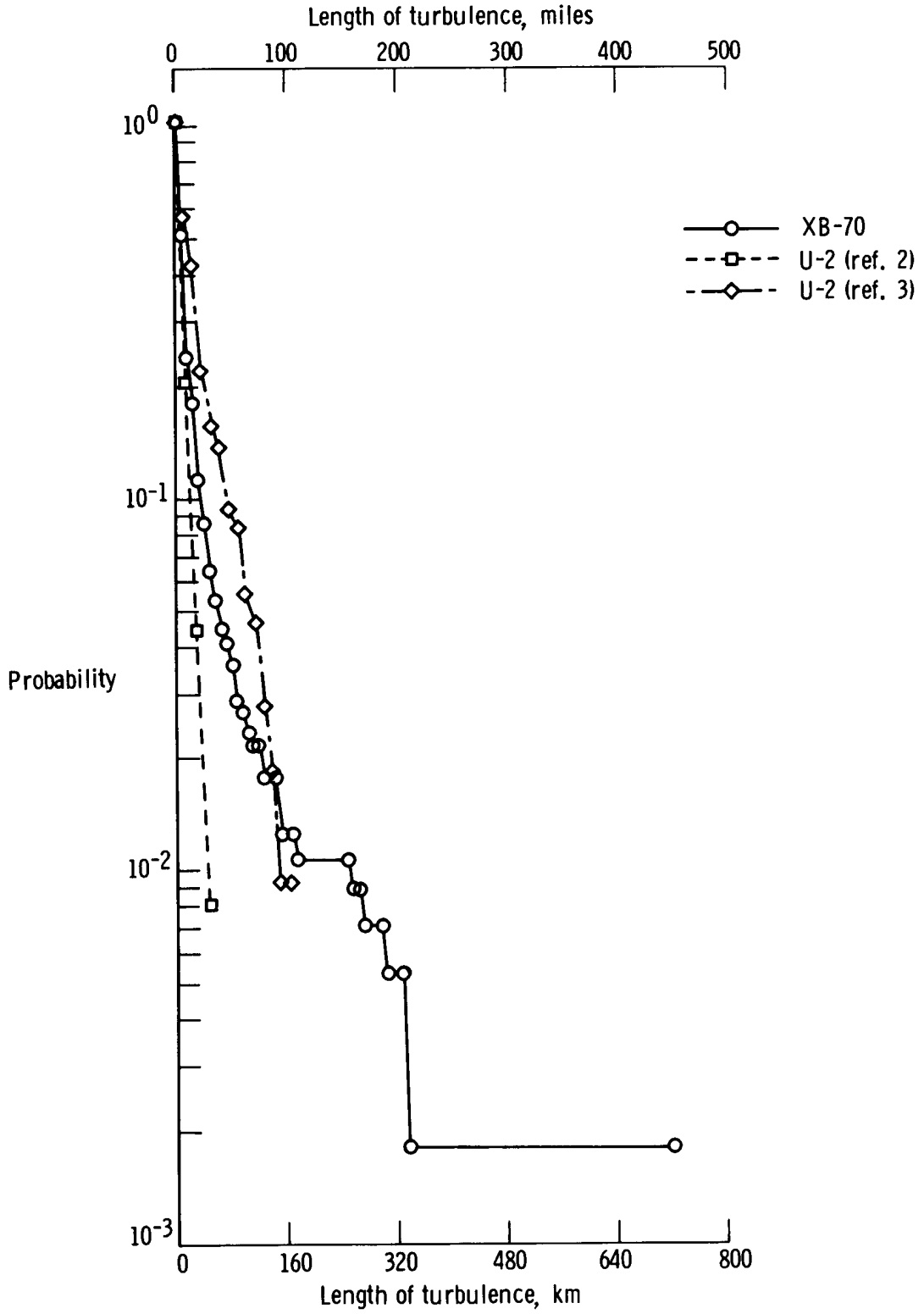

Figure 5. Comparison of the probability that the turbulent area would be equal to or greater than a given length for the XB-70 study with results from other turbulence investigations.

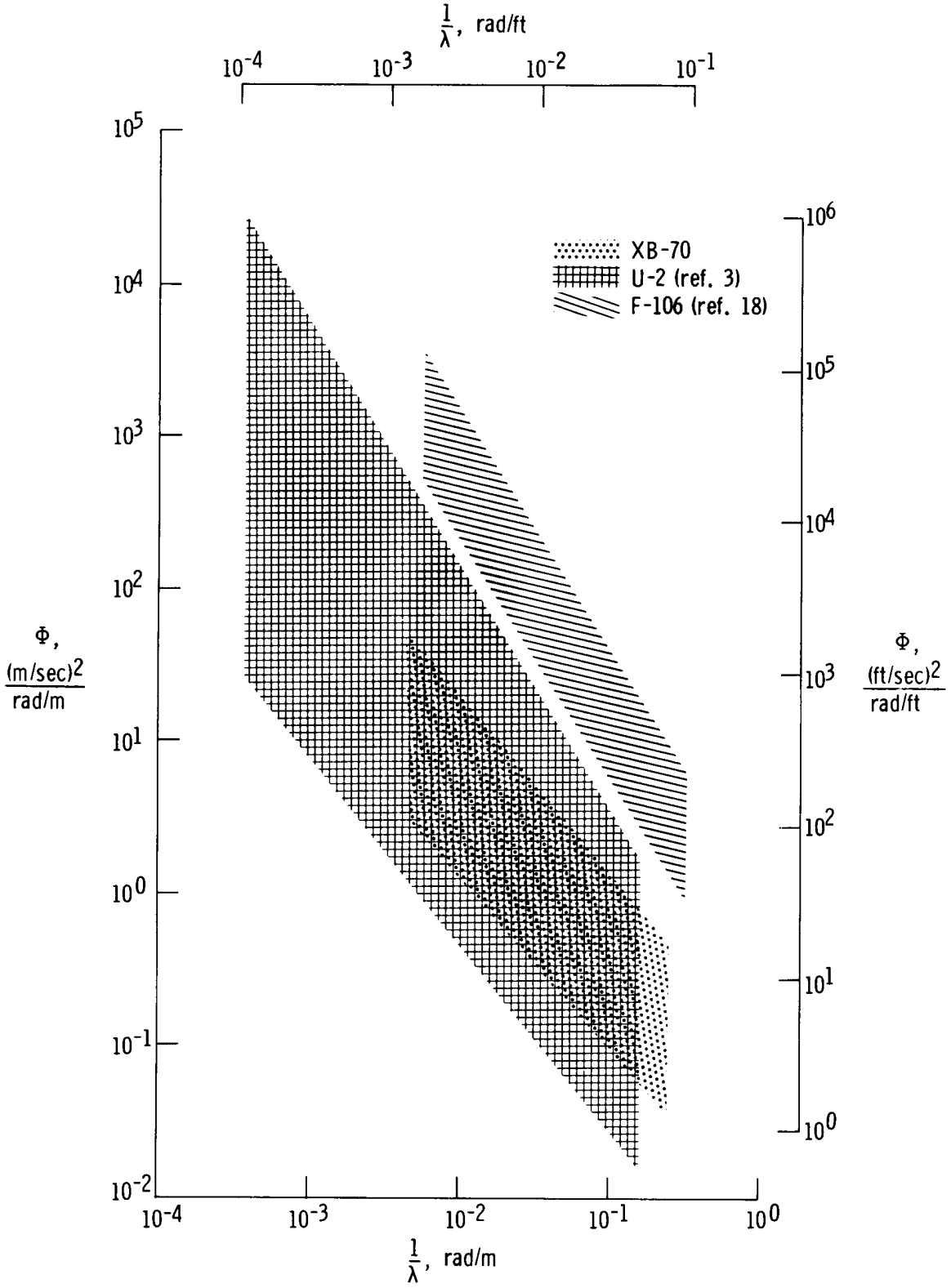

Figure 6. Comparison of gust velocity power spectral envelopes.

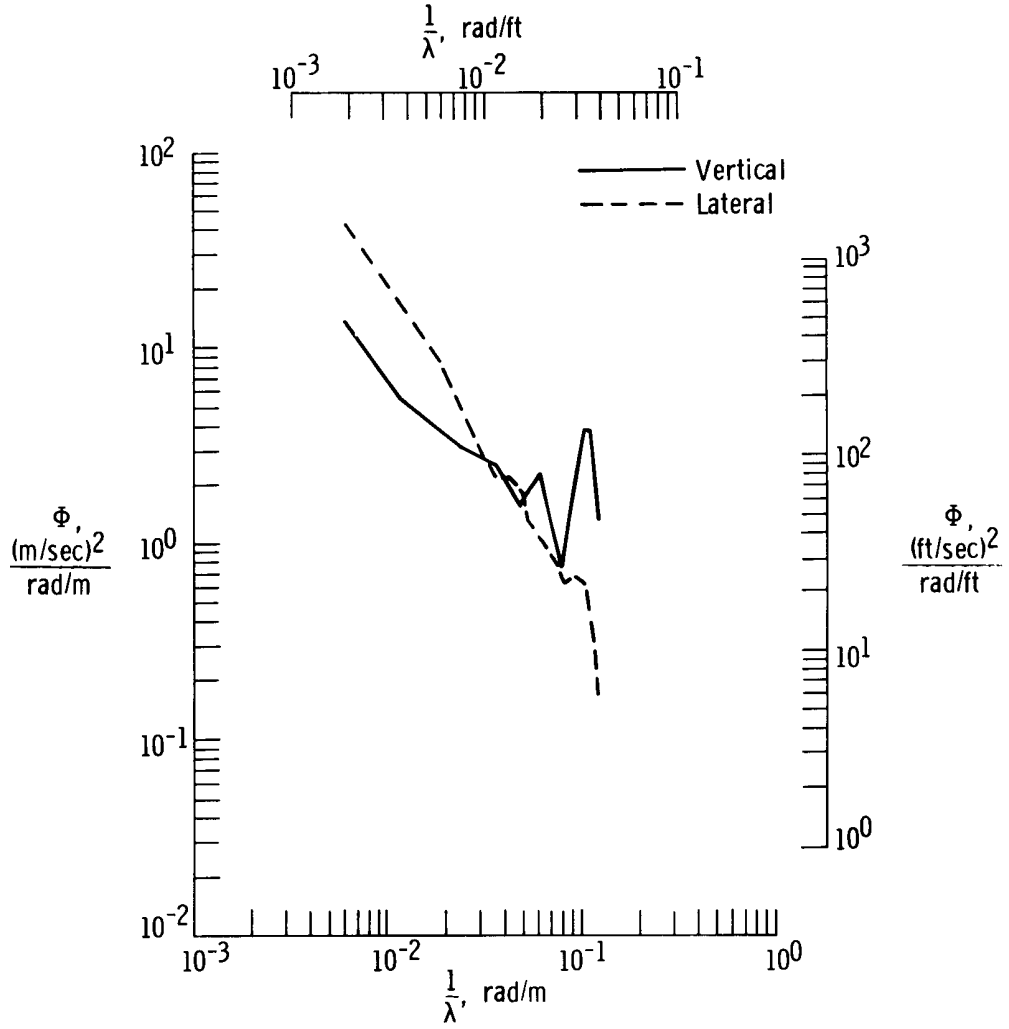

(a) Flight A.

Figure 7. Power spectra of vertical and lateral components of turbulence.

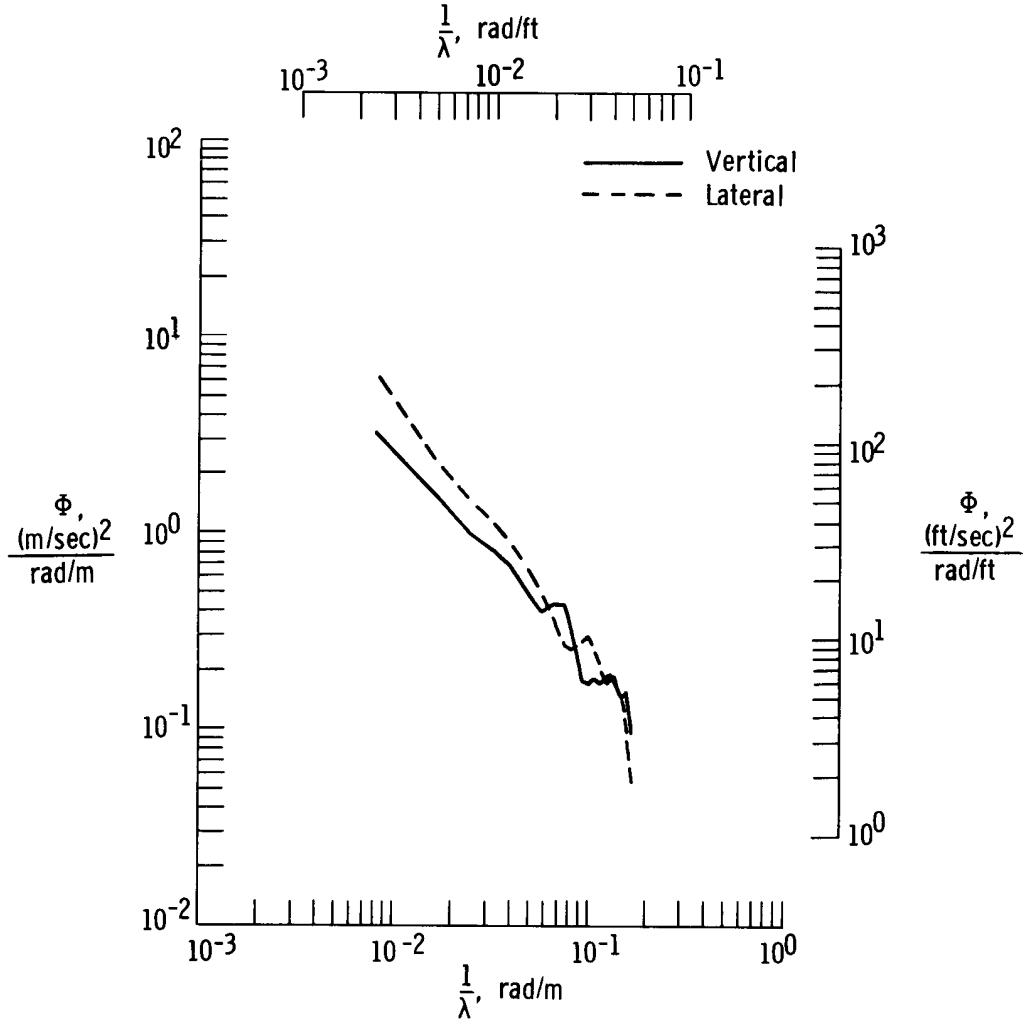

(b) Flight B.

Figure 7. Continued.

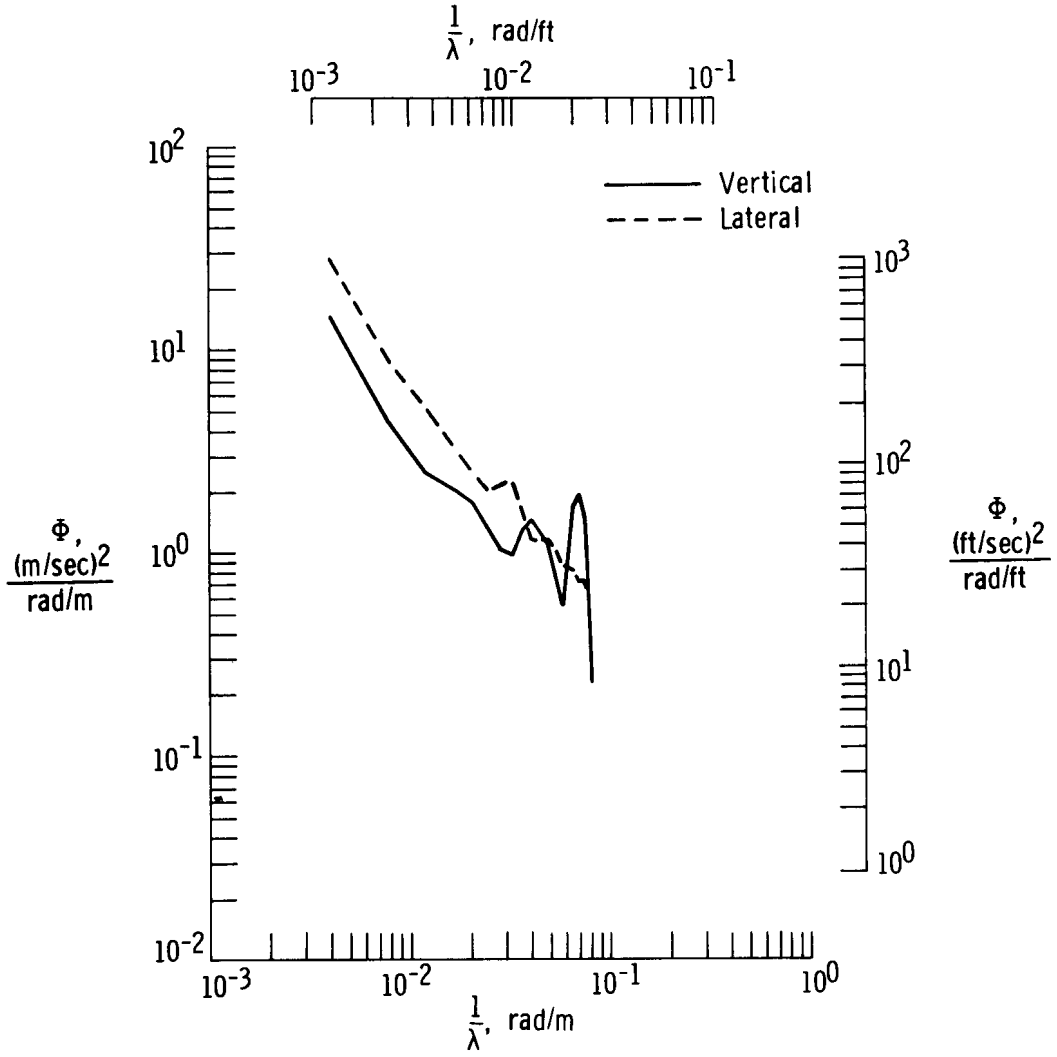

(c) Flight C.

Figure 7. Continued.

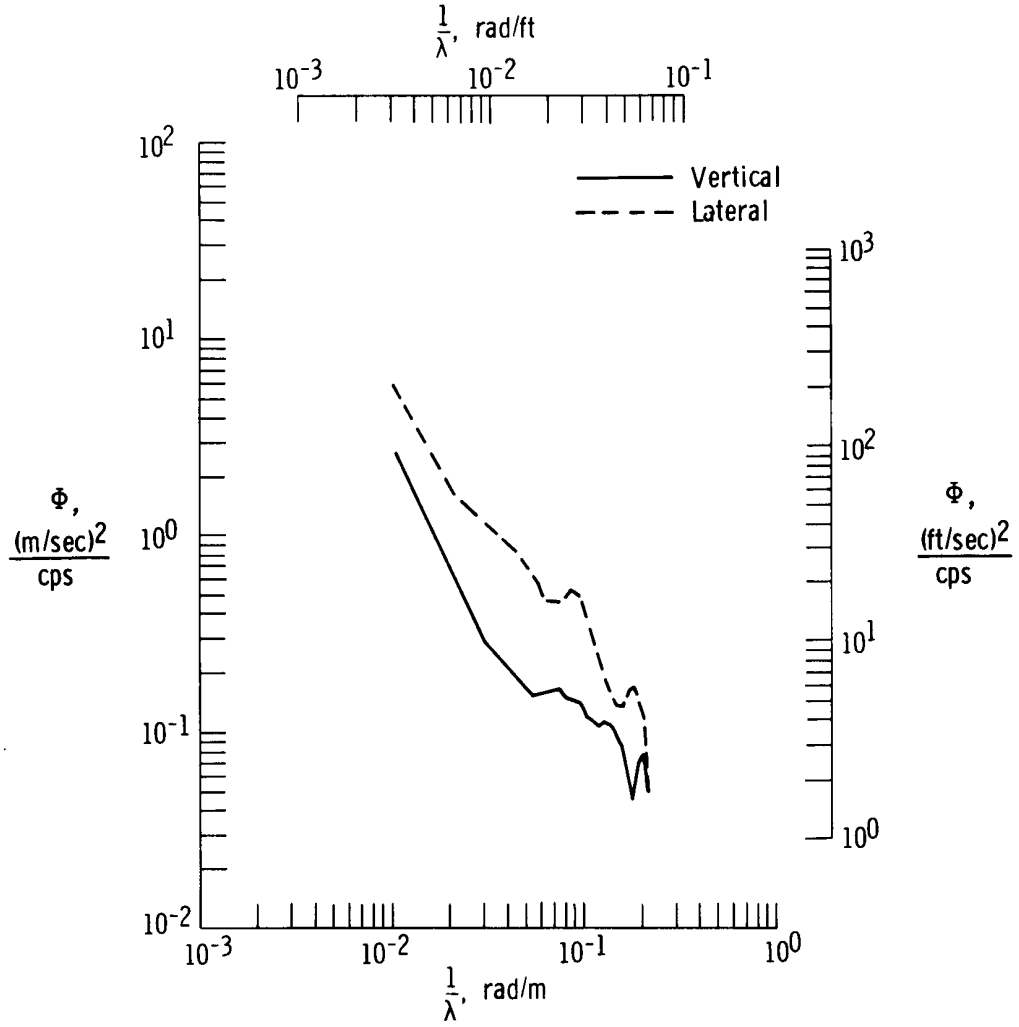

(d) Flight D.

Figure 7. Concluded.

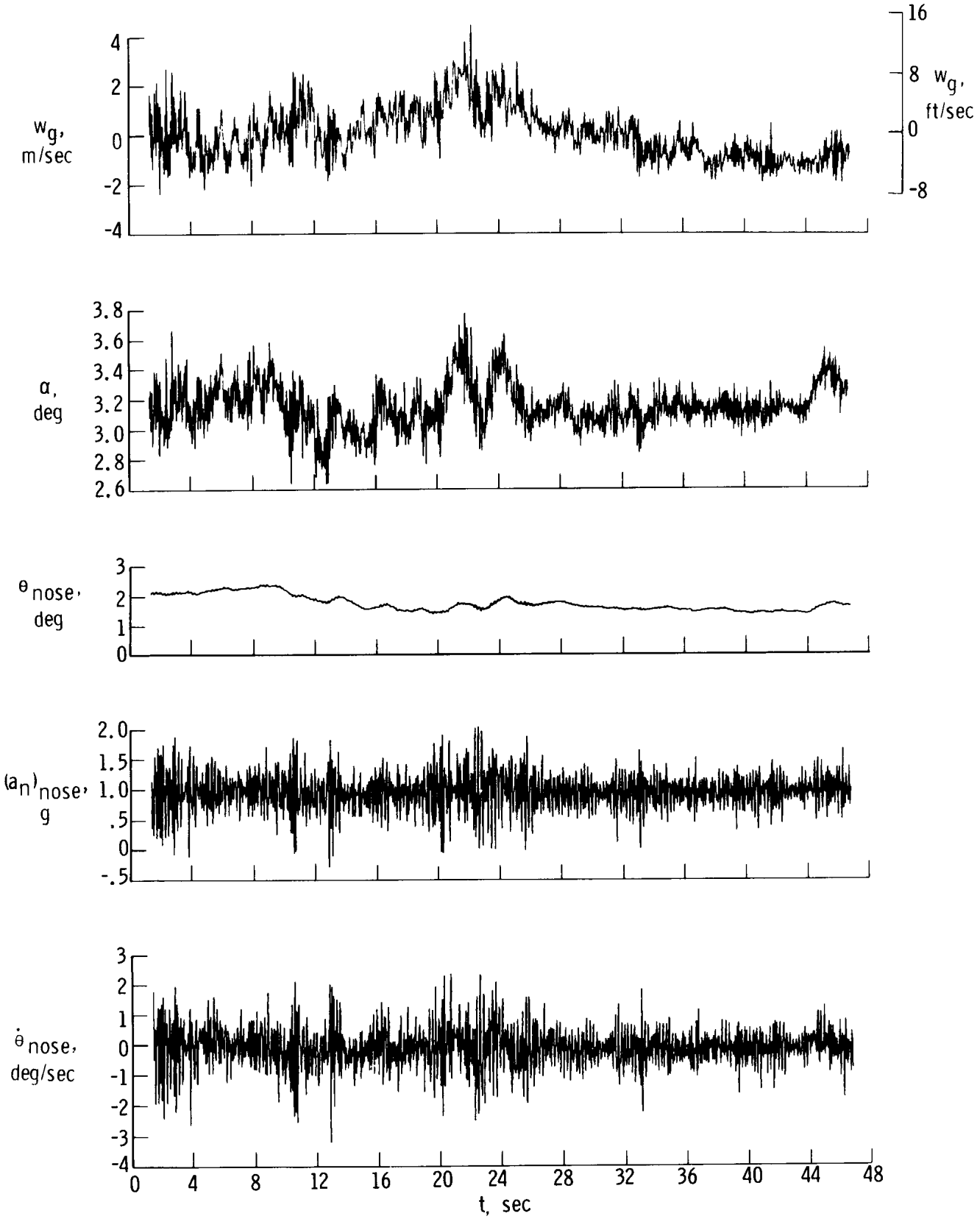

(a) Vertical gust velocity parameters.

Figure 8. Time history of XB-70 response to turbulence. Mach 1.59; h_p = 11,979 m (39,300 ft); $\delta_{t_p} = 65°$.

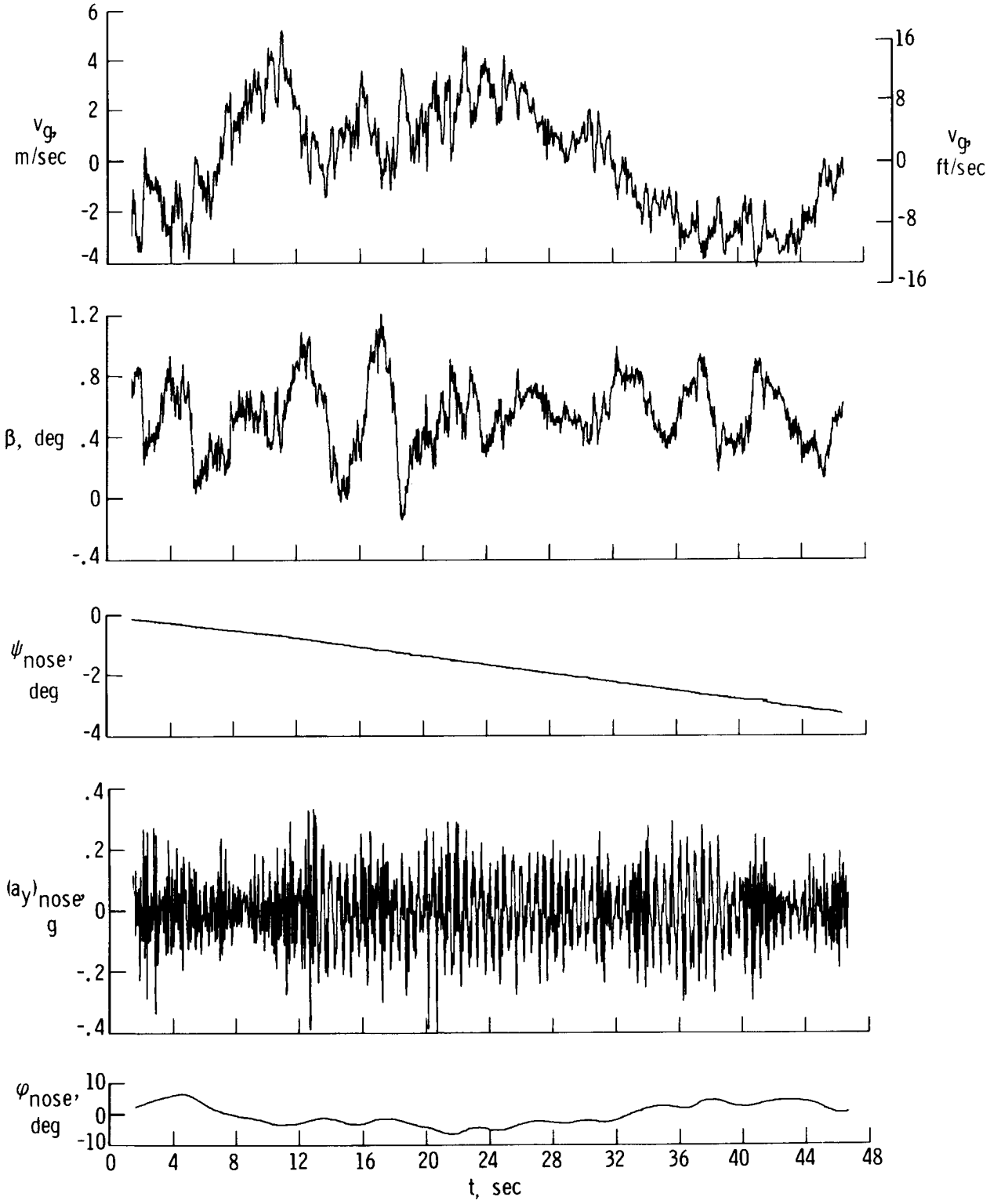

(b) Lateral gust velocity parameters.

Figure 8. Continued.

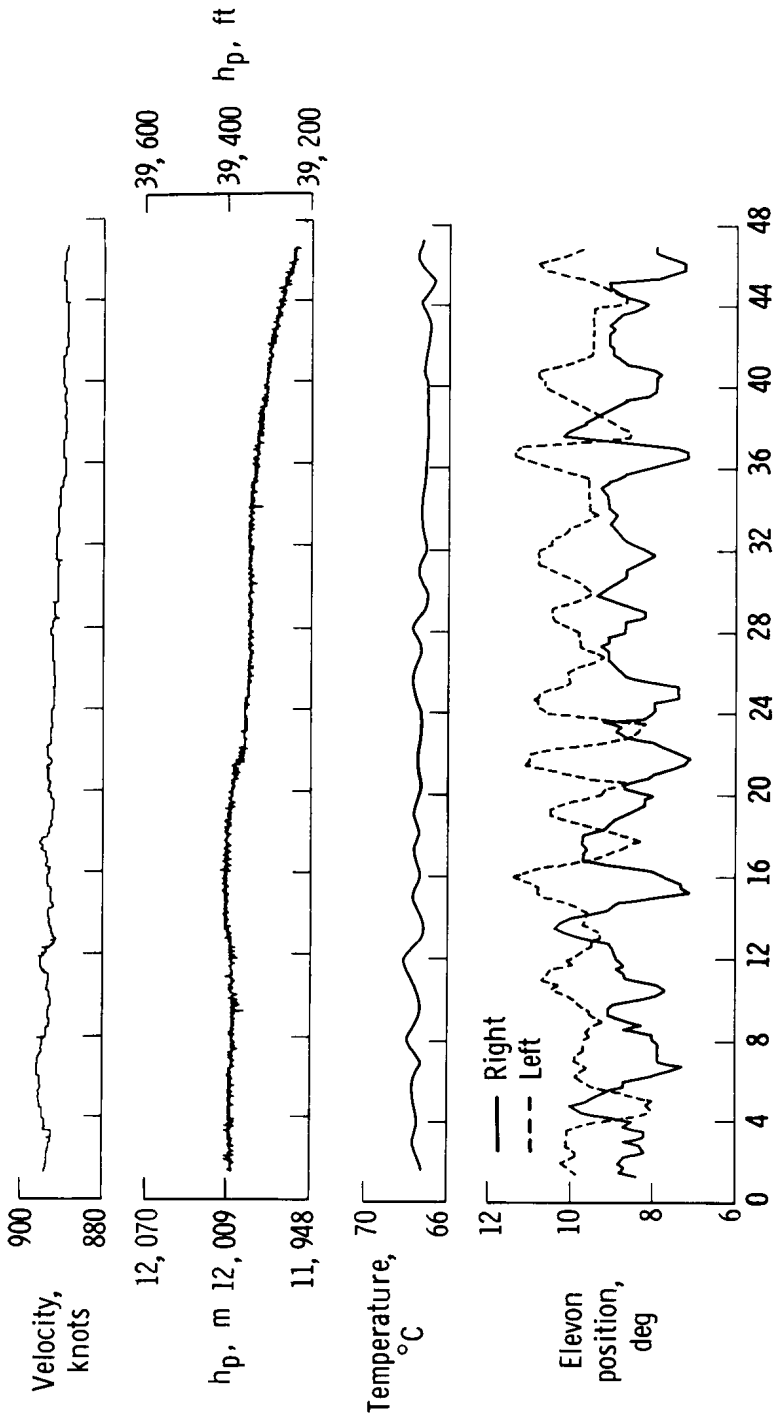

(c) Basic airplane parameters.

Figure 8. Continued.

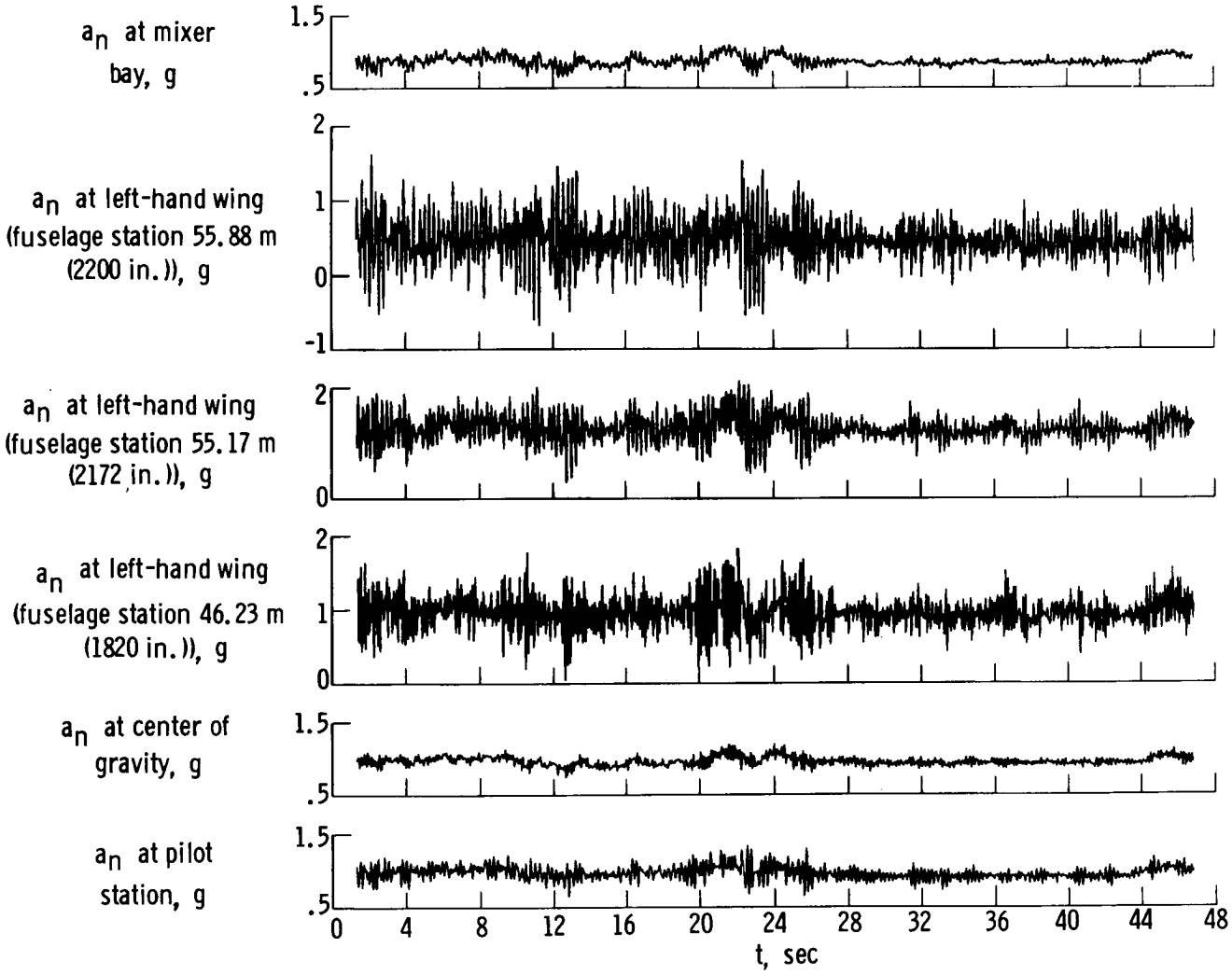

(d) Airplane vertical response parameters.

Figure 8. Continued.

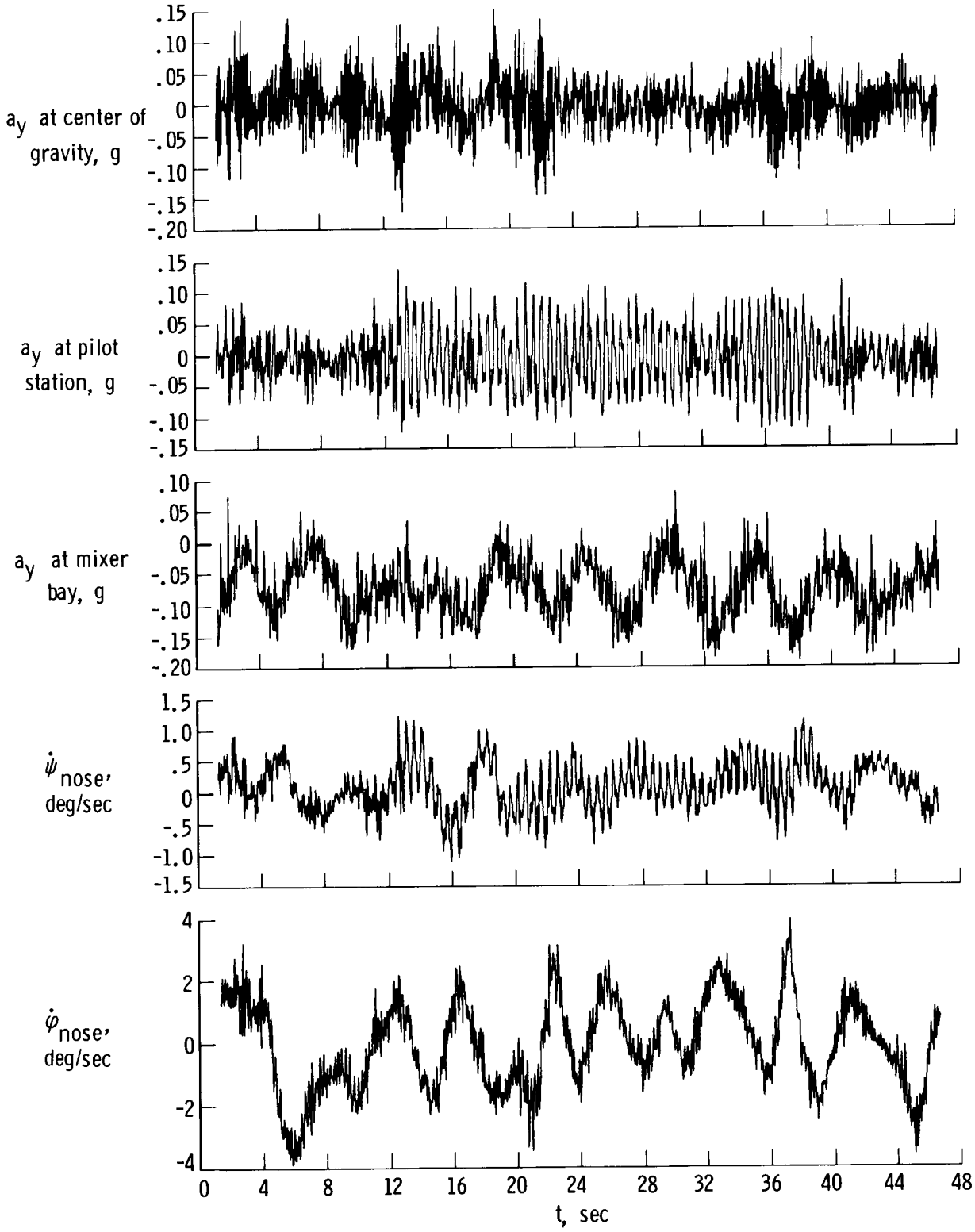

(e) Airplane lateral response parameters.

Figure 8. Concluded.

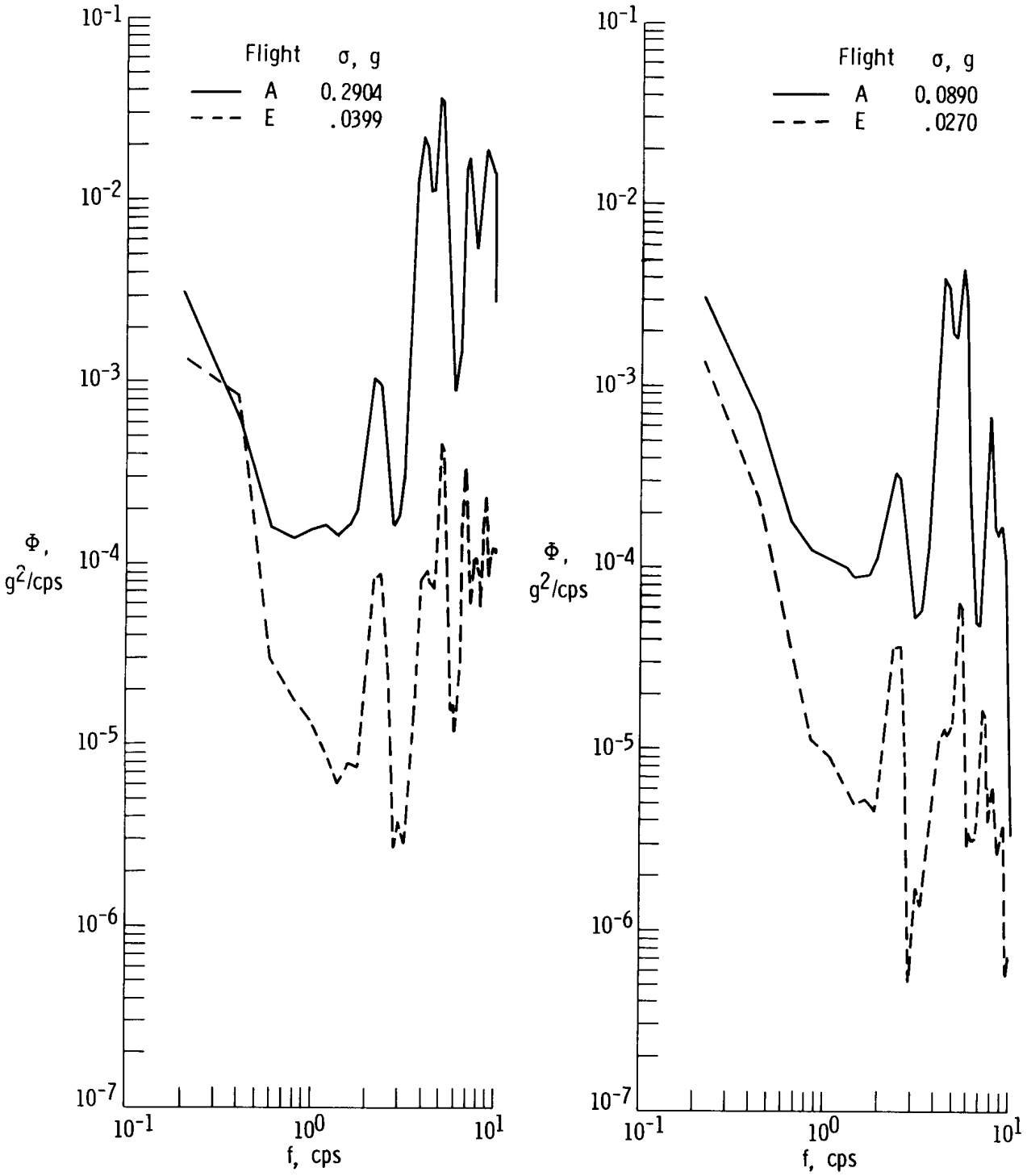

(a) Normal acceleration at the airplane nose.

(b) Normal acceleration at the pilot station.

Figure 9. Comparison of XB-70 normal acceleration response power spectra for a maximum intensity and a minimum intensity turbulence encounter.

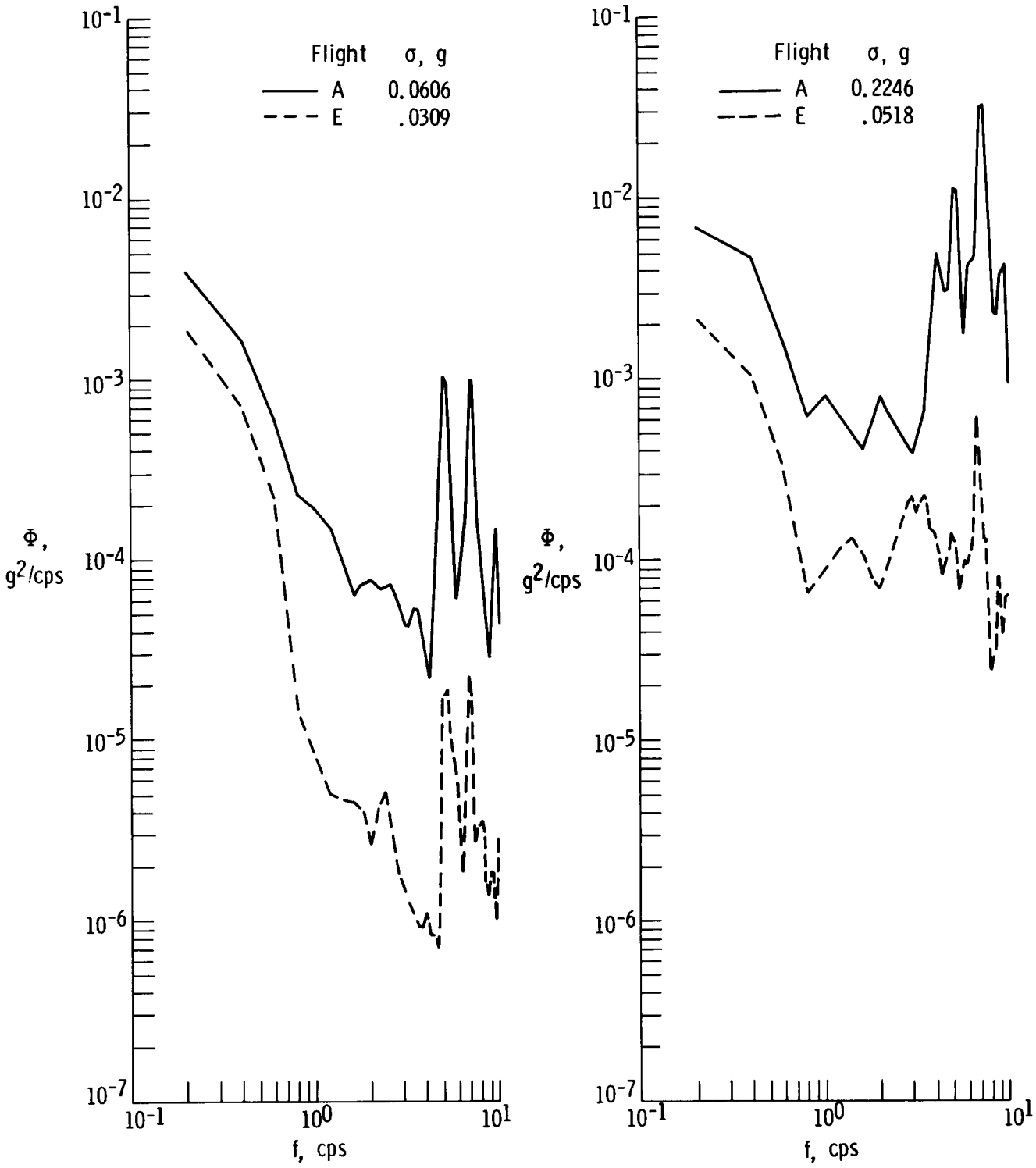

(c) Normal acceleration at the center of gravity.

(d) Normal acceleration at wing fuselage station 46.23 meters (1820 inches).

Figure 9. Continued.

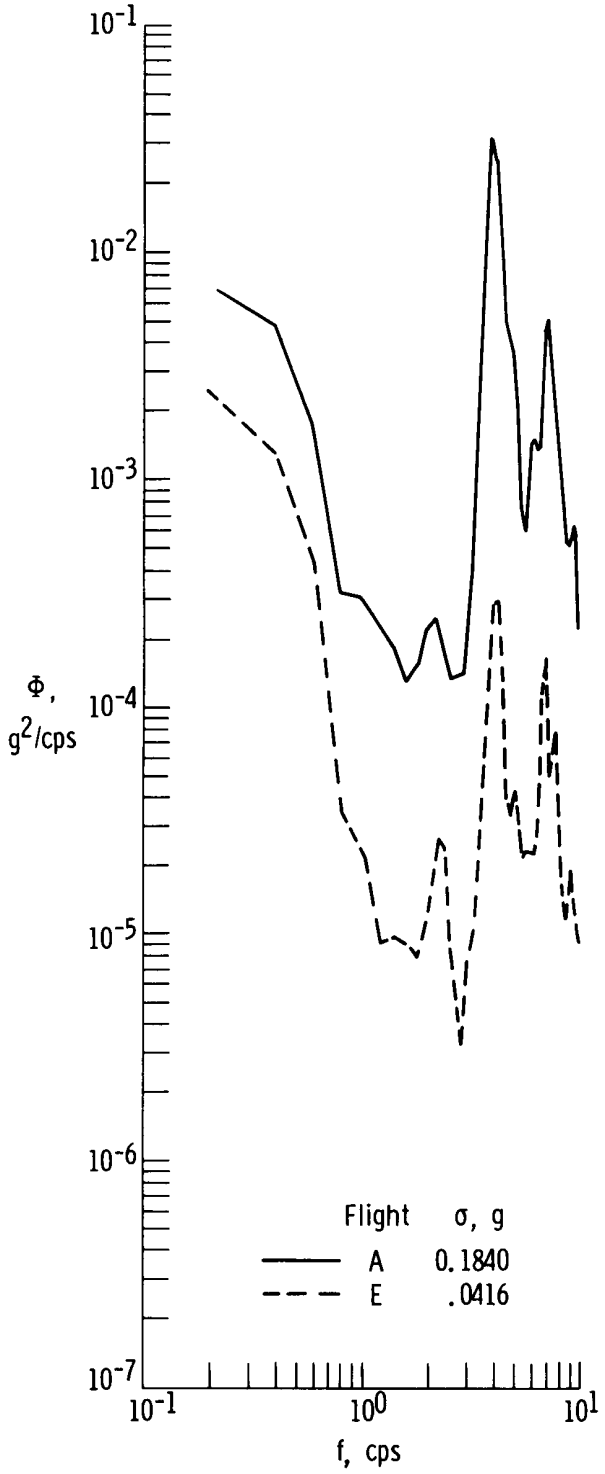

(e) Normal acceleration at wing fuselage station 55.17 meters (2172 inches).

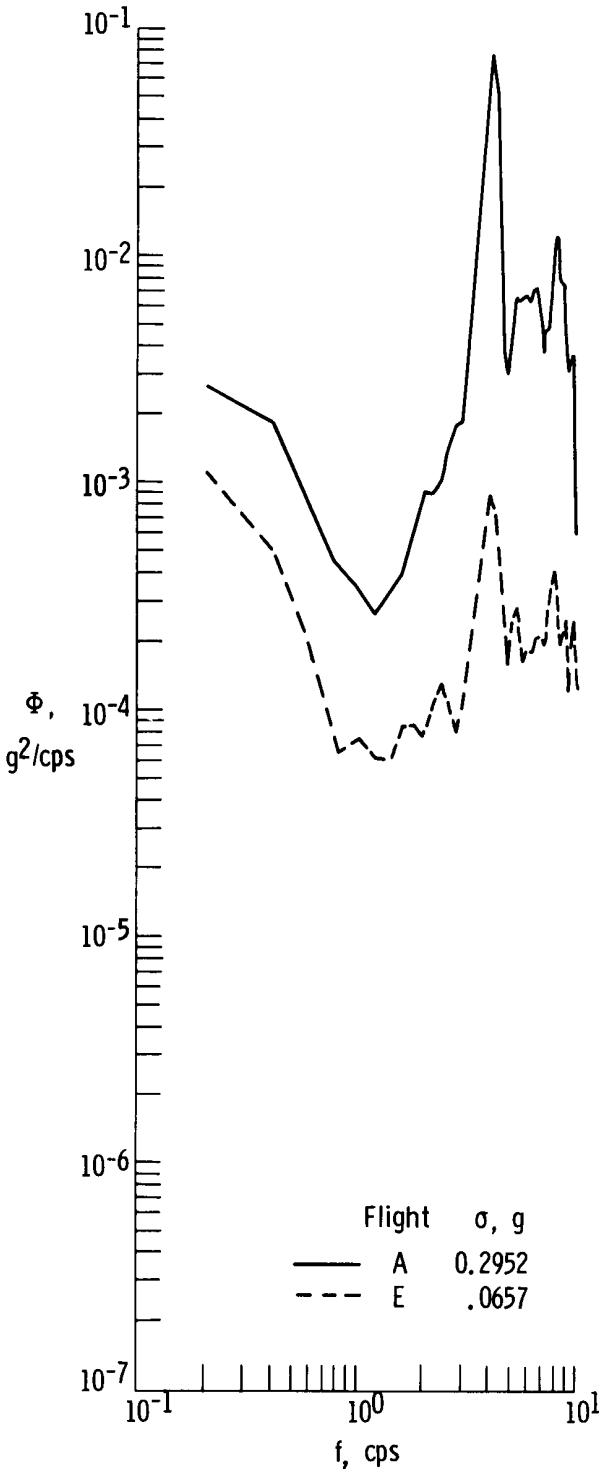

(f) Normal acceleration at wing fuselage station 55.88 meters (2200 inches).

Figure 9. Continued.

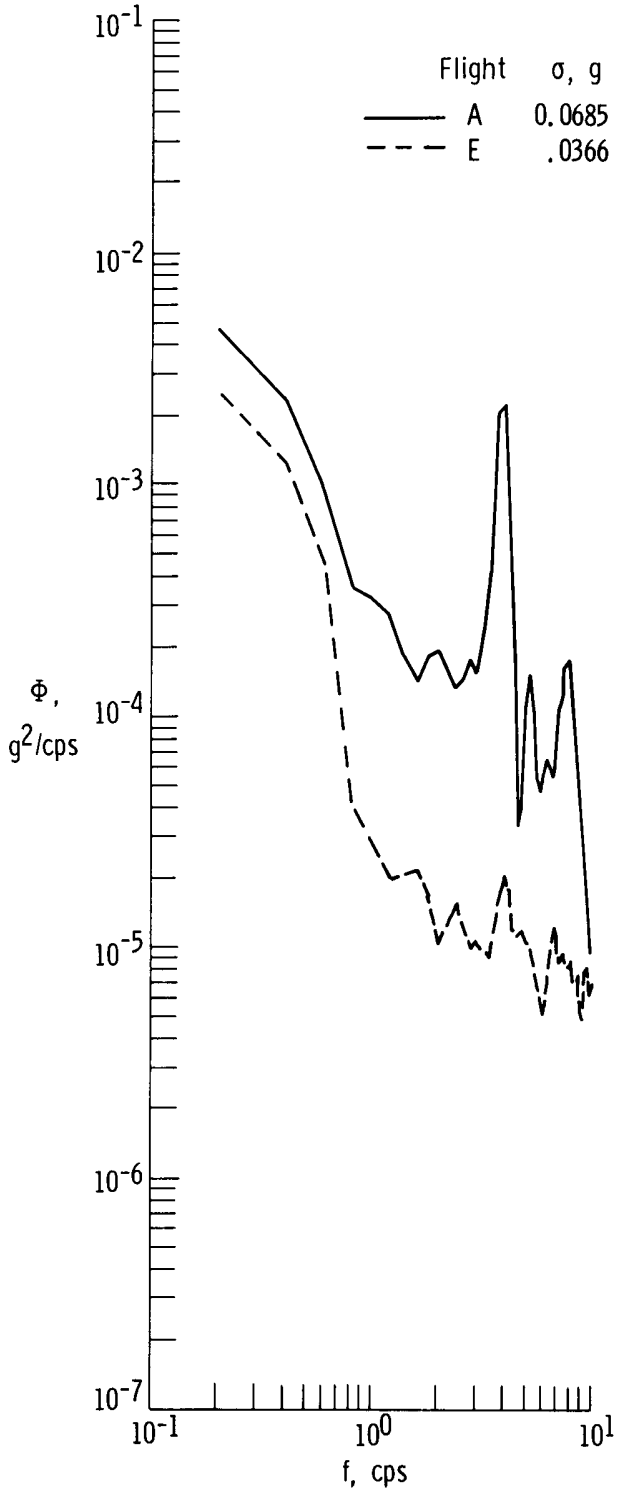

(g) Normal acceleration at the mixer bay.

Figure 9. Concluded.

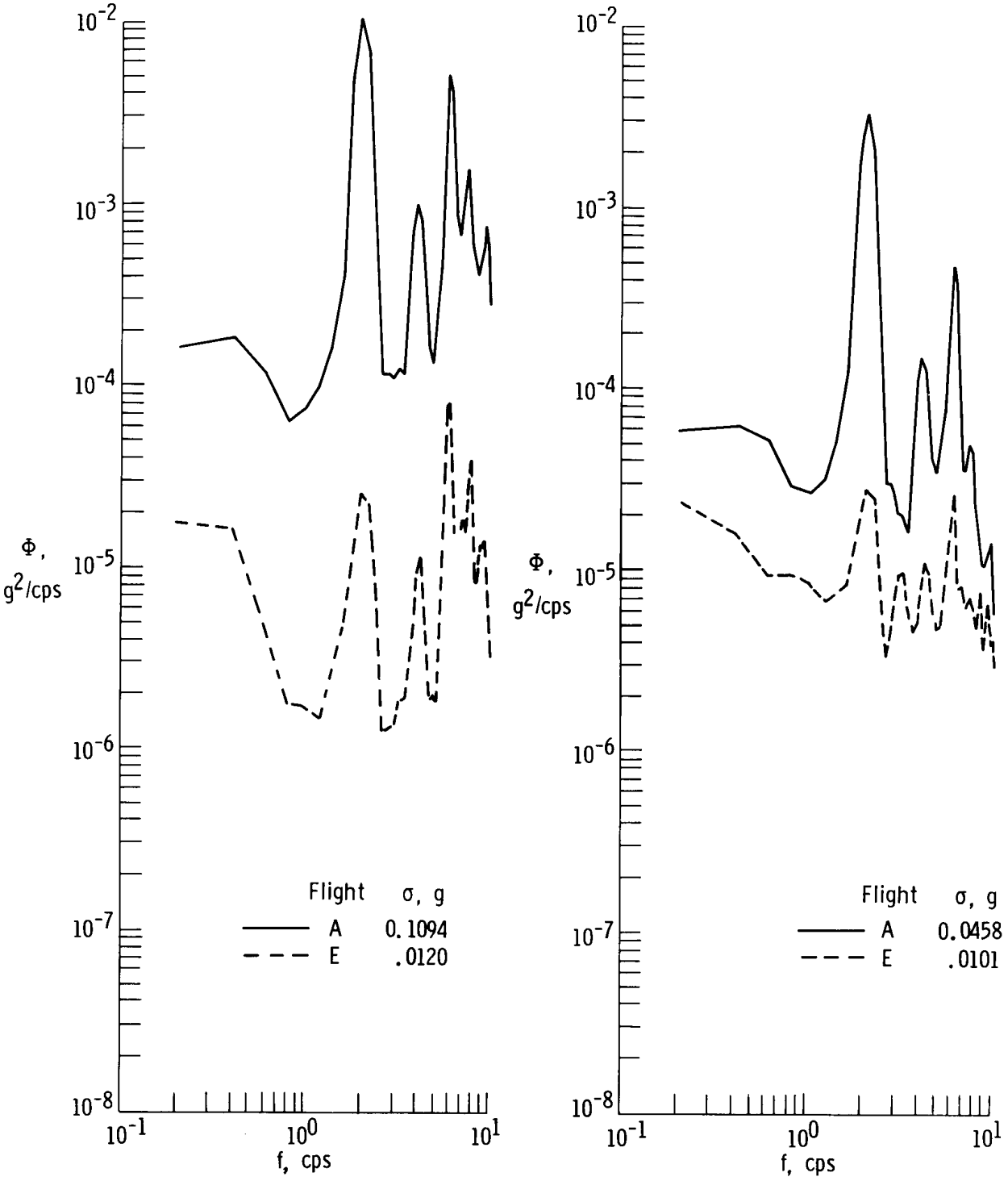

(a) Lateral acceleration at the airplane nose.

(b) Lateral acceleration at the pilot station.

Figure 10. Comparison of XB-70 lateral acceleration response power spectra for a maximum intensity and a minimum intensity turbulence encounter.

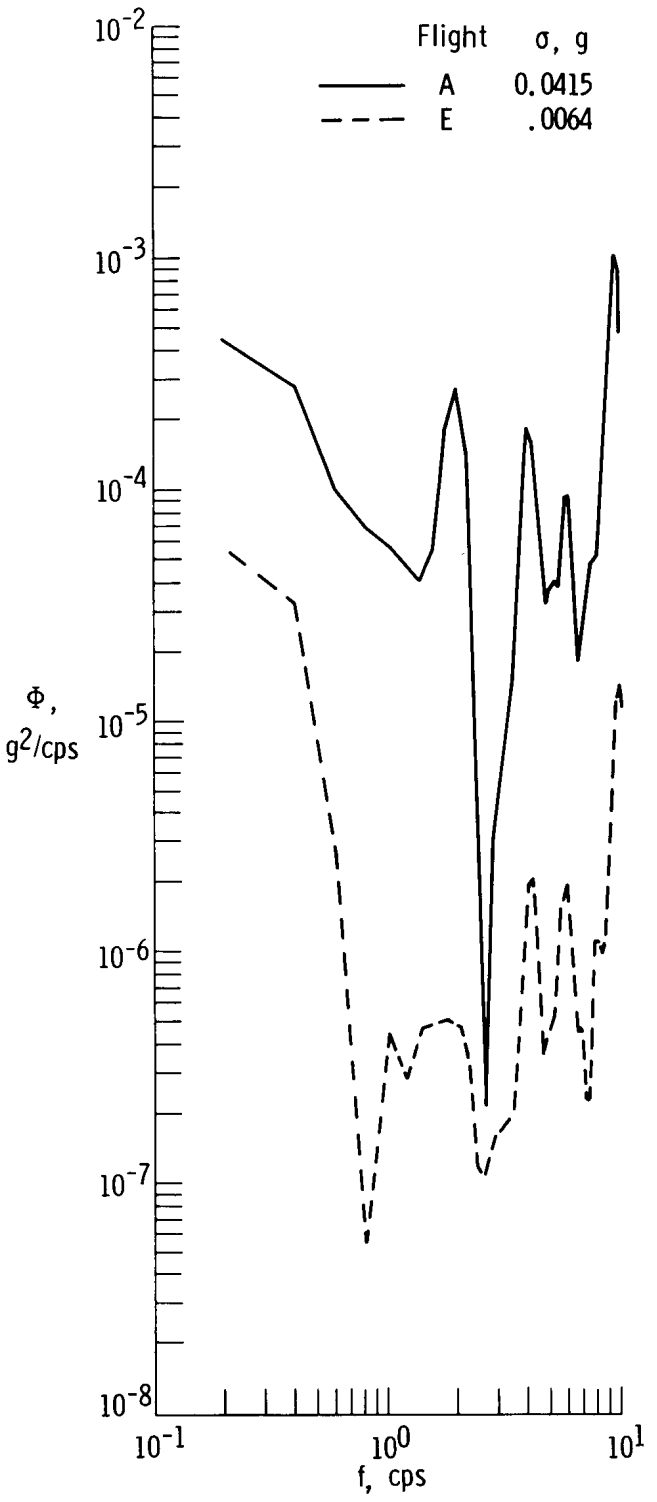

(c) Lateral acceleration at the center of gravity.

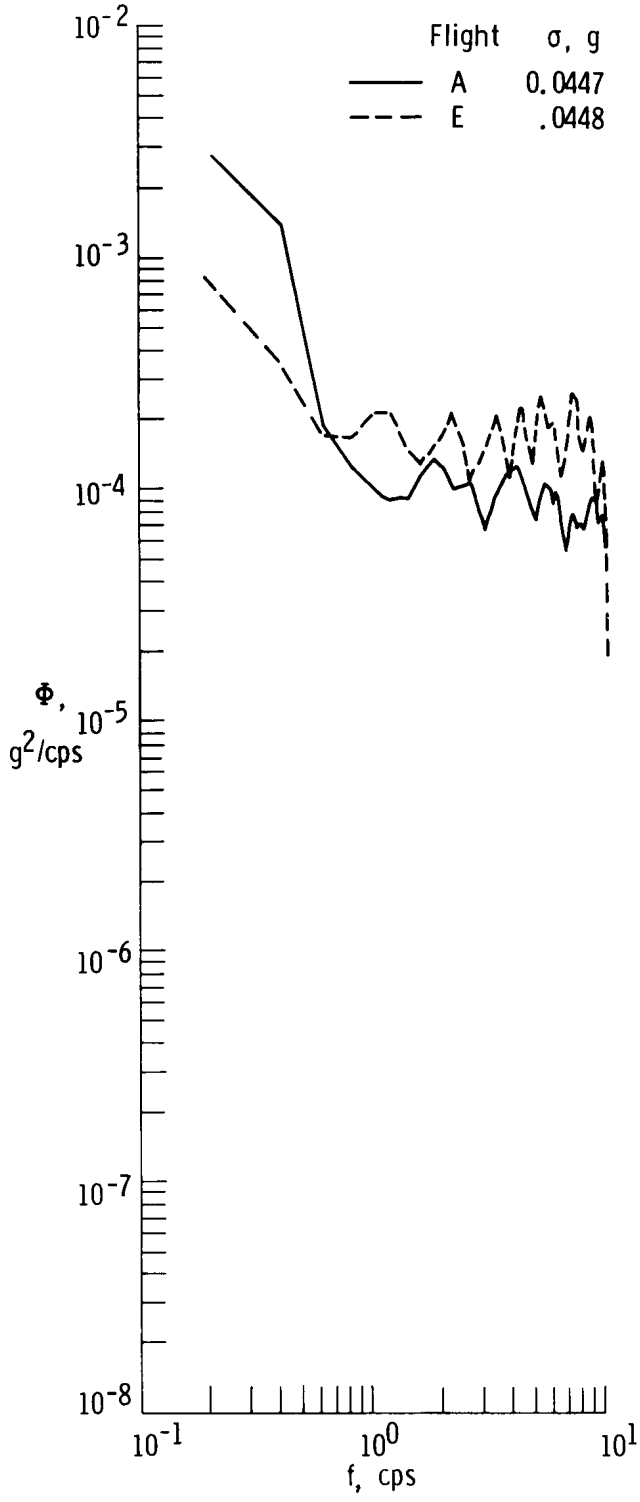

(d) Lateral acceleration at the mixer bay.

Figure 10. Concluded.

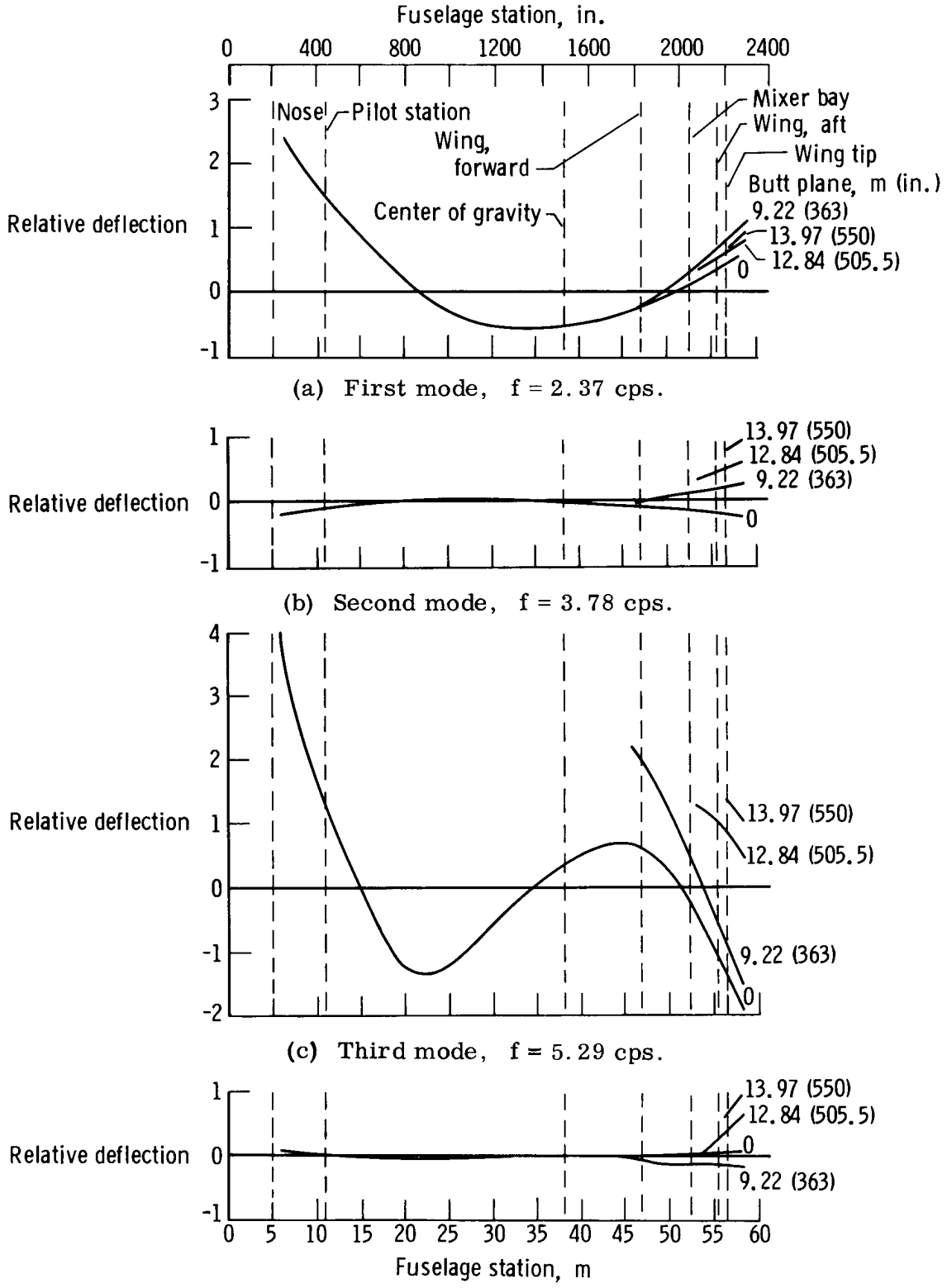

Figure 11. Calculated fuselage vertical deflection (normalized to unit wing-tip deflection) for first four symmetrical modes of the XB-70 airplane. Median weight; $\delta_{t_p} = 65°$.

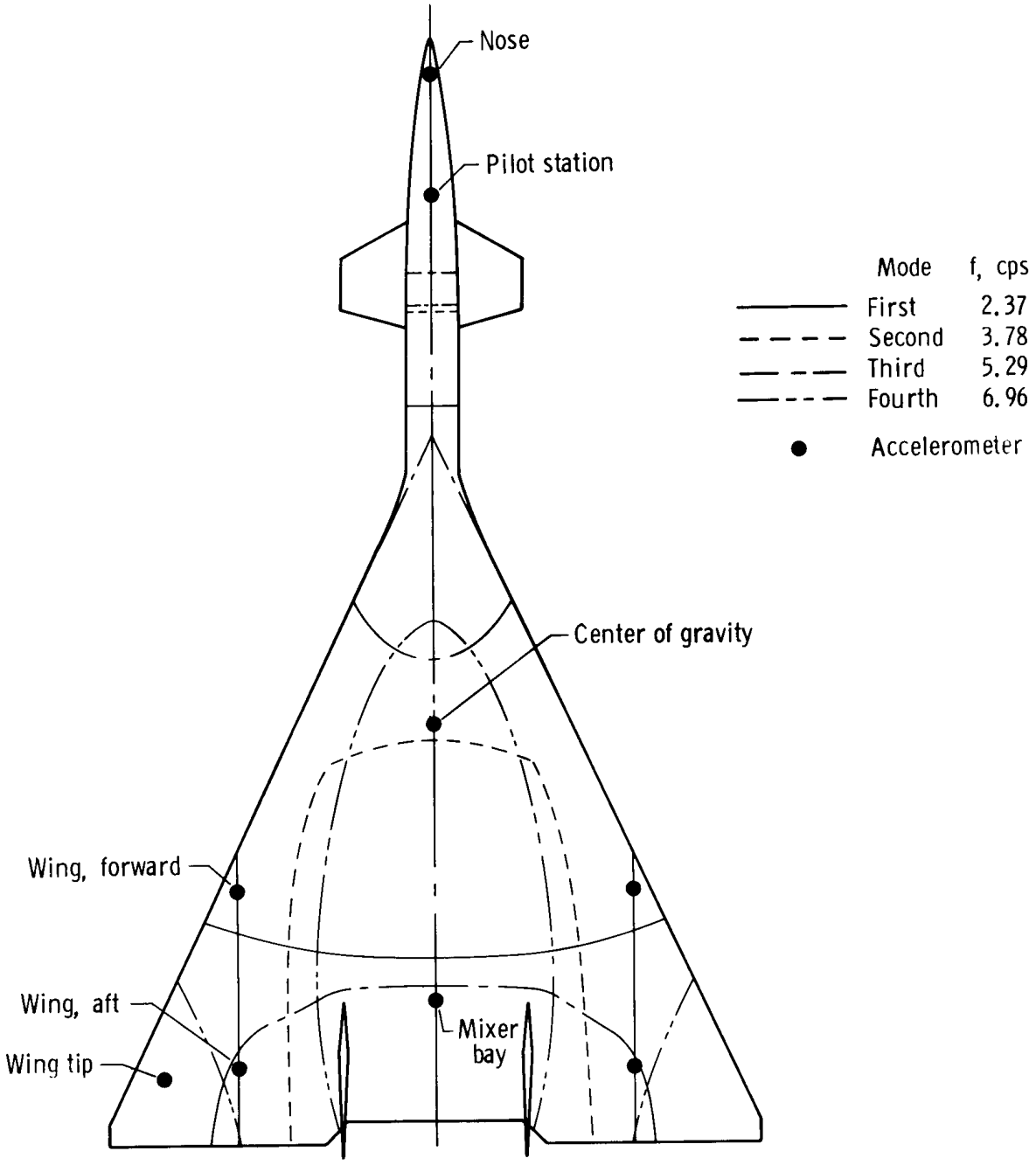

(e) Plan view of calculated node lines.

Figure 11. Concluded.

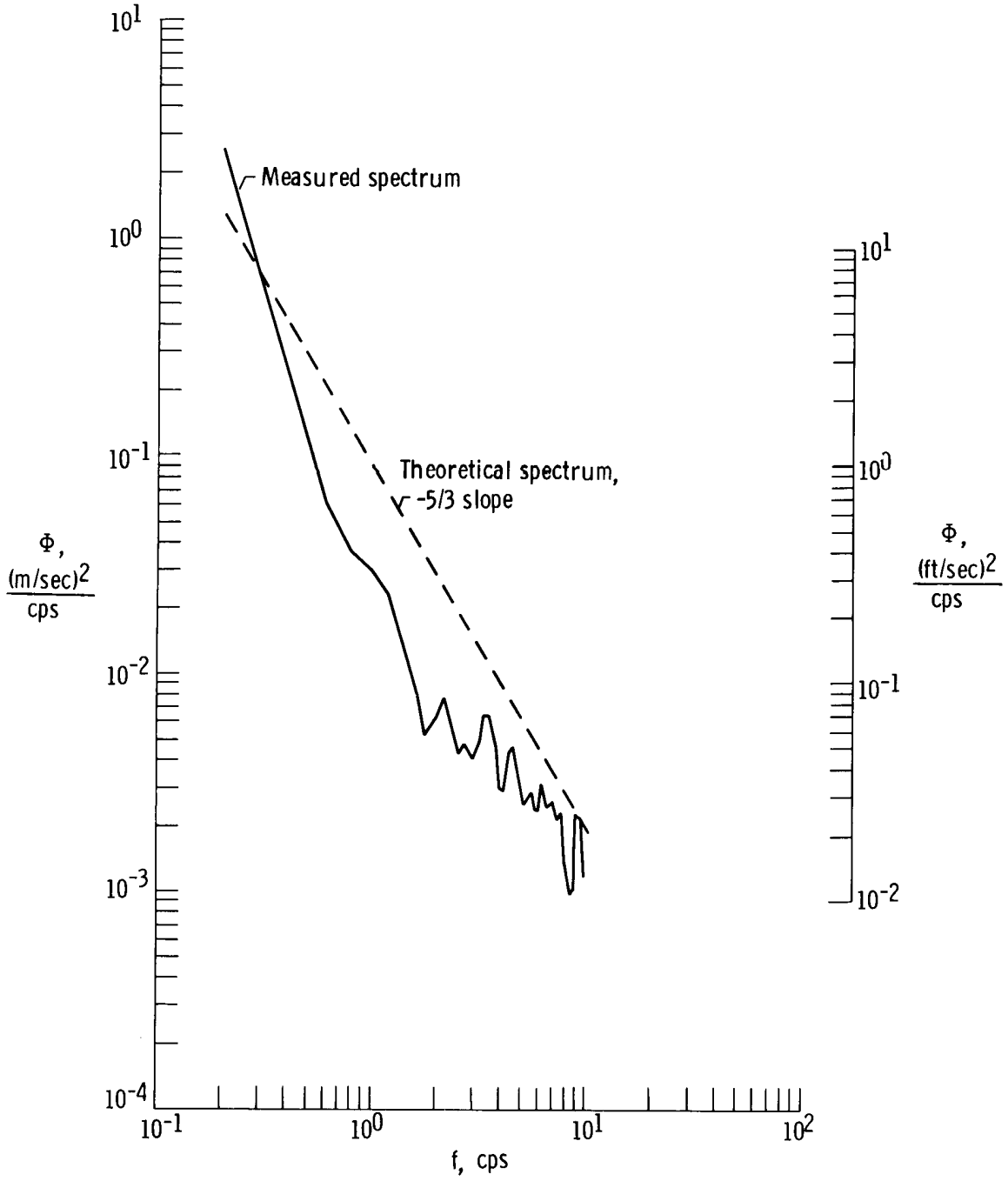

Figure 12. Comparison of vertical component of turbulence input spectrum for flight D with theoretical turbulence model. Mach 0.88; B_e = 0.4 cps; T_r = 30.5 sec; η = 24.4; σ_1 = 0.6120 m/sec (2.0078 ft/sec).

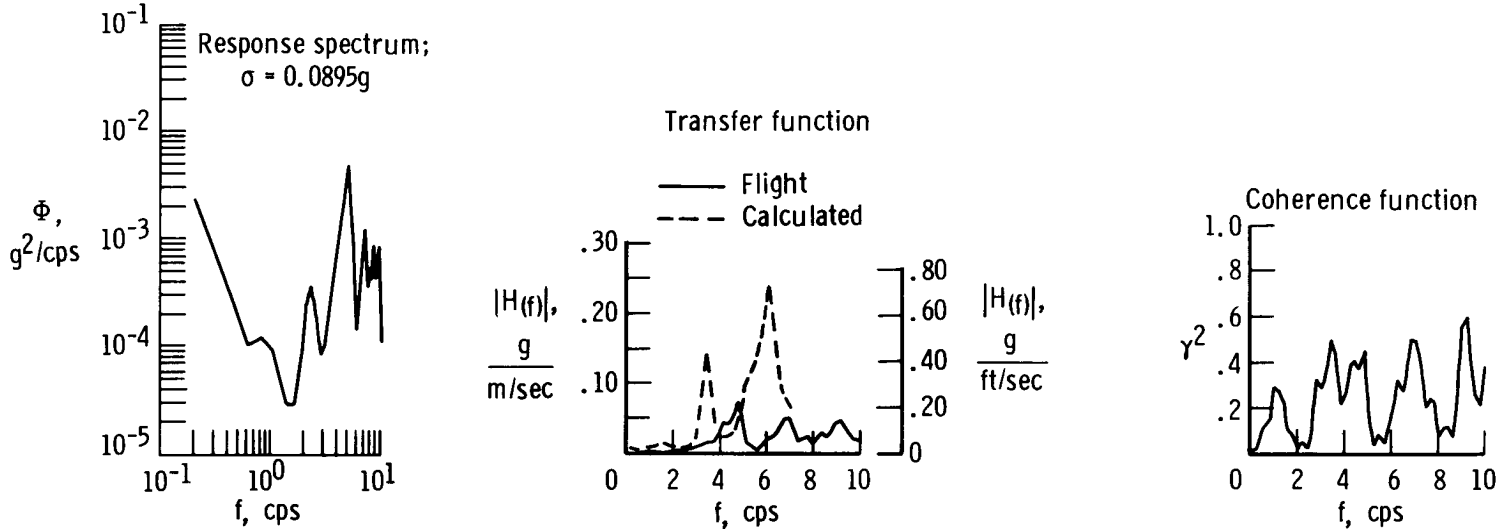

(a) Normal acceleration at the airplane nose.

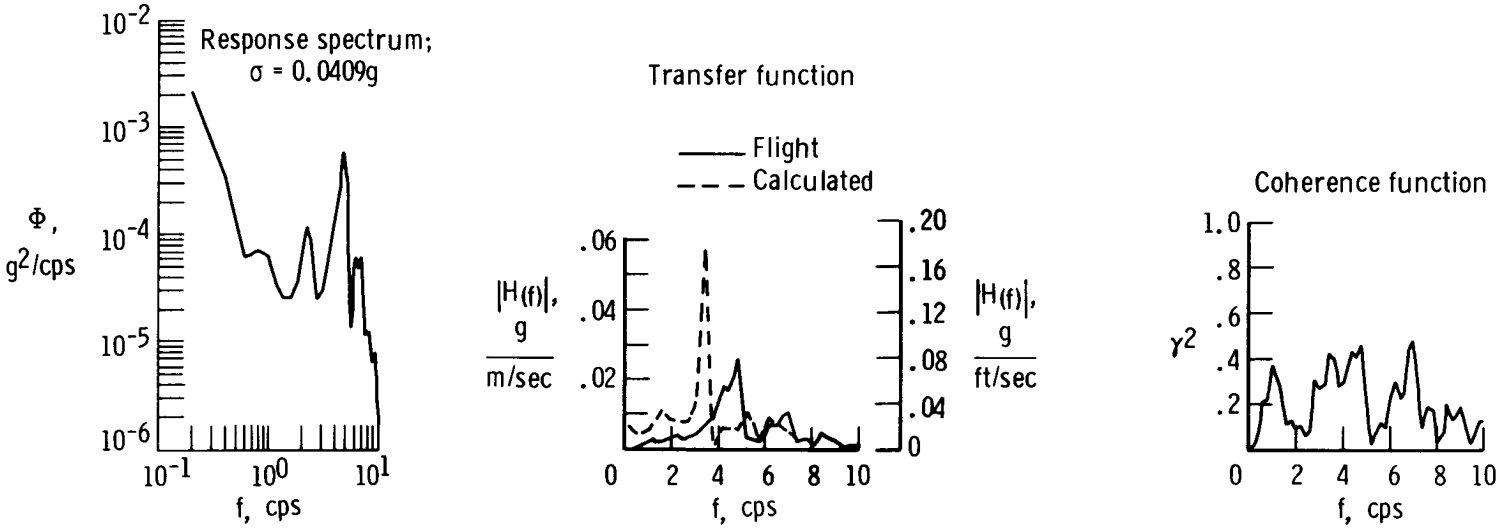

(b) Normal acceleration at the pilot station.

Figure 13. Comparison of frequency response spectra, frequency response transfer functions, and coherence functions for flight D with theoretical frequency response transfer functions for various accelerometer locations. B_e = 0.4 cps; T_r = 30.5 sec; η = 24.4.

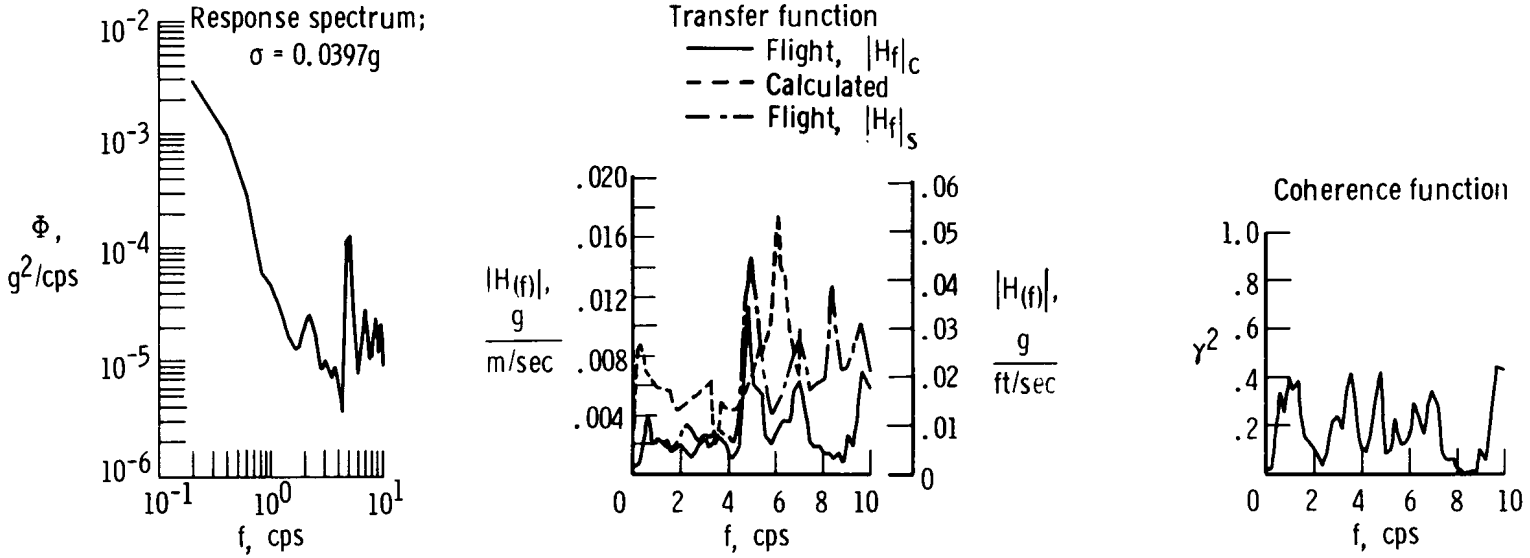

(c) Normal acceleration at center of gravity.

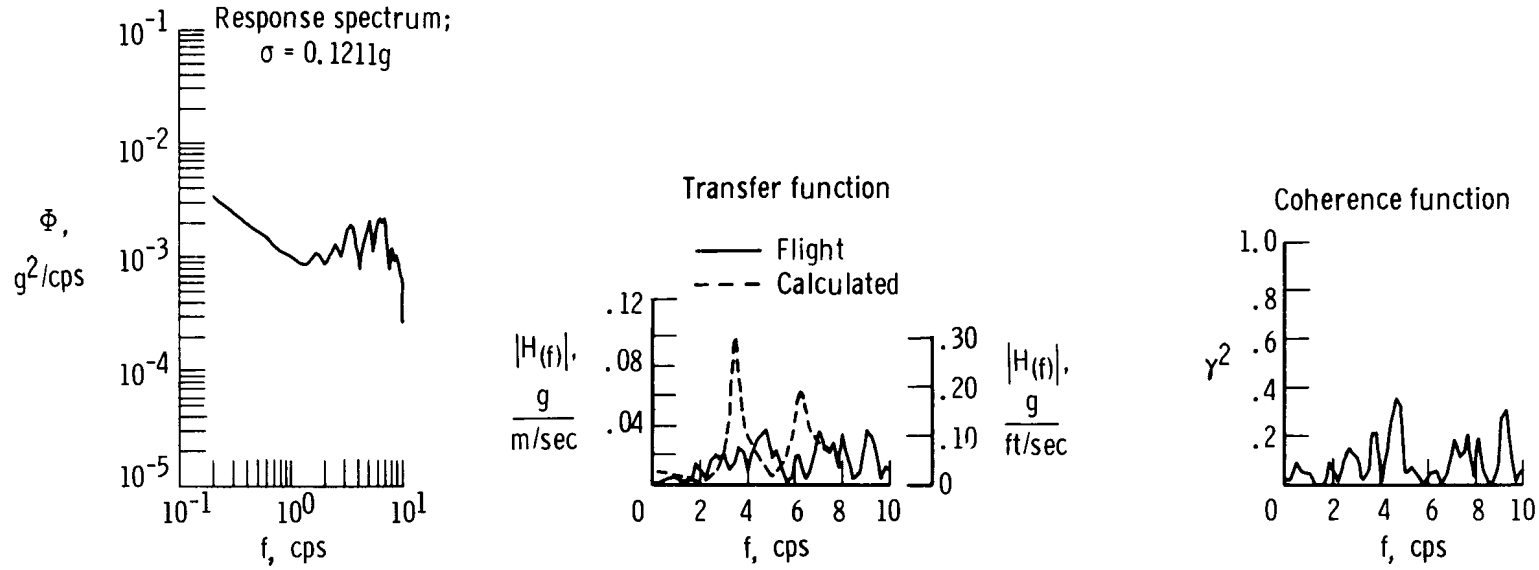

(d) Normal acceleration at wing fuselage station 46.23 meters (1820 inches).

Figure 13. Continued.

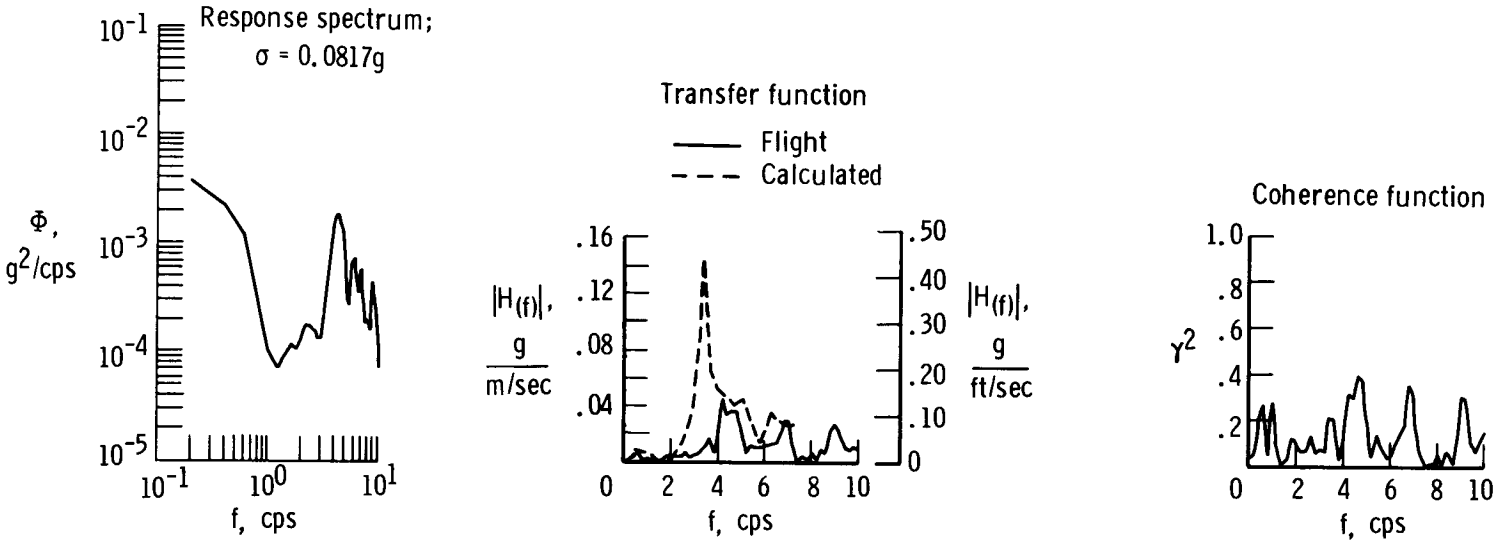

(e) Normal acceleration at wing fuselage station 55.17 meters (2172 inches).

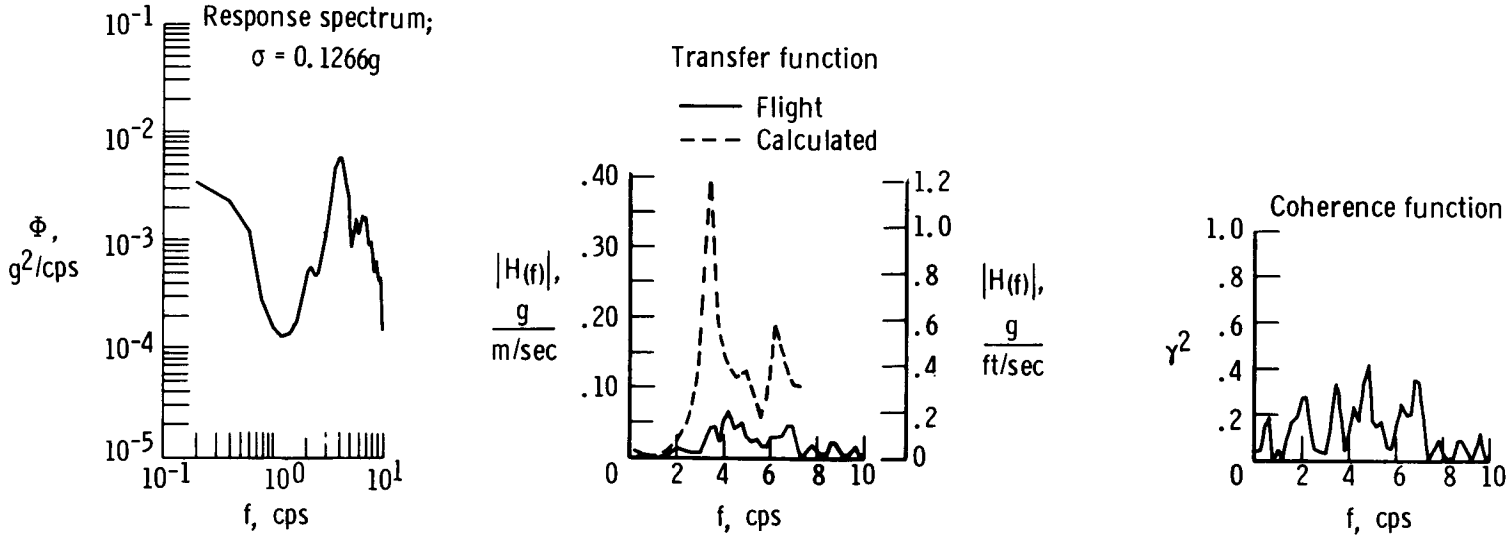

(f) Normal acceleration at wing fuselage station 55.88 meters (2200 inches).

Figure 13. Continued.

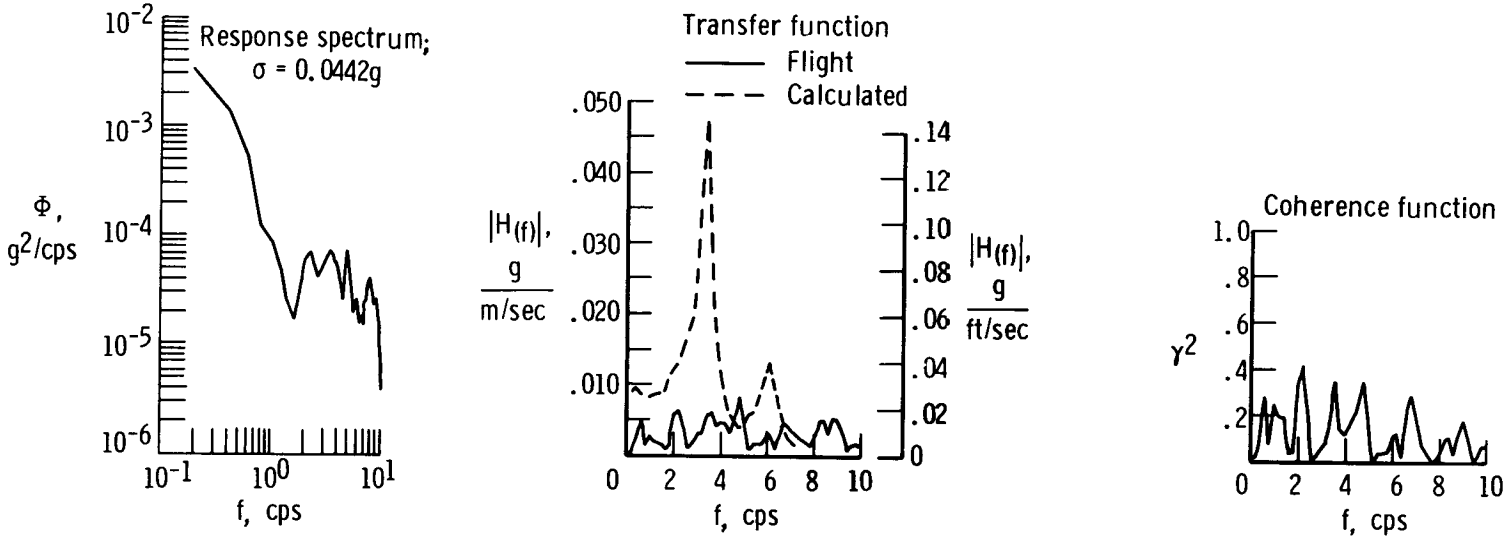

(g) Normal acceleration at the mixer bay.

Figure 13. Concluded.

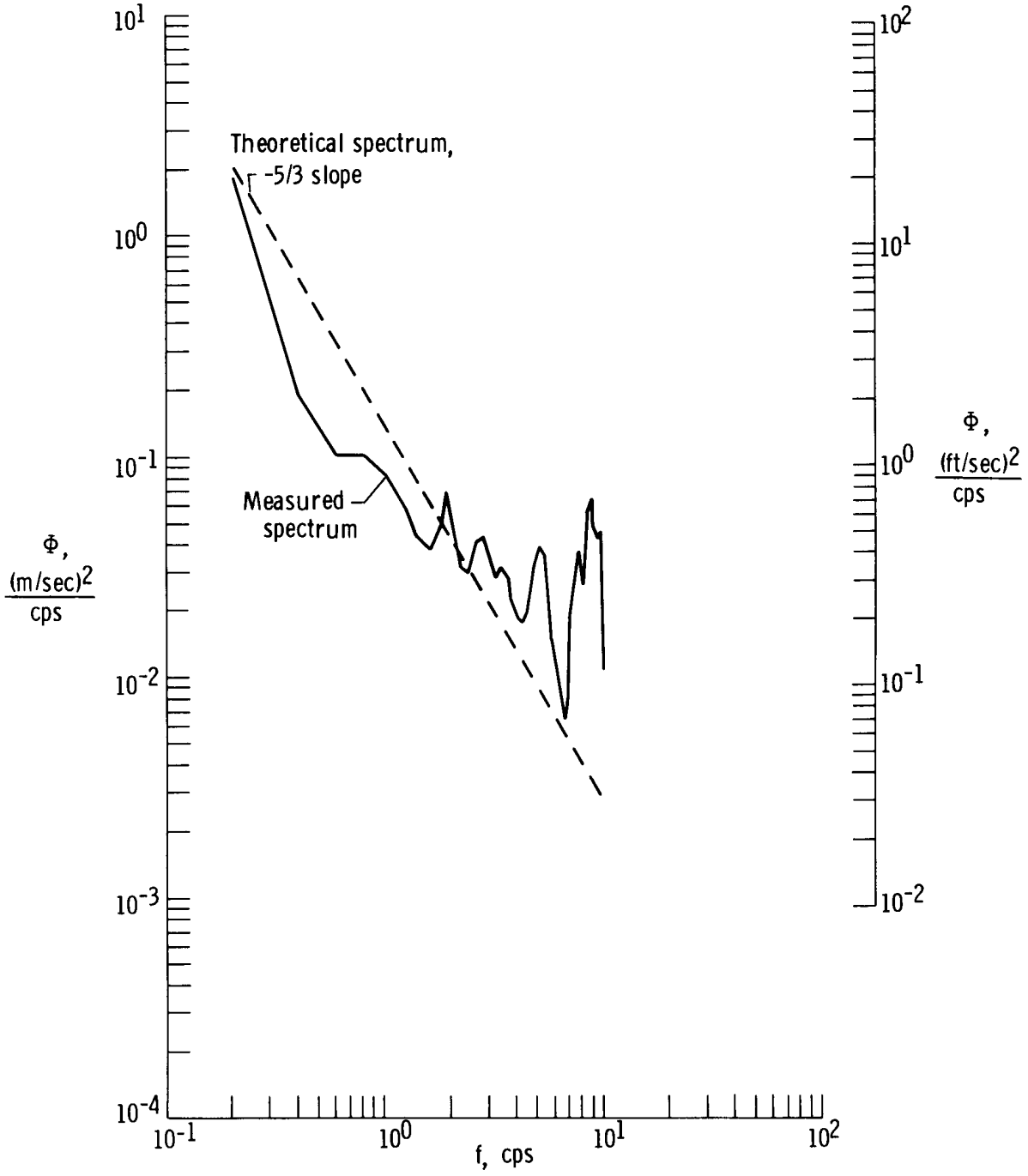

Figure 14. Comparison of vertical component of turbulence input spectrum for flight A with theoretical turbulence model. Mach 1.59; B_e = 0.4 cps; T_r = 45.4 sec; η = 36.3; σ_1 = 0.7604 m/sec (2.4946 ft/sec).

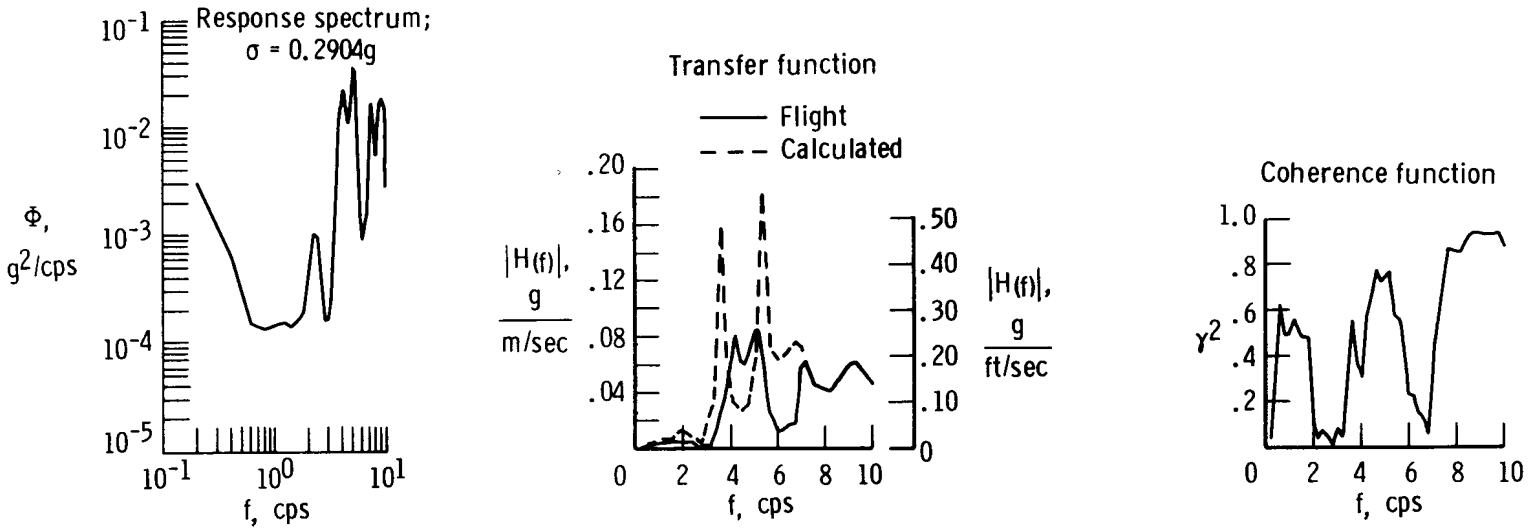

(a) Normal acceleration at the airplane nose.

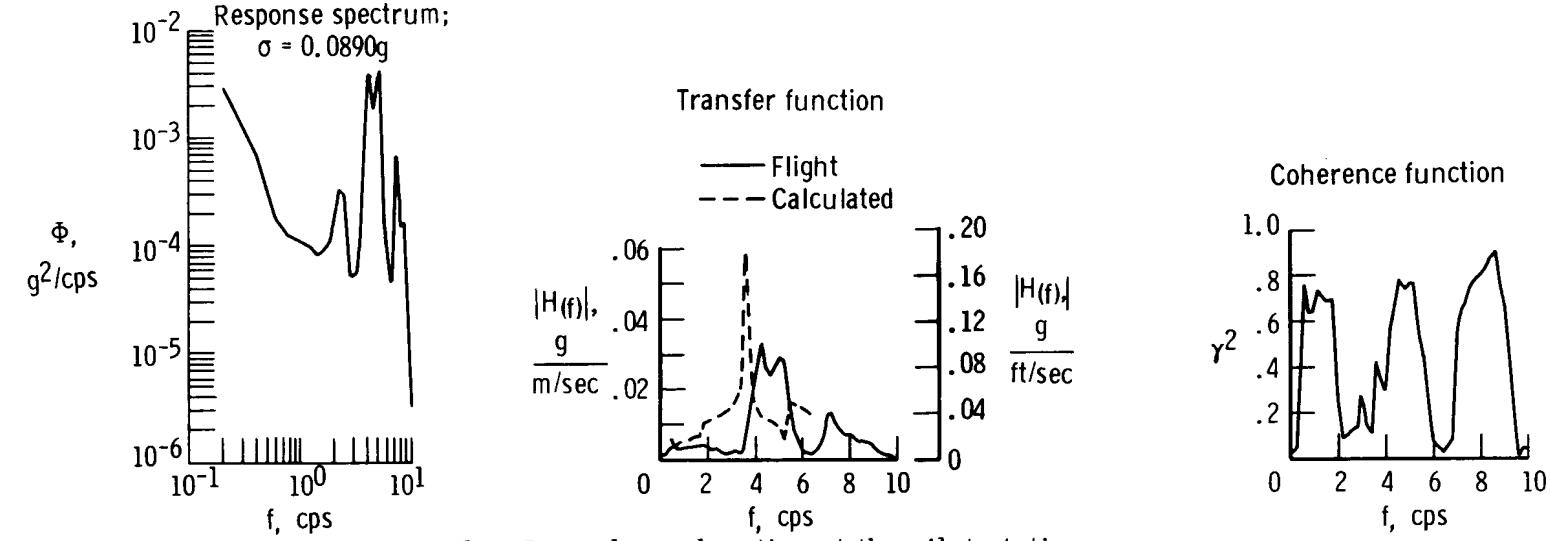

(b) Normal acceleration at the pilot station.

Figure 15. Comparison of frequency response spectra, frequency response transfer functions, and coherence functions for flight A with theoretical frequency response transfer functions for various accelerometer locations. $B_e = 0.4$ cps; $T_r = 45.4$ sec; $\eta = 36.3$.

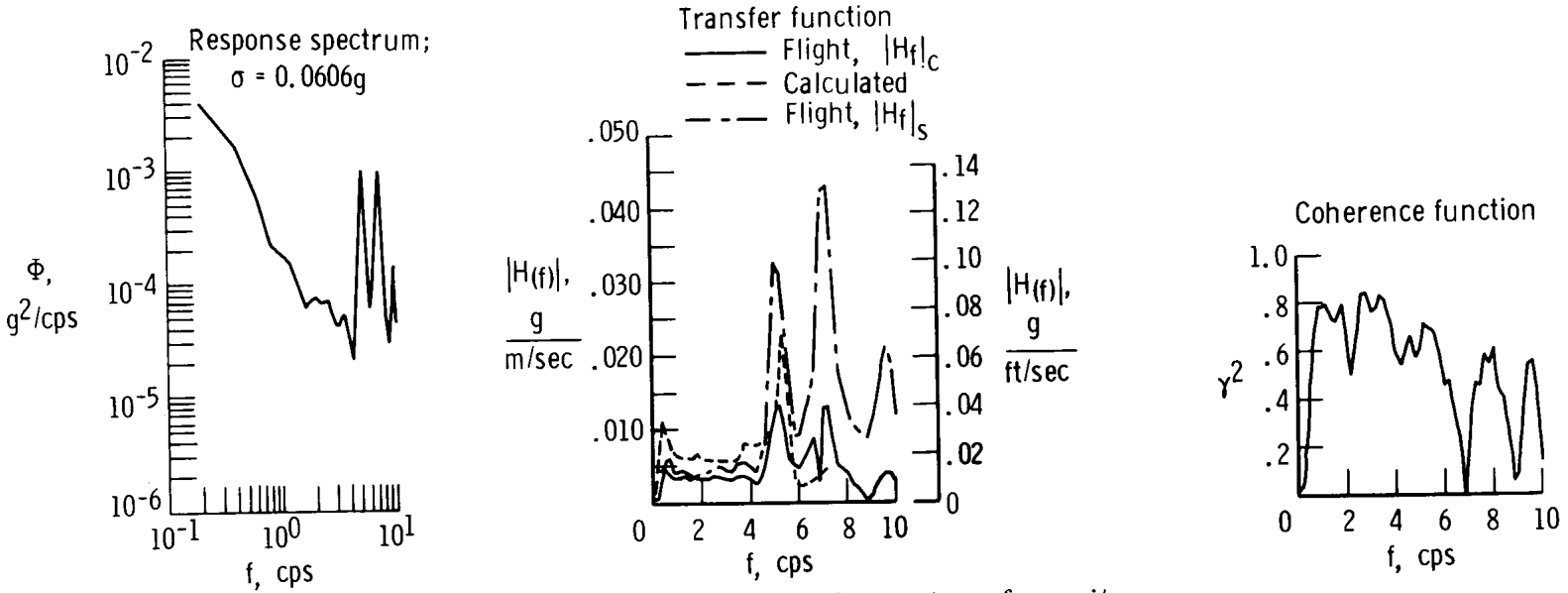

(c) Normal acceleration at the center of gravity.

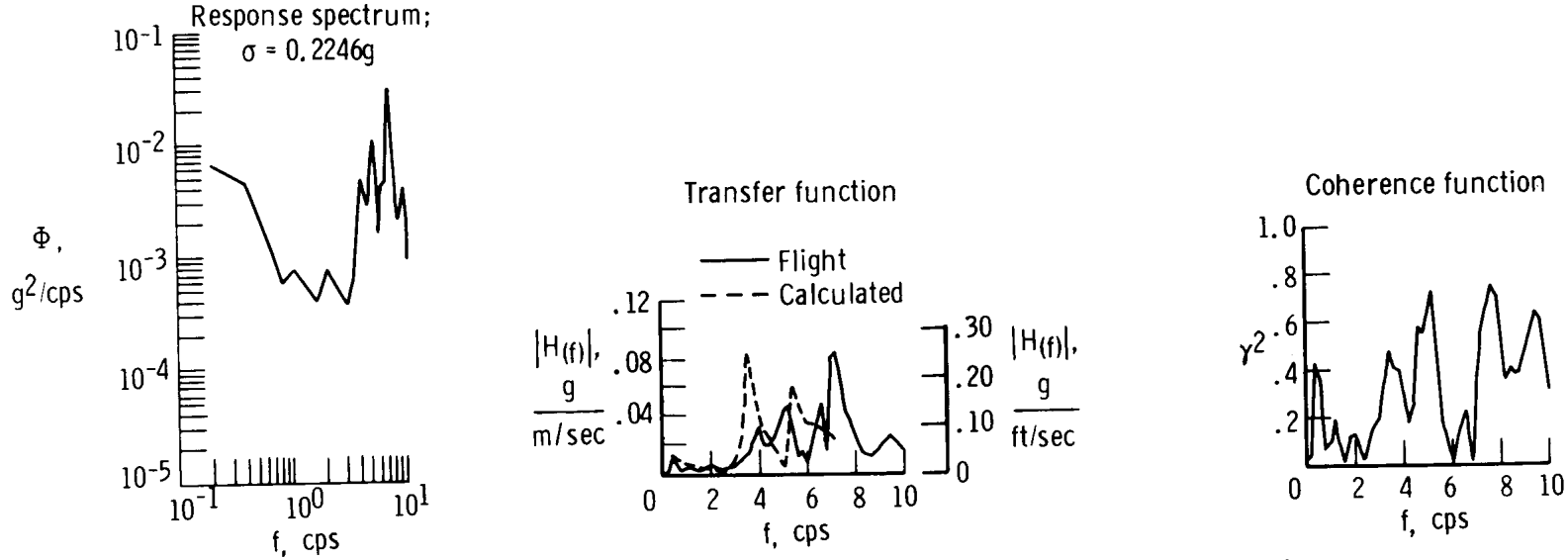

(d) Normal acceleration at wing fuselage station 46.23 meters (1820 inches).

Figure 15. Continued.

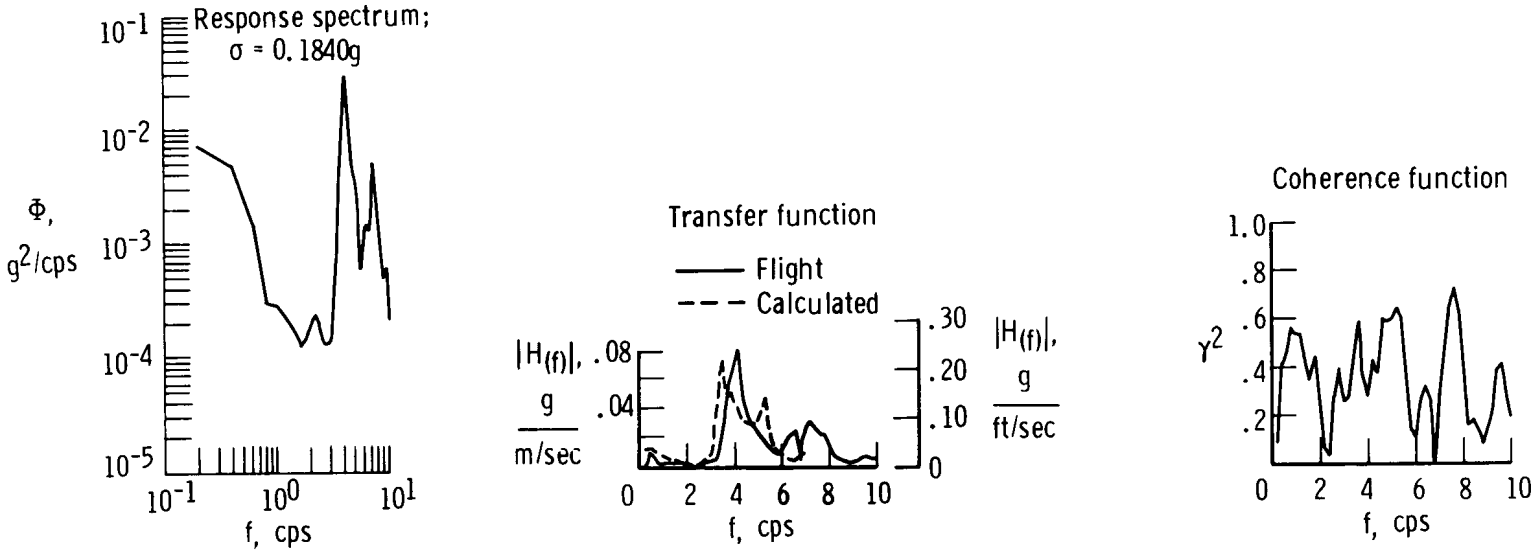

(e) Normal acceleration at wing fuselage station 55.17 meters (2172 inches).

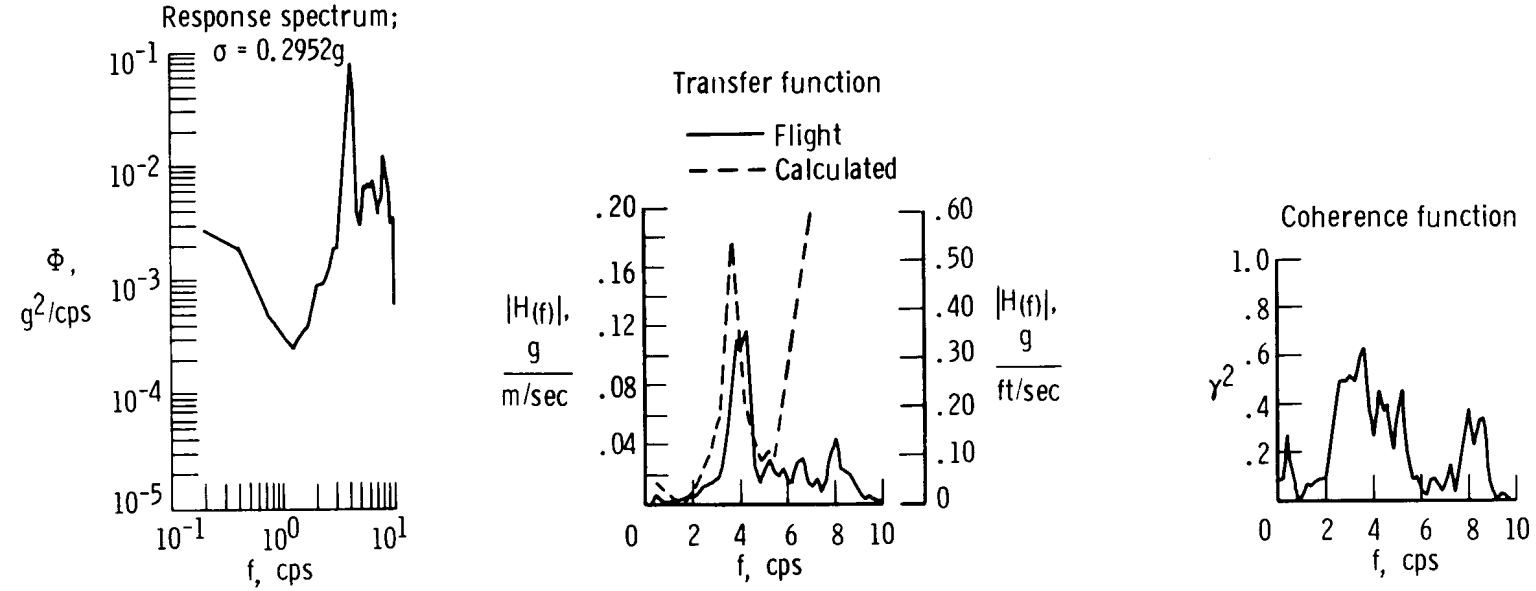

(f) Normal acceleration at wing fuselage station 55.88 meters (2200 inches).

Figure 15. Continued.

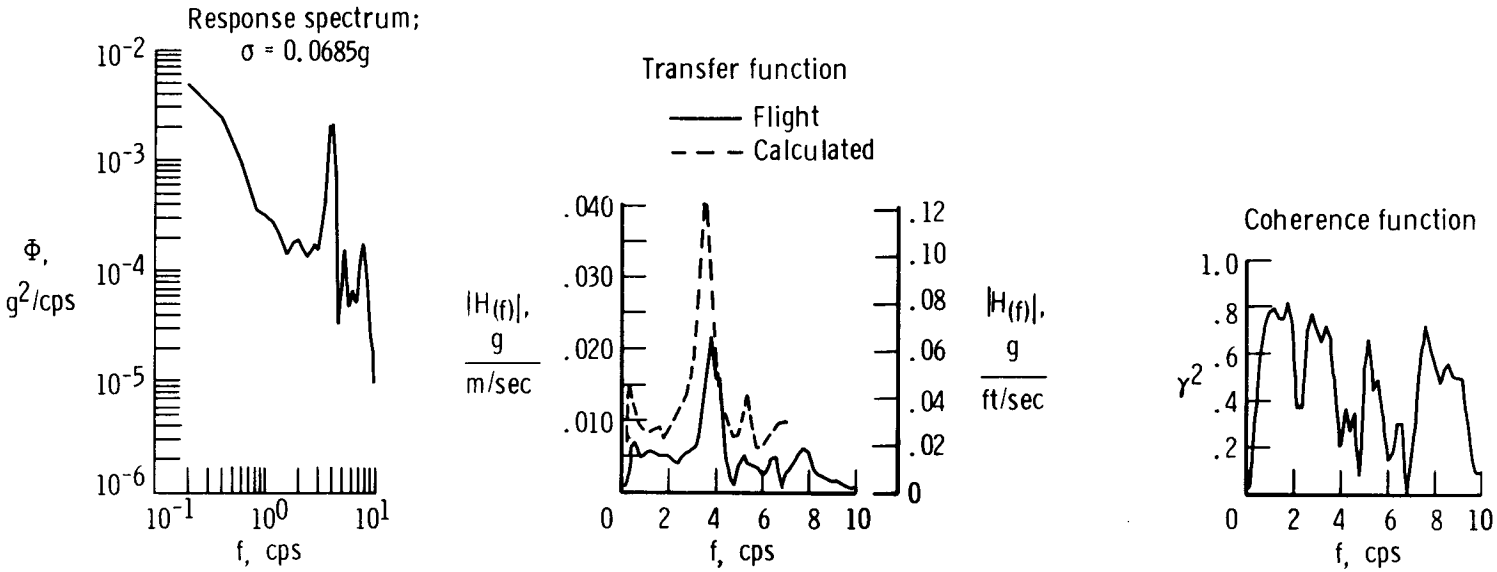

(g) Normal acceleration at the mixer bay.

Figure 15. Concluded.

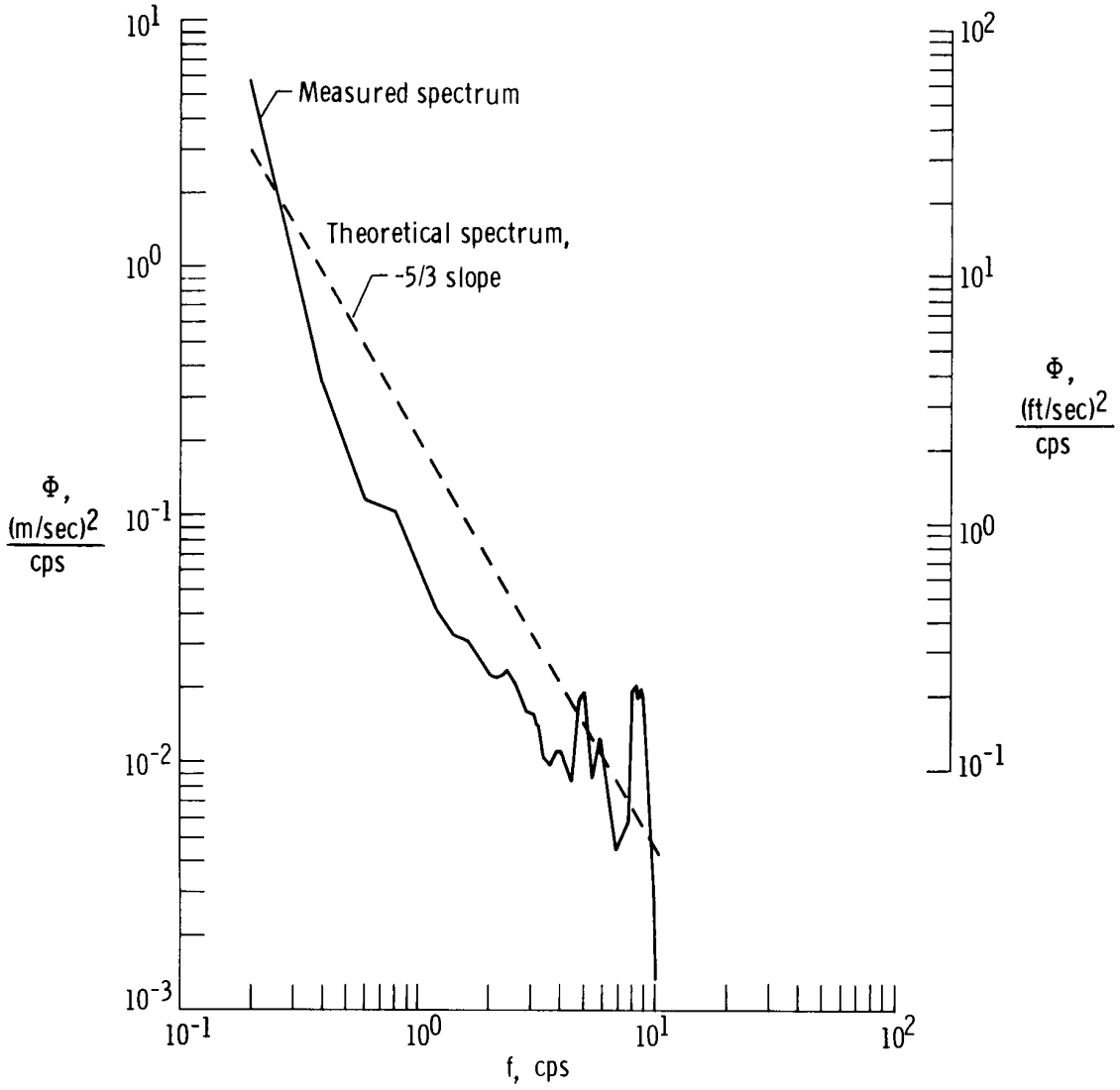

Figure 16. Comparison of vertical component of turbulence input spectrum for flight C with theoretical turbulence mode. Mach 2.35; B_e = 0.4 cps; T_r = 53.5 sec; η = 42.8; σ_1 = 0.9226 m/sec (3.0270 ft/sec).

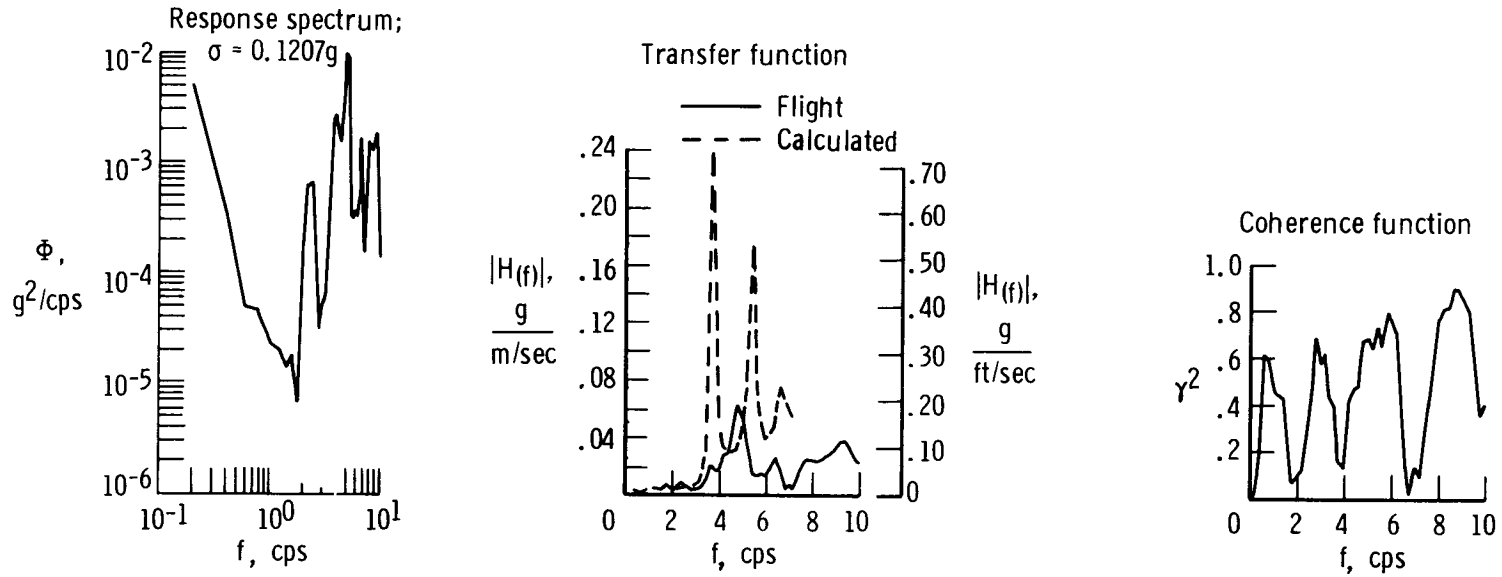

(a) Normal acceleration at the airplane nose.

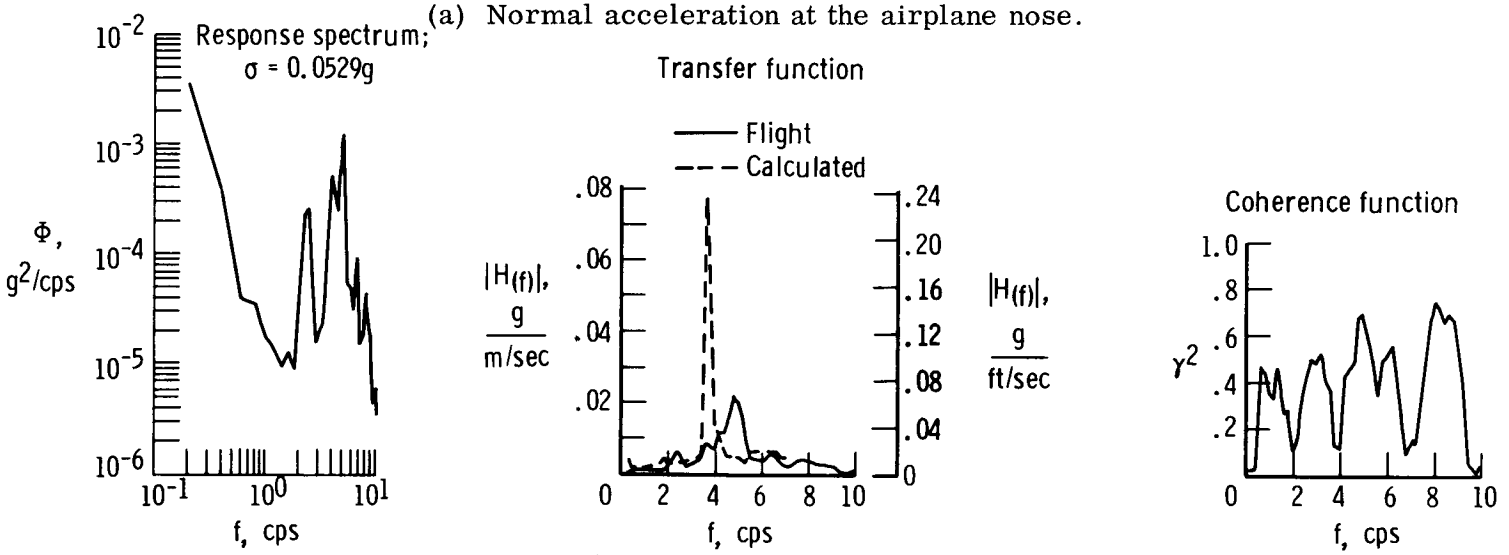

(b) Normal acceleration at the pilot station.

Figure 17. Comparison of frequency response spectra, frequency response transfer functions, and coherence functions for flight C with theoretical frequency response transfer functions for various accelerometer locations. $B_e = 0.4$ cps; $T_r = 53.5$ sec; $\eta = 42.8$.

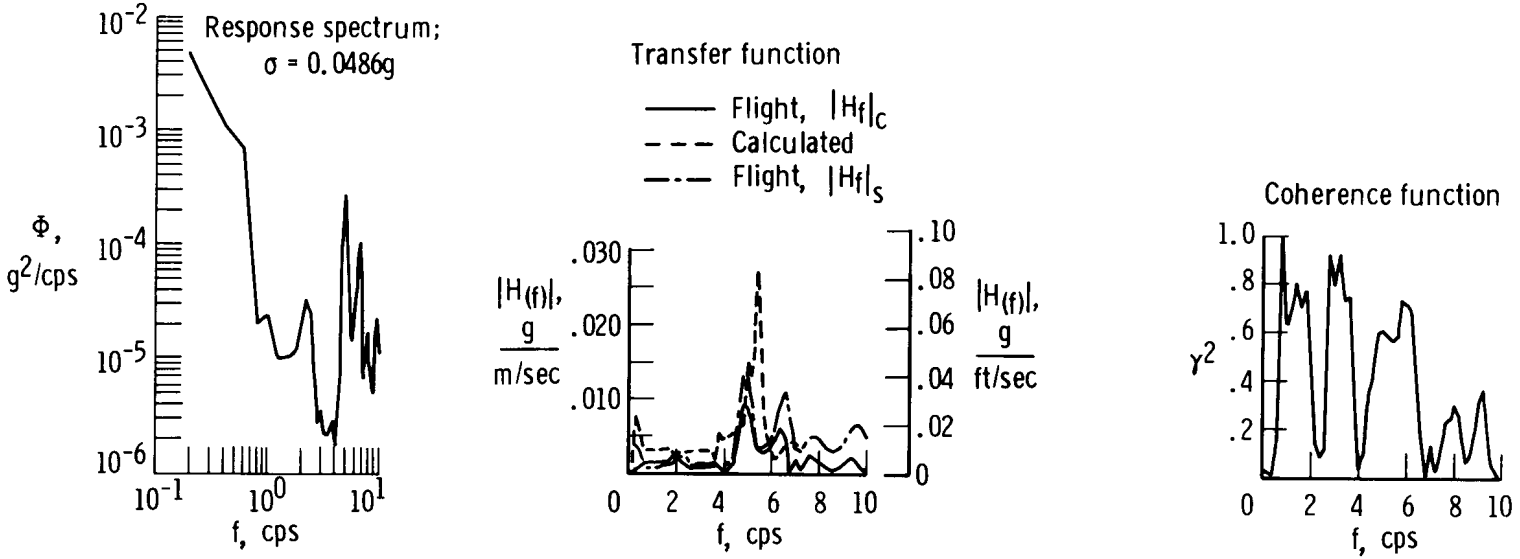

(c) Normal acceleration at the center of gravity.

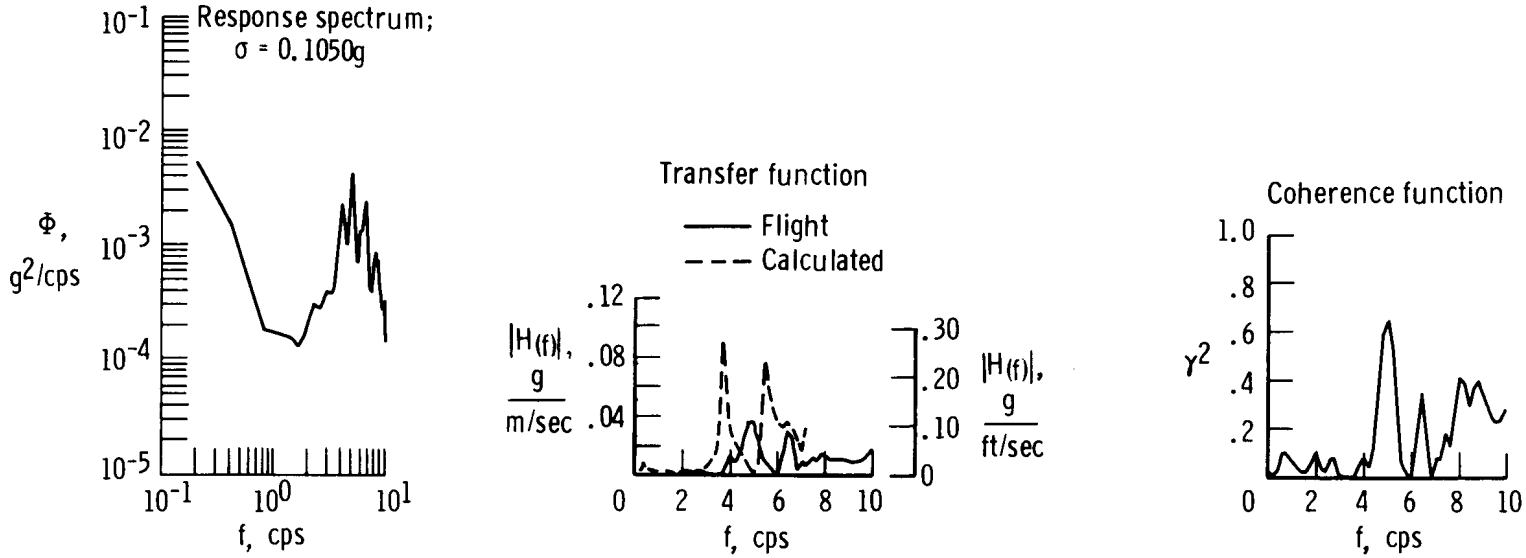

(d) Normal acceleration at wing fuselage station 46.23 meters (1820 inches).

Figure 17. Continued.

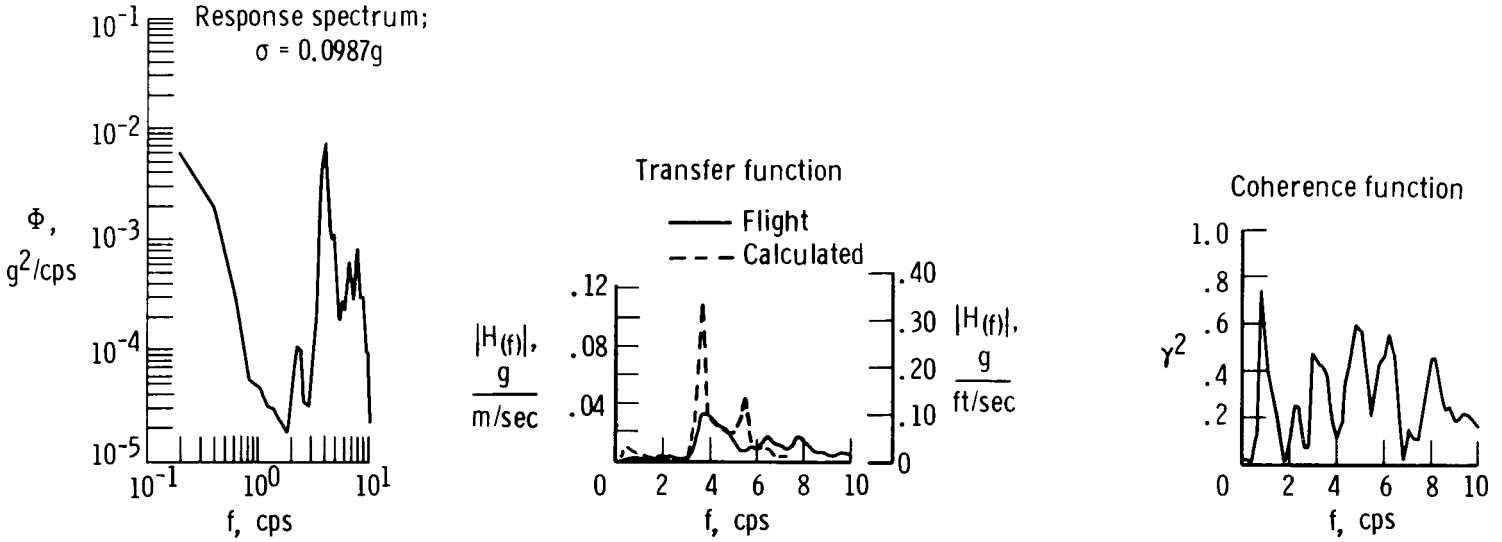

(e) Normal acceleration at wing fuselage station 55.17 meters (2172 inches).

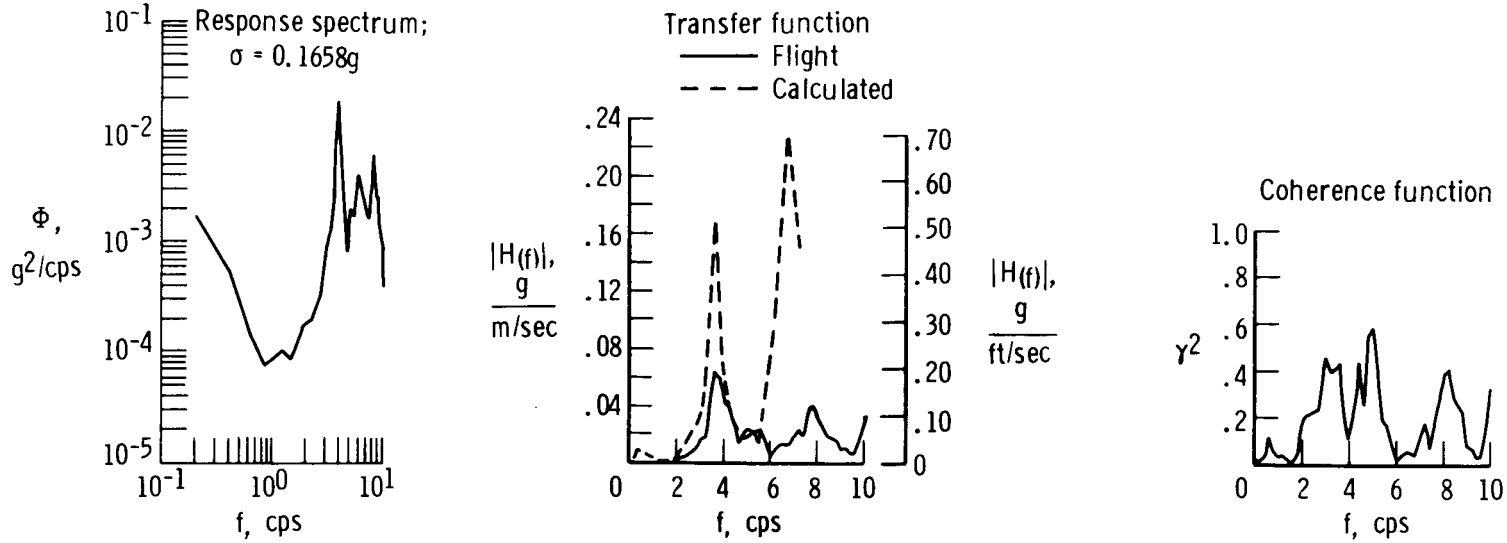

(f) Normal acceleration at wing fuselage station 55.88 meters (2200 inches).

Figure 17. Continued.

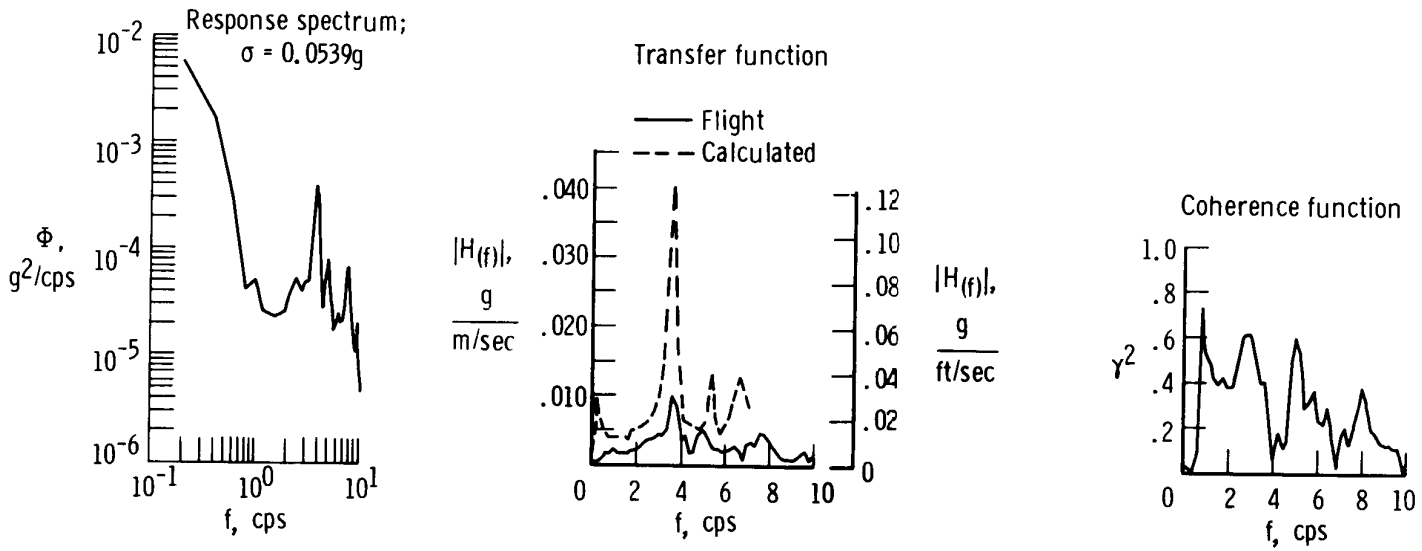

(g) Normal acceleration at the mixer bay.

Figure 17. Concluded.

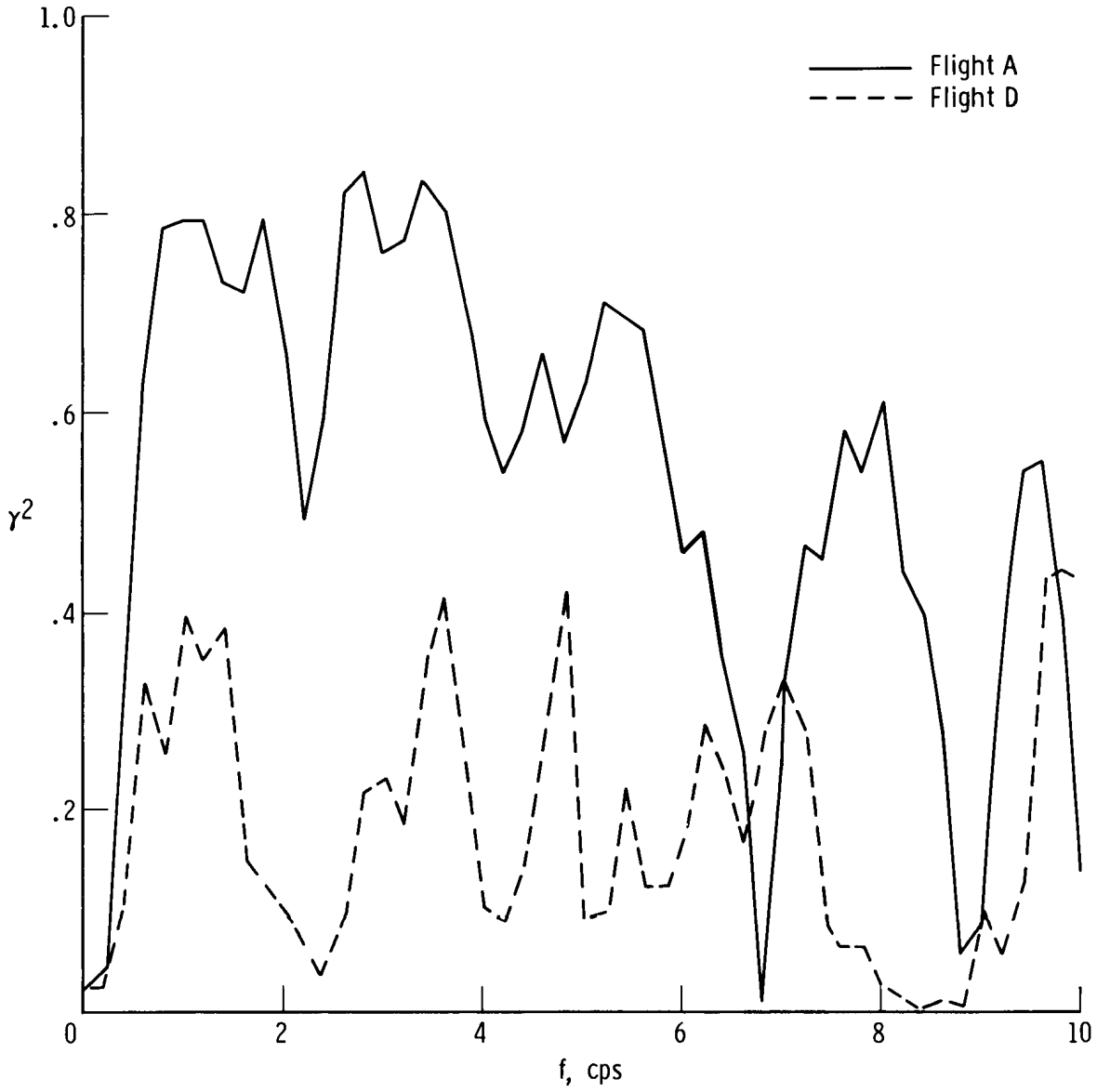

Figure 18. Comparison of coherence function at the center of gravity for a high and a low intensity turbulence encounter.

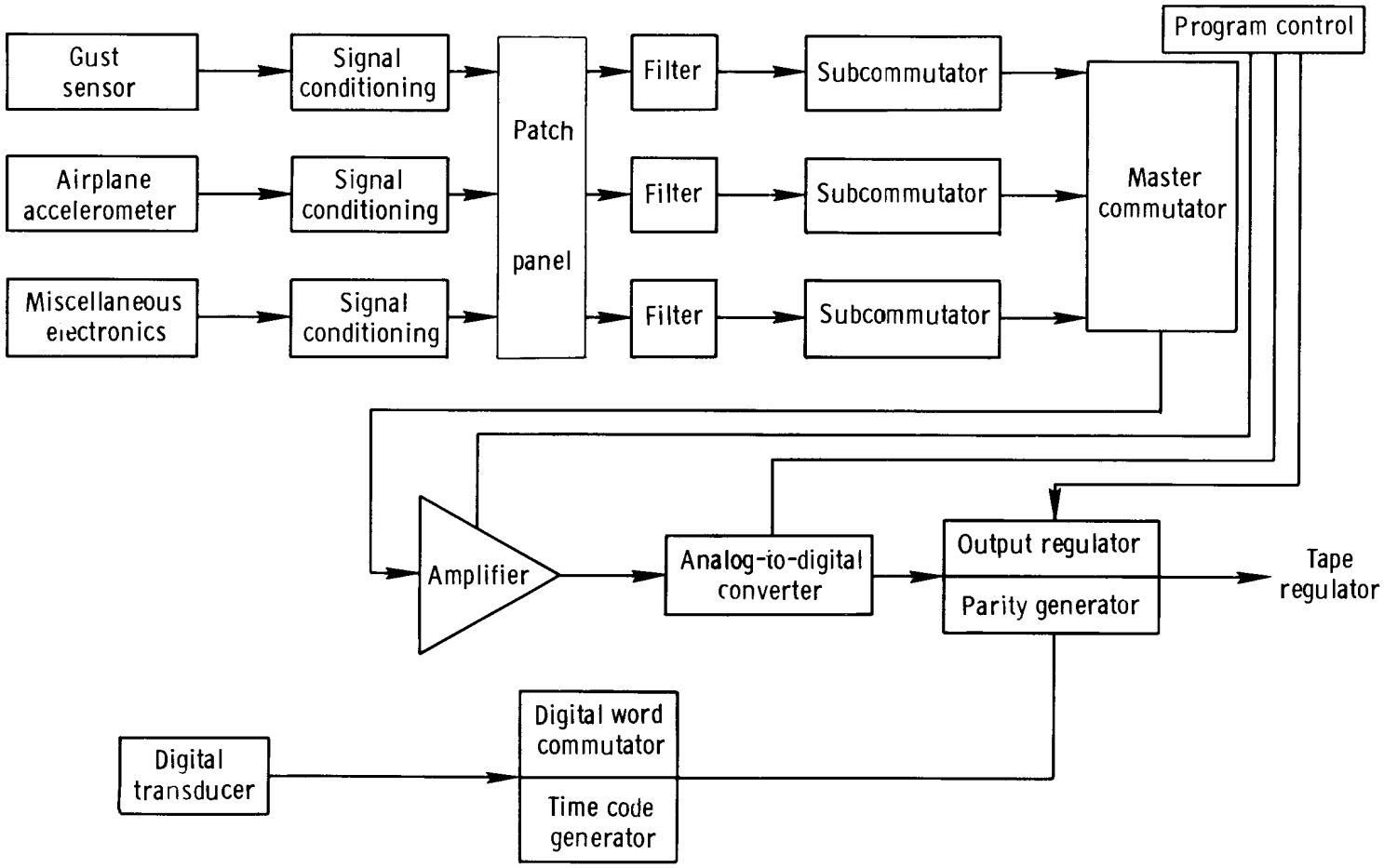

Figure 19. Block diagram of XB-70 airborne digital data-acquisition system.

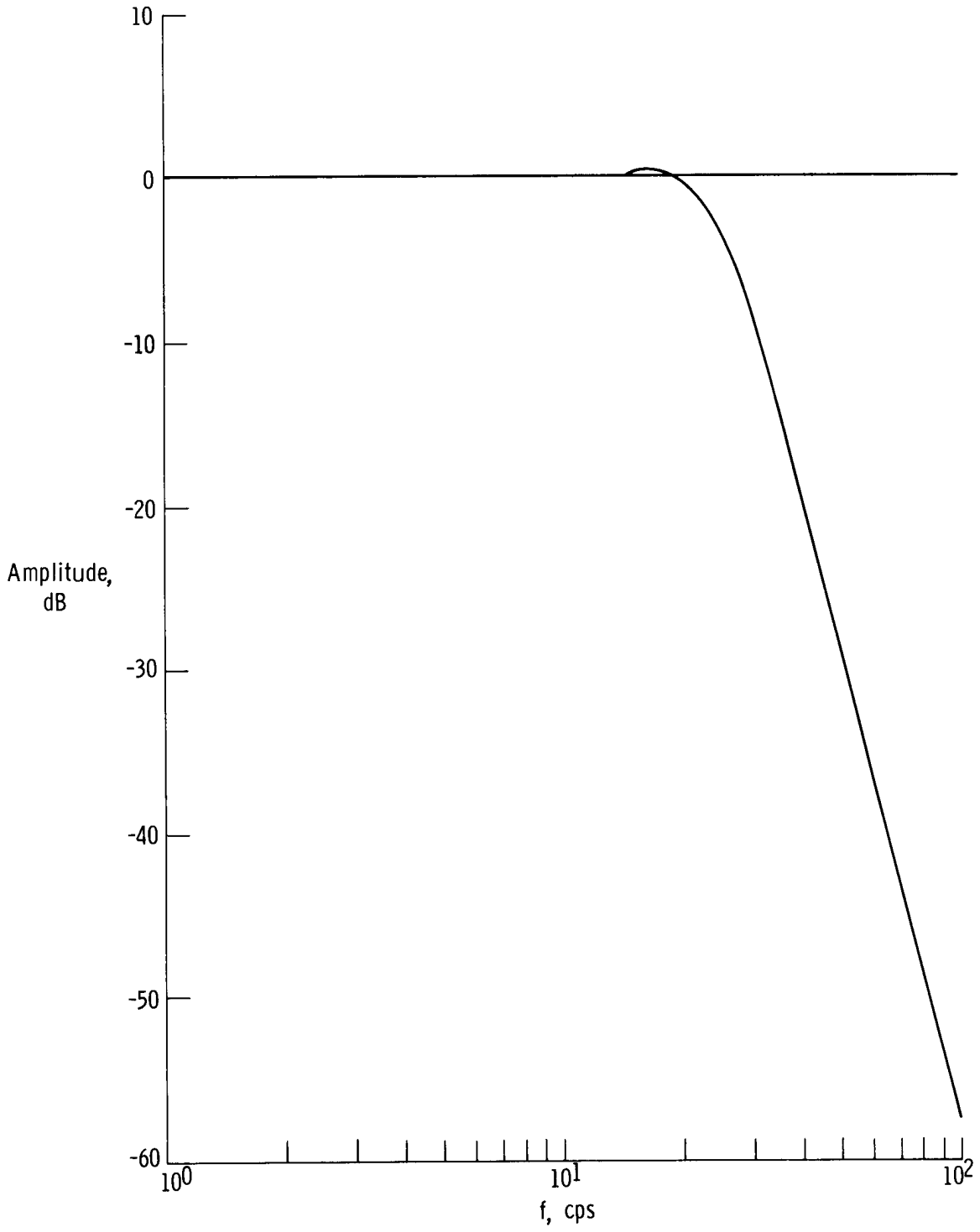

Figure 20. Frequency response of XB-70 turbulence response passive low-pass filter.

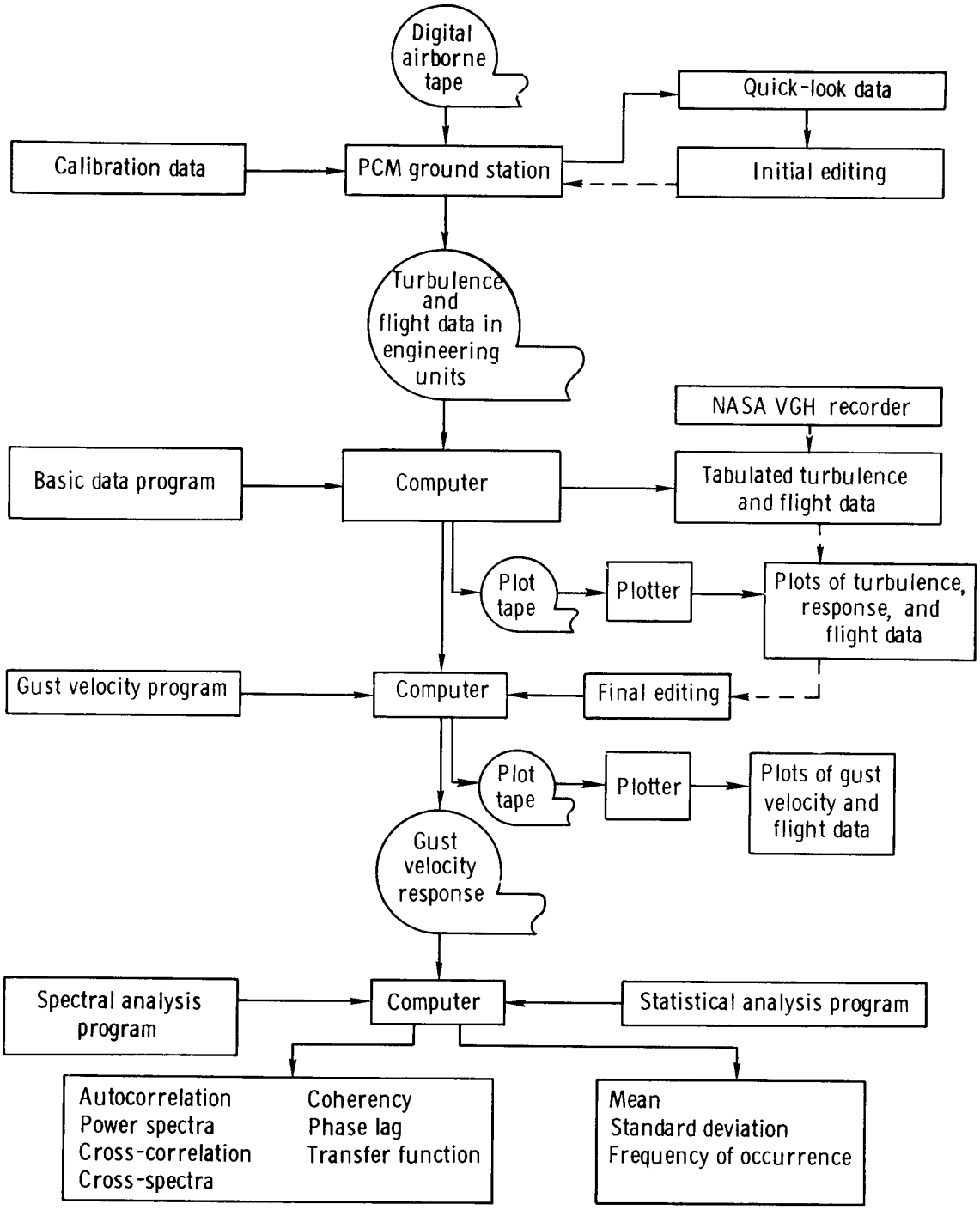

Figure 21. Data-processing flow chart.

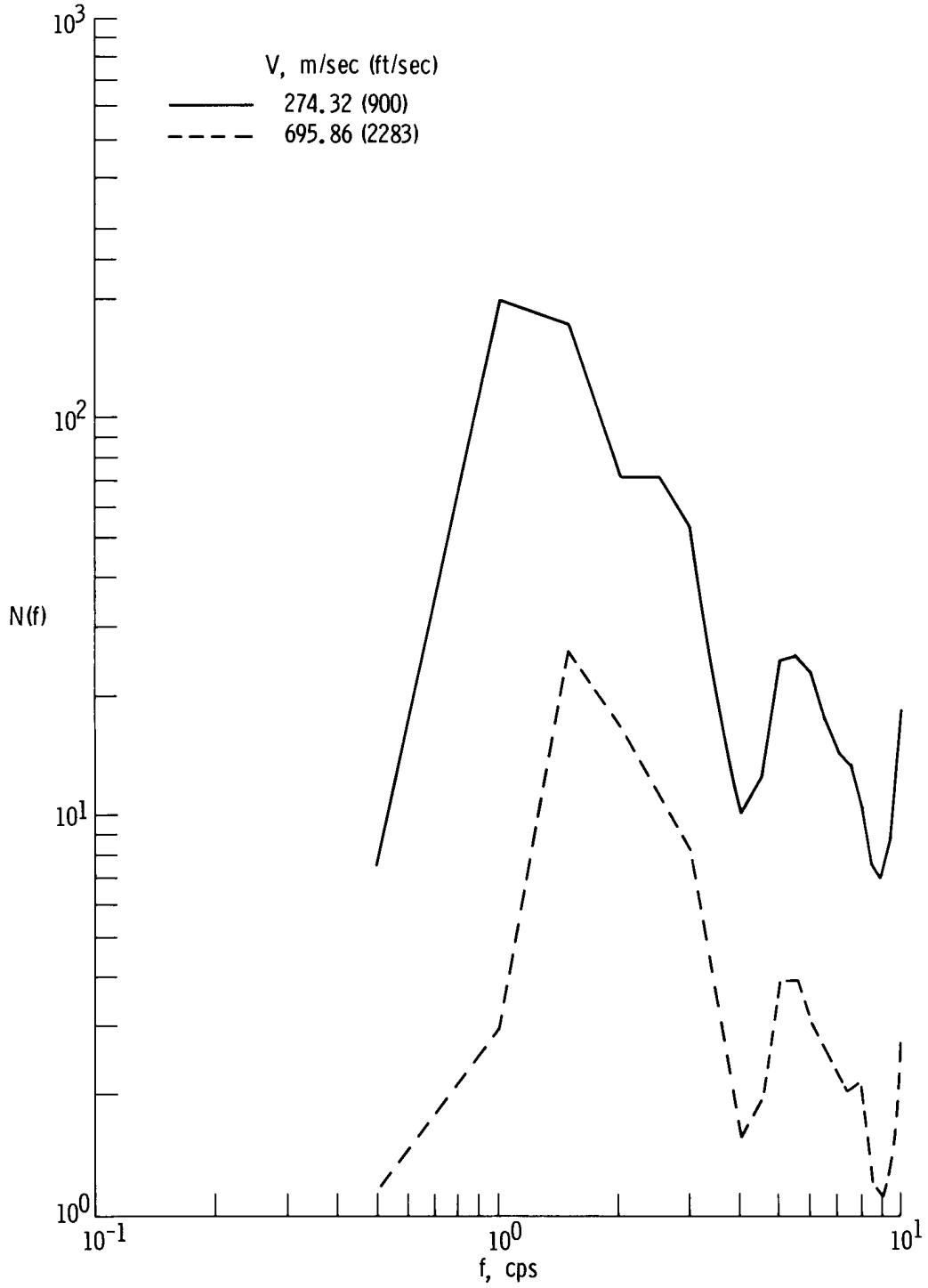

Figure 22. Comparison of equivalent signal-to-noise ratios for two flight conditions.

Figure 23. Geographic area covered in XB-70 flight tests.

Encounter number	Greenwich mean time	$(\Delta a_n)_{max}$, g	Distance in turbulence, km (miles)	h_p, m (ft)
1	1738	0.127	6.8 (4.2)	12, 649 (41, 500)

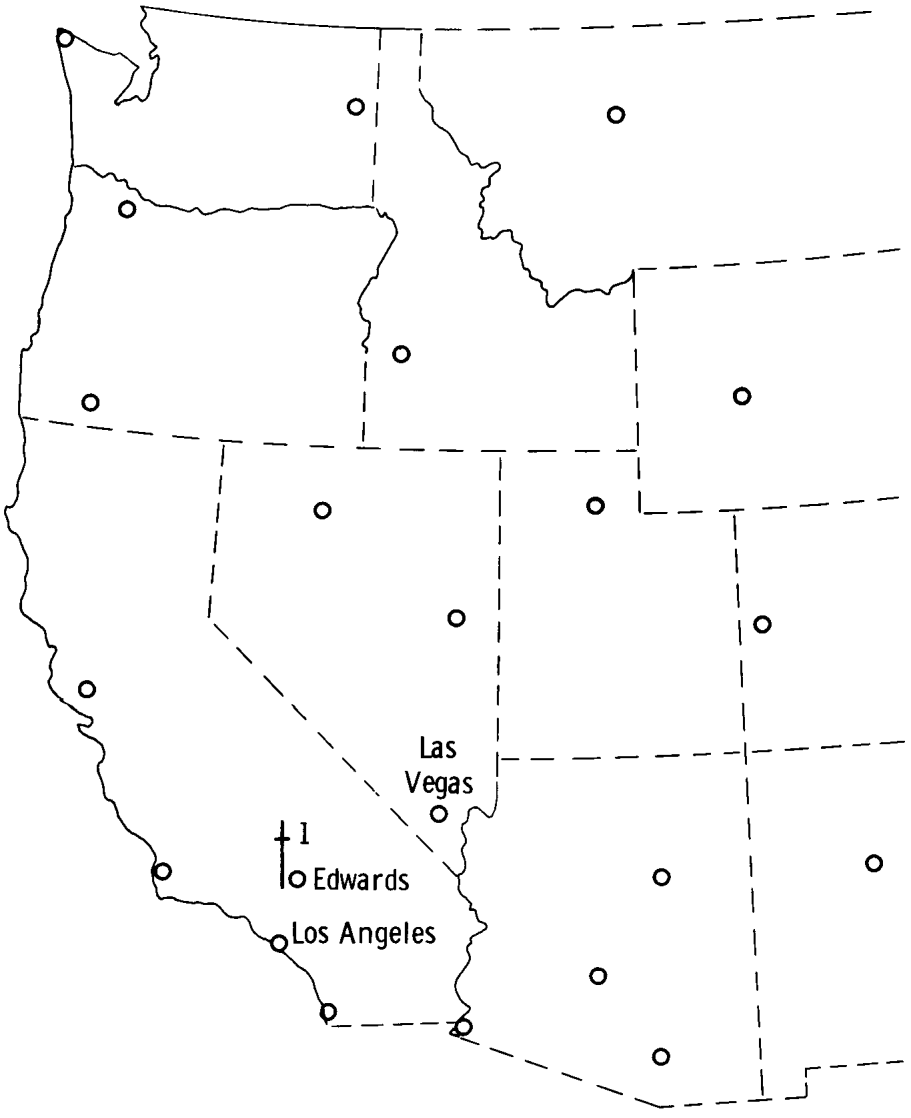

(a) Flight 63, June 2, 1967.

Figure 24. XB-70 turbulence encounter data.

Encounter number	Greenwich mean time	$(\Delta a_n)_{max}$, g	Distance in turbulence, km (miles)	h_p, m (ft)
1	1751	0.143	9.8 (6.1)	15, 636 (51, 300)
2	1753	.254	46.8 (29.1)	15, 758 (51, 700)
3	1755	.254	4.3 (2.7)	15, 362 (50, 400)
4	1804	.111	58.0 (36.0)	14, 021 (46, 000)

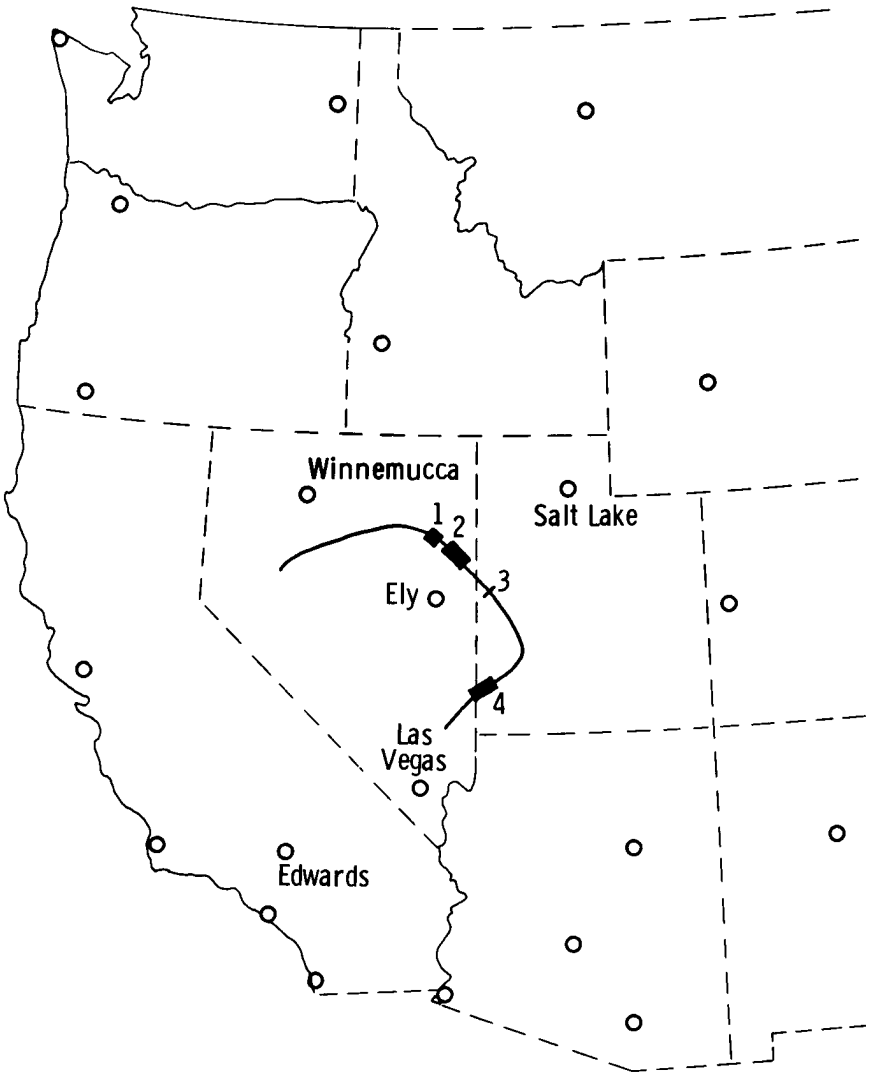

(b) Flight 64, June 22, 1967.

Figure 24. Continued.

Encounter number	Greenwich mean time	$(\Delta a_n)_{max}$, g	Distance in turbulence, km (miles)	h_p, m (ft)
1	1630	0.095	3.5 (2.2)	16, 703 (54, 800)
2	1631	.095	2.4 (1.5)	16, 825 (55, 200)
3	1632	.111	5.5 (3.4)	17, 252 (56, 600)
4	1643	.095	6.3 (3.9)	17, 191 (56, 400)
5	1647	.095	7.7 (4.8)	16, 398 (53, 800)

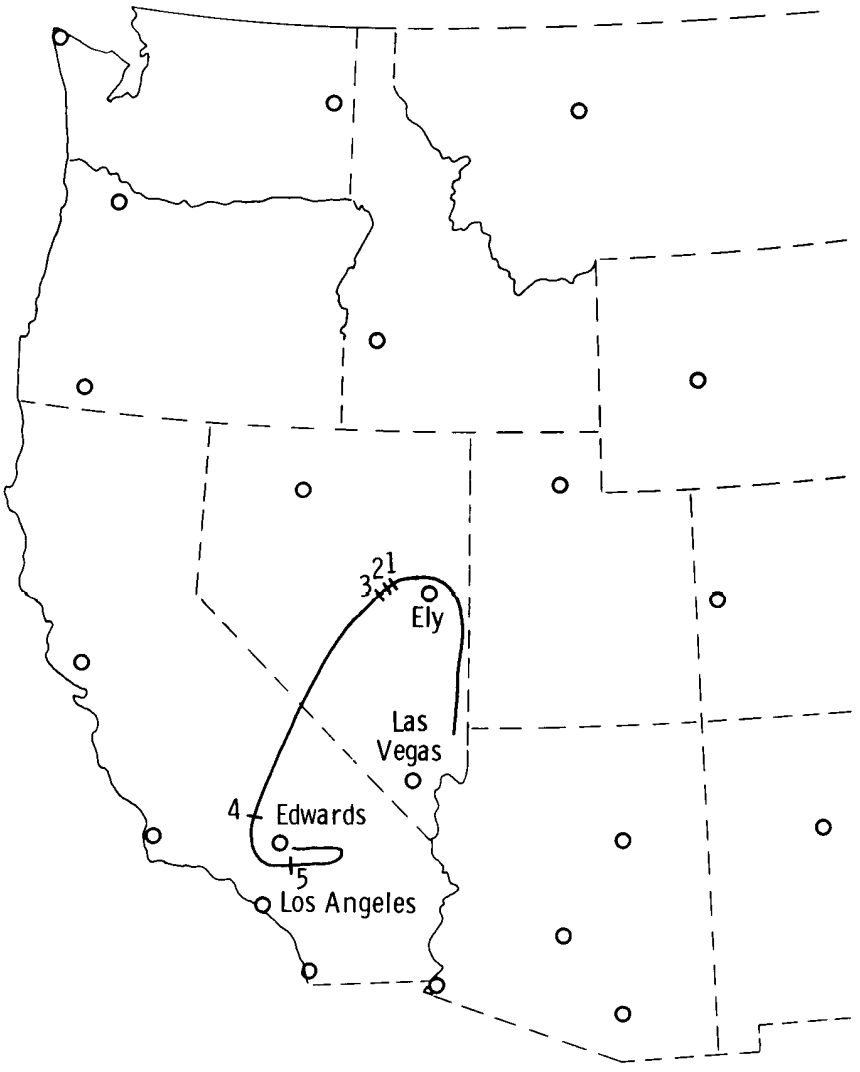

(c) Flight 66, August 24, 1967.

Figure 24. Continued.

Encounter number	Greenwich mean time	$(\Delta a_n)_{max}$, g	Distance in turbulence, km (miles)	h_p, m (ft)
1	1544	0.127	10.0 (6.2)	12, 741 (41, 800)
2	1553	.095	5.3 (3.3)	16, 398 (53, 800)
3	1601	.095	15.0 (9.3)	17, 374 (57, 000)
4	1639	.127	14.0 (8.7)	16, 215 (53, 200)

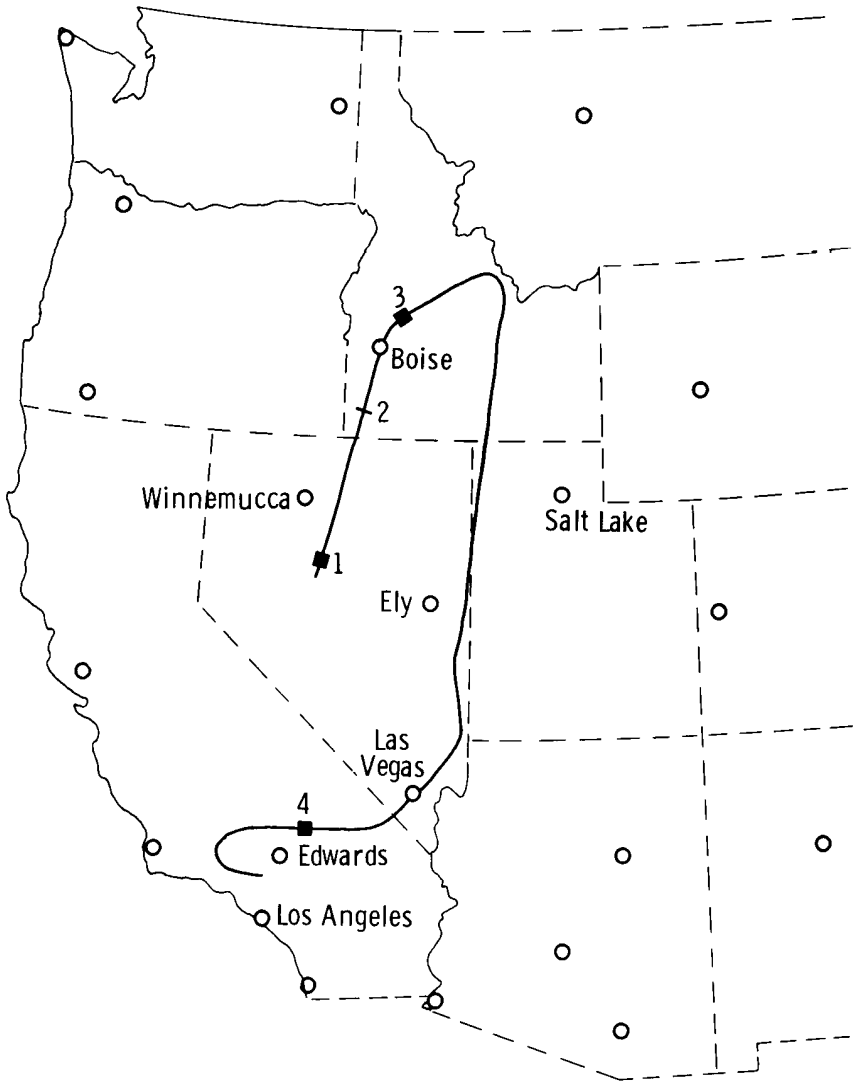

(d) Flight 67, September 8, 1967.

Figure 24. Continued.

Encounter number	Greenwich mean time	$(\Delta a_n)_{max}$, g	Distance in turbulence, km (miles)	h_p, m (ft)
1	1638	0.127	63.9 (39.7)	15, 758 (51, 700)
2	1643	.095	23.0 (14.3)	16, 398 (53, 800)
3	1648	.111	3.4 (2.1)	16, 612 (54, 500)
4	1649	.127	15.4 (9.6)	16, 764 (55, 000)
5	1650	.095	6.8 (4.2)	16, 764 (55, 000)
6	1652	.254	9.5 (5.9)	16, 886 (55, 400)
7	1656	.095	10.9 (6.8)	16, 947 (55, 600)
8	1657	.095	26.2 (16.3)	16, 825 (55, 200)
9	1658	.127	19.5 (12.1)	16, 947 (55, 600)
10	1702	.143	8.2 (5.1)	16, 886 (55, 400)
11	1720	.111	8.7 (5.4)	15, 484 (50, 800)
12	1724	.127	12.4 (7.7)	13, 106 (43, 000)

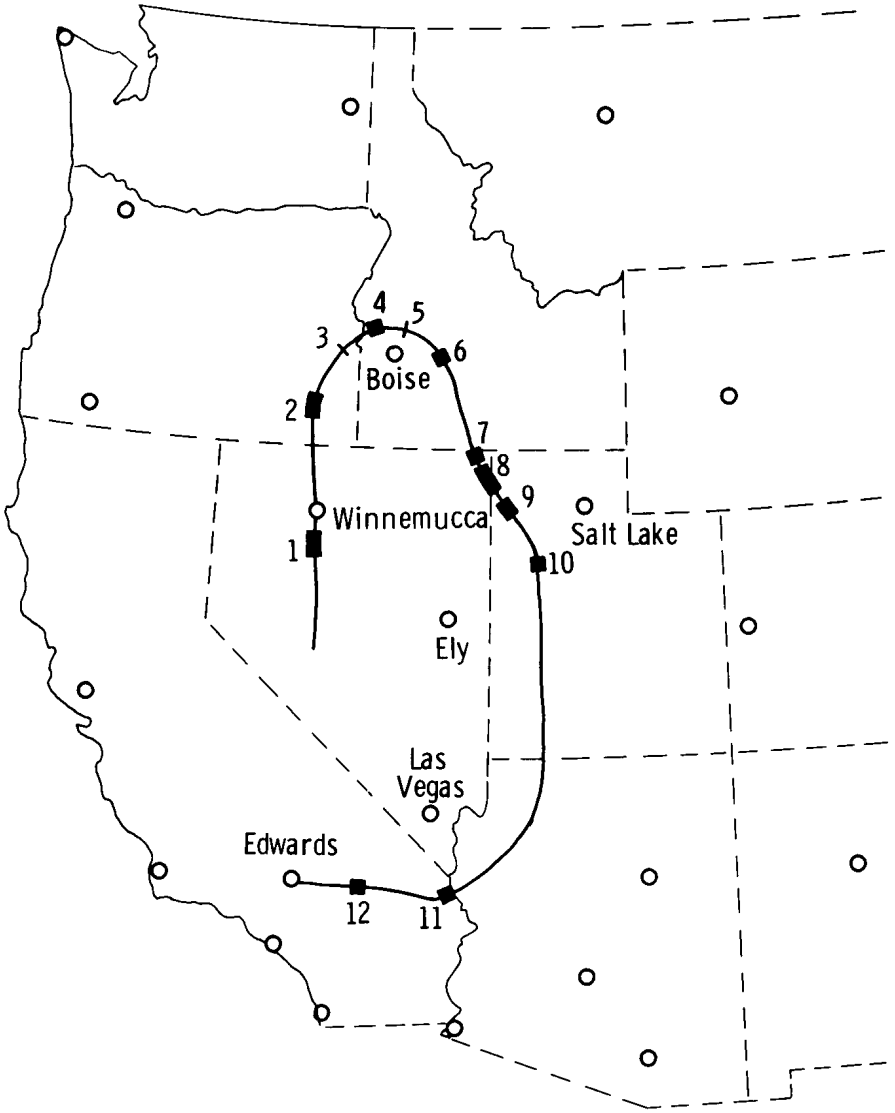

(e) Flight 68, October 11, 1967.

Figure 24. Continued.

Encounter number	Greenwich mean time	$(\Delta a_n)_{max}$, g	Distance in turbulence, km (miles)	h_p, m (ft)
1	1737	0.095	41.8 (26.0)	16, 520 (54, 200)
2	1738	.095	9.5 (5.9)	16, 947 (55, 600)
3	1758	.111	12.9 (8.0)	18, 898 (62, 000)
4	1802	.127	29.3 (18.2)	19, 141 (62, 800)
5	1804	.143	82.1 (51.0)	19, 202 (63, 000)
6	1814	.111	11.9 (7.4)	17, 313 (56, 800)
7	1815	.143	38.6 (24.0)	16, 581 (54, 400)

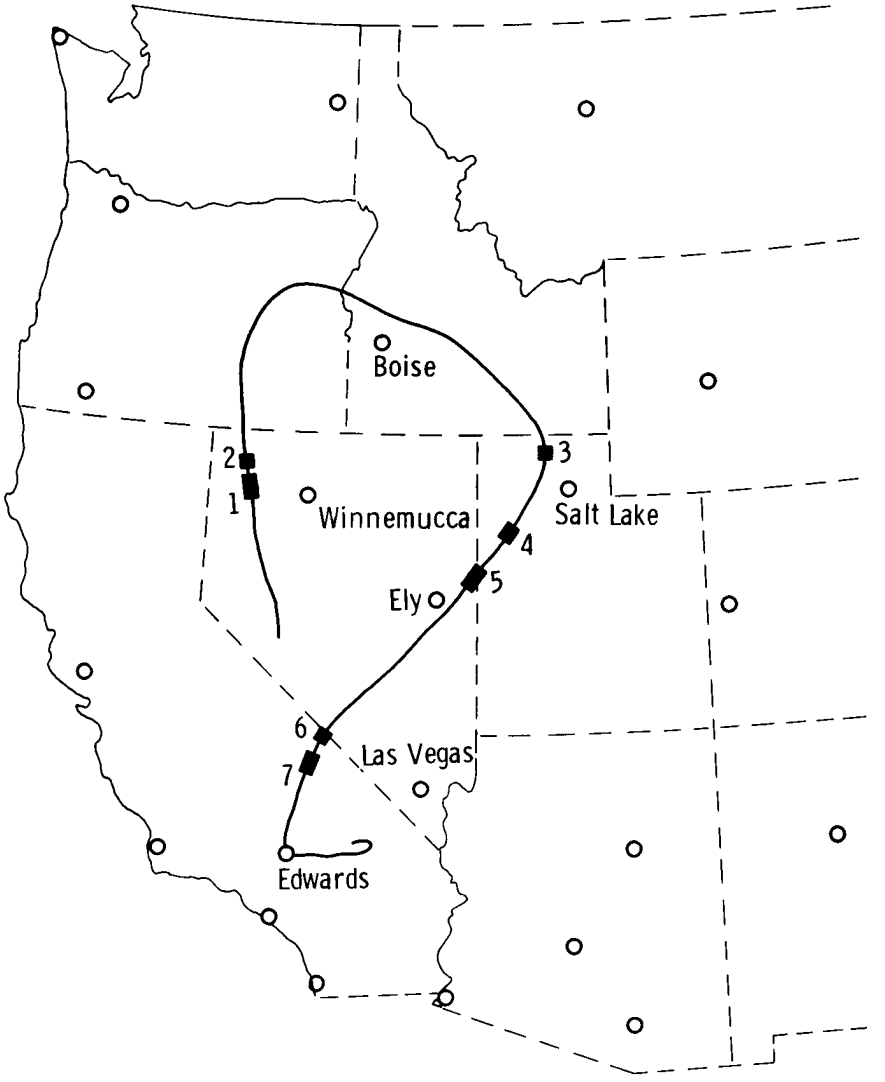

(f) Flight 69, November 2, 1967.

Figure 24. Continued.

Encounter number	Greenwich mean time	$(\Delta a_n)_{max}$, g	Distance in turbulence, km (miles)	h_p, m (ft)
1	1559	0.095	10.6 (6.6)	16,093 (52,800)

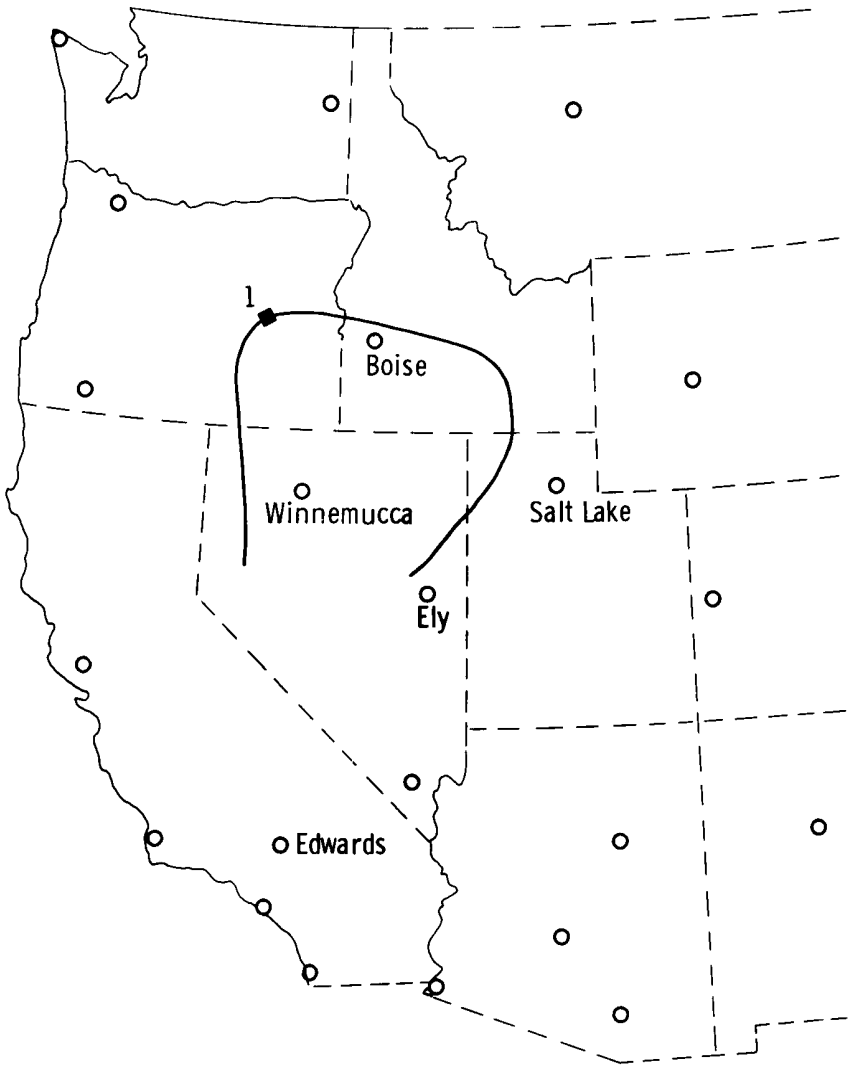

(g) Flight 77, August 16, 1968.

Figure 24. Continued.

Encounter number	Greenwich mean time	$(\Delta a_n)_{max}$, g	Distance in turbulence, km (miles)	h_p, m (ft)
1	1806	0.095	13.8 (8.6)	14, 783 (48, 500)
2	1808	.143	10.3 (6.4)	14, 966 (49, 100)
3	1814	.095	11.9 (7.4)	13, 289 (43, 600)
4	1826	.254	17.1 (10.6)	12, 527 (41, 100)
5	1830	.318	16.9 (10.5)	12, 436 (40, 800)

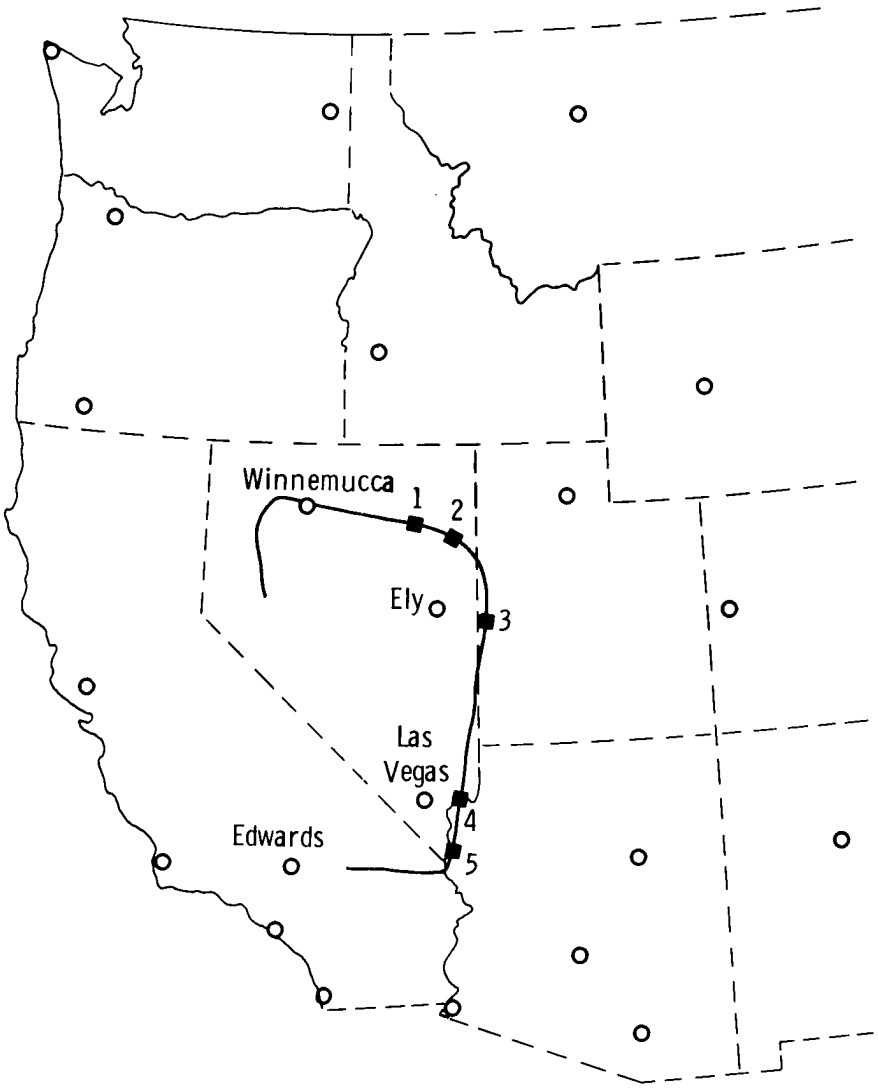

(h) Flight 79, October 18, 1968.

Figure 24. Continued.

Encounter number	Greenwich mean time	$(\Delta a_n)_{max}$, g	Distance in turbulence, km (miles)	h_p, m (ft)
1	2045	No VGH recorder	11.4 (7.1)	12, 863 (42, 200)
2	2056	No VGH recorder	37.2 (23.1)	17, 008 (55, 800)

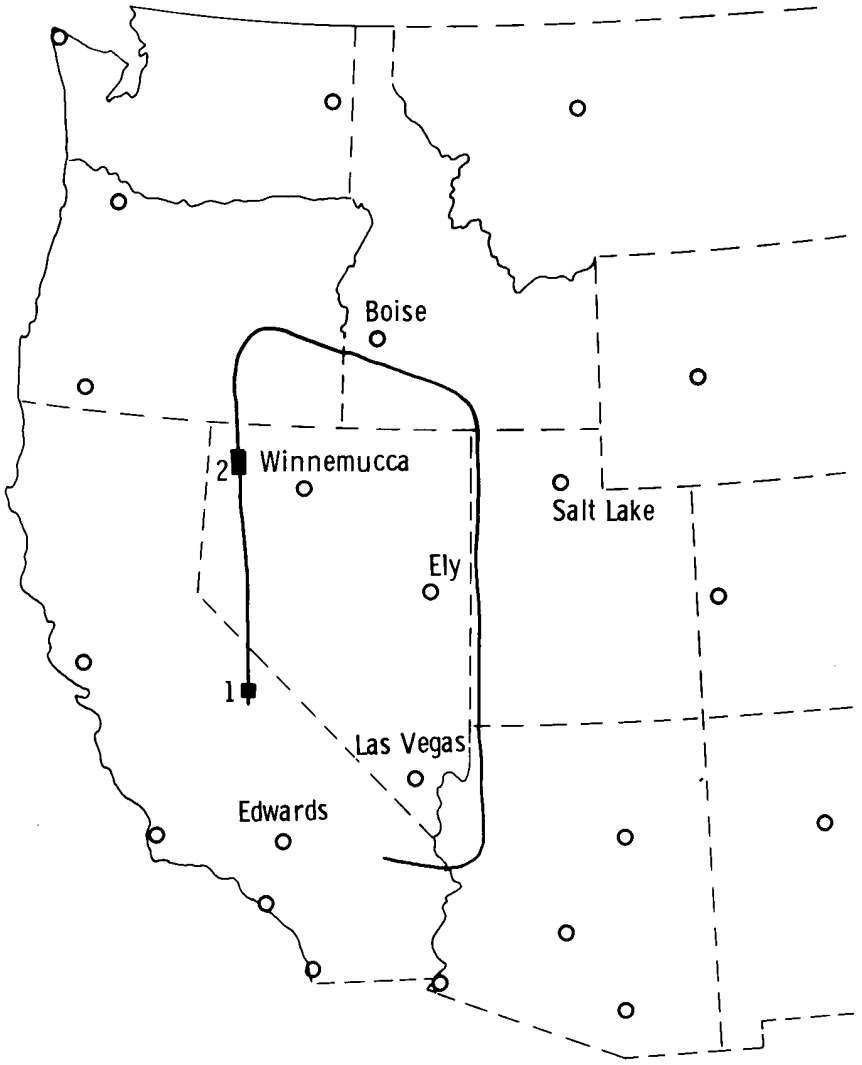

(i) Flight 82, December 17, 1968.

Figure 24. Concluded.

NASA-Langley, 1971 — 2 H-631